ELSEVIER

Contents lists available at ScienceDirect

Materials Today Catalysis

journal homepage: www.journals.elsevier.com/materials-today-catalysis





MXene-based catalysts: A review

Ali Hamzehlouy a, Masoud Soroush a,b,*

- ^a Department of Chemical and Biological Engineering, Drexel University, Philadelphia, PA 19104, USA
- b Department of Materials Science and Engineering, Drexel University, Philadelphia, PA 19104, USA

ARTICLE INFO

Keywords:
MXenes
Catalysts
Chemical reactions
Hydrogen evolution
Oxygen evolution
Oxygen reduction
Carbon dioxide reduction
CO oxidation

ABSTRACT

Two-dimensional (2D) materials, such as graphene, hexagonal boron nitride, 2D metal-organic frameworks, layered double hydroxides, transition metal dichalcogenides, and MXenes, have garnered significant attention in catalysis due to their exceptional properties and structures. Notably, recent studies have revealed the promising catalytic activity of MXene-based catalysts for many reactions, including hydrogen evolution, oxygen evolution, oxygen reduction, nitrogen reduction, carbon dioxide reduction, alcohol oxidation, hydrogenation, dehydrogenation, methanol conversion, dry reforming of methane, and CO oxidation. This review offers a summary of recent advances in the field, contextualizing the progress made. Additionally, it delves into existing challenges while presenting prospects for future developments in this domain.

1. Introduction

Two-dimensional (2D) materials, including graphene [1,2], hexagonal boron nitride (h-BN) [3], 2Dmetal-organic frameworks (MOFs) [4], layered double hydroxides (LDHs) [5], transition metal dichalcogenides (TMDs) [6], 2D transition metal carbides [7], and MXenes [8–10] have attracted significant interest owing to their outstanding properties and structures. Consequently, they have shown capabilities in applications in many areas, including catalysis, sensors, nanocomposites, actuators, antimicrobial materials, and electromagnetic interference shielding [11–16]. It is also long known that carbides (nonnoble metals containing carbon) can be alternatives to expensive late transition metals as catalysts to accelerate various reactions [17]. For instance, Levy et al. [18] investigated the effect of inserting carbon into tungsten (W), which led to tungsten carbide (WC) formation. Their findings revealed that the catalytic performance of WC was comparable to that of pure metals like platinum in reactions, including the formation of water from hydrogen and oxygen at room temperature, the reduction of tungsten trioxide by hydrogen in the presence of water, and the isomerization of 2,2-dimethylpropane to 2-methylbutane. As for the formation of water from hydrogen and oxygen, the chemisorption of hydrogen and oxygen, and subsequent removal of adsorbed oxygen by hydrogen with the formation of water have been long assessed for platinum (Pt) [19], palladium (Pd) [20], and rhodium (Rh) [21]. However, it is unlikely for these processes to take place on other transition metals because they establish robust interactions with oxygen, hindering its removal. In contrast, primary

outcomes have indicated that the incorporation of carbon into tungsten alters the electron distribution. In other words, carbon significantly decreases the high reactivity of tungsten toward oxygen via the introduction of its valence electrons to those of the metal.

In particular, few-layered transition metal carbides, nitrides, and carbonitrides, called MXenes, are novel groups of 2D nanomaterials that have received great interest worldwide due to their extraordinary chemical and physical characteristics [22–25]. They were discovered in 2011 at Drexel University, and since then, research on these 2D materials has exponentially increased [26]. MXenes have the general chemical formula of $M_{n+1}X_nT_x$ (n=1–4), where M is an early transition metal (including Sc, Ti, Zr, Hf, V, Nb, Ta, Cr, and Mo), X is a carbon and/or nitrogen atom, and T_x denotes surface terminations (hydroxyl, oxygen, fluorine, etc.) [27,28]. So far, more than 50 types of MXenes have been synthesized. $T_{13}C_2T_x$ is the most widely studied MXene.

MXenes have been synthesized using different methods. A widely-used method is the selective etching of A element from a ternary $M_{n+1}AX_n$ phase called a MAX phase, where A is an element of the IIIA or IVA group. Single- or a-few-layer MXenes are obtained by the exfoliation and delamination of multi-layer MXenes (Fig. 1) [29–31]. It should be noted that the interlayer bonds are much weaker than intralayer ones in the MAX phase, so a robust etchant can detach the A layer from the MAX structure [32]. Etching by hydrofluoric acid (HF) was the first experimental way of obtaining MXenes [33]. However, HF is corrosive and poses a severe threat to the environment, which has necessitated the development of alternative synthesis methods and the optimization of

^{*} Corresponding author at: Department of Chemical and Biological Engineering, Drexel University, Philadelphia, PA 19104, USA. *E-mail address:* ms1@drexel.edu (M. Soroush).

the synthesis steps [9]. Alternative synthesis methods include Lewis acidic etching [34,35], molten salt etching [36,37], electrochemical etching [38], and alkali etching [39]. As a "non-etching" method, chemical vapor deposition (CVD) is a direct synthesis route of MXenes, which results in new morphologies with more easily accessible surfaces and exposed catalytically active edges. In this method, MXenes are fabricated at high temperatures by reacting gaseous precursors, such as a mixture of CH₄ and TiCl₄, on a substrate [40]. Fig. 2 presents some of the fluoride-containing and fluoride-free synthesis routes of MXenes. As Fig. 2(a) shows, Al atoms in the MAX phase are etched out by HF, leading to the production of a MXene [26]. Another approach involves etching Ti₃AlC₂ initially with a solution of hydrochloric acid (HCl) and lithium fluoride (LiF). Subsequently, the product, Ti₃C₂T_x, was repeatedly washed with water to increase the pH to 4-6. Finally, the products were sonicated under inert gas flow, leading to the fabrication of a delaminated Ti₃C₂T_x suspension. To avoid using direct HF directly, a milder LiF initially reacted with HCl to produce HF in this method (Fig. 2 (b)) [41]. Halim et al. [42] produced epitaxial MXene films. First, the Ti₃AlC₂ nanometer film was deposited onto a sapphire (0001) substrate via magnetron sputtering (note that a TiC layer was initially formed as an incubation layer). Afterward, the Al layer was removed by an aqueous HF etchant, resulting in Ti₃C₂T_r MXene (Fig. 2(c)). Yang and coworkers [43] conducted a study on the fabrication of exfoliated Ti₃C₂T_x utilizing an efficient fluoride-free etching method based on the anodic corrosion of Ti₃AlC₂ in a binary aqueous electrolyte comprising NH₄Cl and tetramethylammonium hydroxide (TMA·OH). In this process, aluminum was dissolved, followed by in-situ intercalation of ammonium hydroxide, which subsequently led to the formation of carbide flakes $(Ti_3C_2T_x, T = 0, OH)$ with high yield (over 90%) (Fig. 2(d)).

Due to hazards associated with using hydrochloric acid, fluoride-free methods have been proposed. For instance, Xie *et al.* [44] investigated surface leaching of Ti₃AlC₂ (e-TAC) through a fluoride-free hydrothermal etching method, which leads to the formation of a potential support for Pt nanoparticles (NPs). The novel Pt/e-TAC catalyst exhibited higher chemical stability and oxygen reduction reaction (ORR) activity than a Pt/C catalyst. In another research, Cl-terminated MXenes (Ti₃C₂Cl₂) were synthesized using a fluoride-free route. In this procedure, the Ti₃AlC₂ MAX phase initially underwent a replacement reaction with ZnCl₂, producing a Zn-MAX phase (Ti₃ZnC₂). Next, Cl-terminated MXenes (Ti₃C₂Cl₂) were produced using excess ZnCl₂ and exfoliating the Ti₃ZnC₂ (Fig. 2(e)) [45]. UV-induced etching is another pathway to produce MXenes [46]. In this pathway, Ga was selectively removed

(from Mo_2Ga_2C), leading to the production of a mesoporous Mo_2CT_x MXene, a potential anode for rechargeable batteries (Fig. 2(f)). MXenes have demonstrated attractive features such as high conductivity, light weight, flexibility, and transparency, making them potential candidates for applications such as electromagnetic interference shielding, flexible optoelectronics, sensors, thermal heaters, and nanocomposites [47].

Etching with HF limits termination groups to -F, -O, and -OH [48]. Alternatively, etching in molten inorganic salts leads to the fabrication of MXenes with other surface terminations, including –NH, –S, –Cl, –Se, -Br, and -Te [49]. For instance, the etching of the Ti₃AlC₂ MAX phase in molten ZnCl2 and other molten Lewis acids at a temperature above 500 °C brings about the formation of Ti₃C₂Cl₂ MXene containing pure -Cl termination groups [50]. Likewise, etching with molten Lewis acid CdBr2 has resulted in preparing Br-terminated Ti3C2Br2 and Ti2CBr2 MXenes. MXenes synthesized through this strategy have -Cl and -Br terminations that form weaker (M-F and M-Br) bonds with transition metals from the outer layers of MXene sheets (Ti, Mo, Nb, V), in comparison to M-F and M-O bonds in MXenes prepared via traditional routes. These surface bonds allow for the occurrence of installation and removal reactions where halide ions, i.e., Cl and Br, exchange for other atoms and functional groups, forming MXenes with tunable terminations. Therefore, these chemical transformations and modifications can enable substantial control over the chemistry, structure, and properties of MXene materials [51].

MXenes with n>3 can be synthesized through epitaxial growth (e.g., depositing alternating layers of nitrogen molecules (N₂) and early transition metal). Computational studies, including density functional theory (DFT) methods have supported the usefulness of this method. In this method, N₂ molecules are initially adsorbed onto the surface of a MXene precursor possessing M₂X stoichiometry, followed by the formation of M₂XN₂ MXenes. In summary, computational studies have shown that the epitaxial growth leads to the synthesis of pristine MXenes with alternating N-transition metal layers, rendering these nanomaterials more layers beyond seven [51].

In recent years, the catalytic activities of MXenes, as heterogeneous catalysts, have been studied for many reactions [52,53]. This has primarily been motivated by the scarcity and high cost of noble metals used in noble-metal-based catalysts [54] and the inexpensiveness and abundance of the elements comprising MXenes [31].

This review paper aims to highlight the most recent advances in applying MXenes as catalysts. This paper describes the latest advances in the use of MXenes as catalysts in electrocatalysis reactions, including

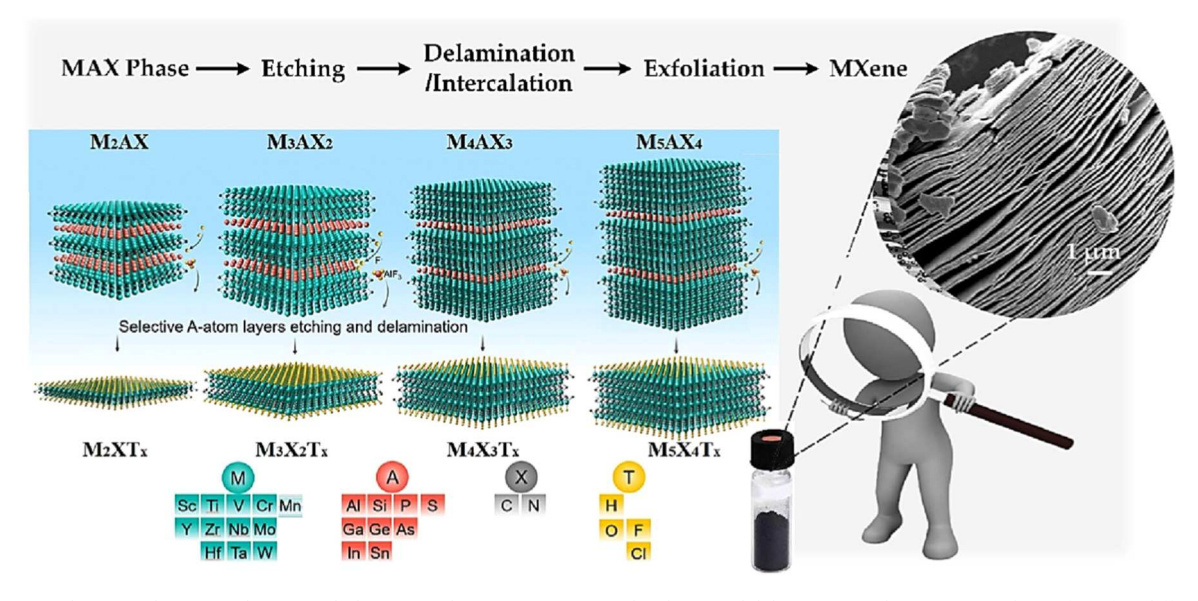


Fig. 1. MXene synthesis involves several steps, including MAX phase preparation, acid etching, and delamination. These steps are shown for a few different MXenes. Reprinted with permission from [9].

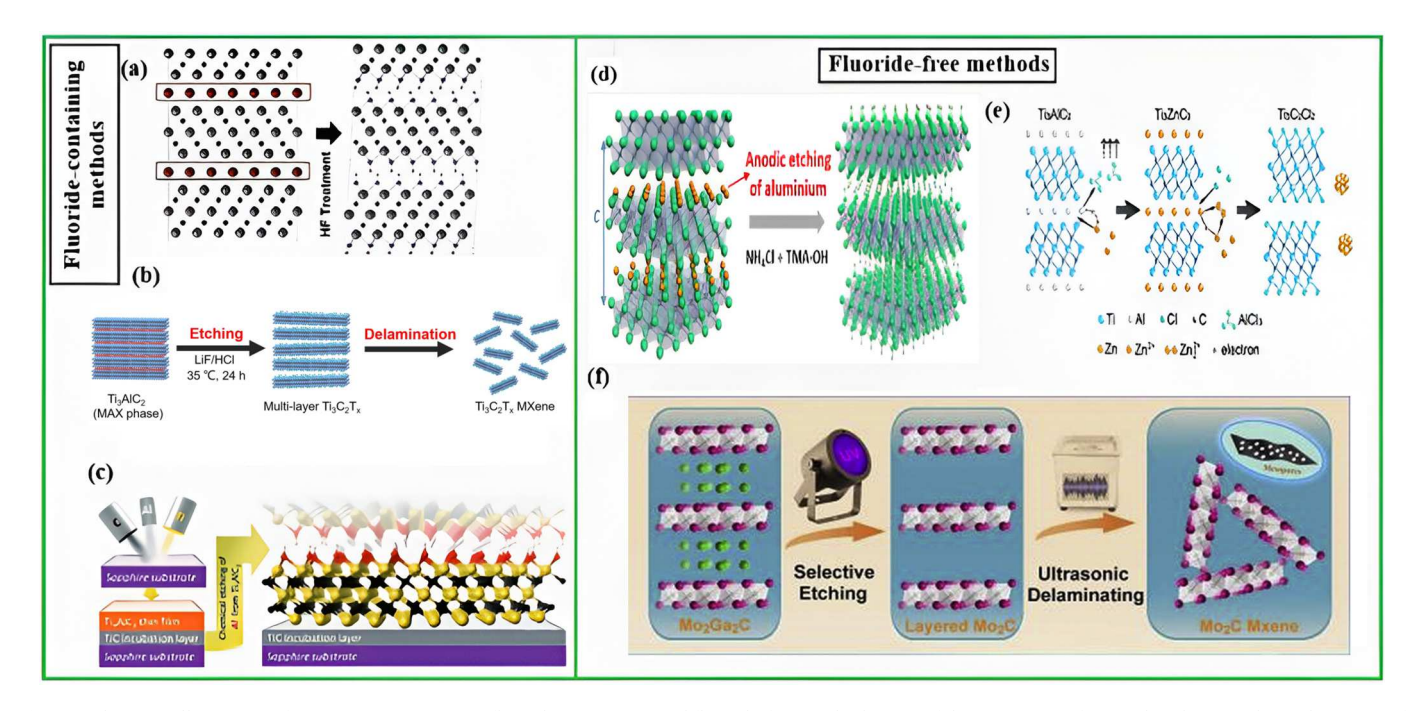


Fig. 2. Schematic illustration of MXene preparation via fluoride-containing and fluoride-free methods: (a) Exfoliation process for Ti_3AlC_2 showing the replacement of Al atoms by -OH after reaction with HF[26]. (b) MAX phase was etched in a solution of acid and fluoride salt and washed with water to adjust pH toward 4-6. The resulting sediment behaves like clay and can be rolled to produce flexible, freestanding films or molded and dried to yield conducting objects of the desired shape. HCl and milder LiF was used instead of aggressive HF. [41] (c) Schematic diagram of OH-terminated $Ti_3C_2T_x$ after selective etching of Al from the deposited Ti_3AlC_2 by bi-fluoride salts etching [42]. (d) Anodic etching of bulk Ti_3AlC_2 in a binary aqueous electrolyte [43]. (e) The replacement reaction between the MAX phase and late transition-metal halides generates Zn-based MAX phases and Cl-terminated MXenes [45]. (f) UV-induced selective etching route of removing the double Ga layers from Mo_2Ga_2C precursor to generate Mo_2CT_x [46].

(a) Reprinted with permission from [26]. (b) Reprinted with permission from [41]. (c) Reprinted with permission from ref [42]. (d) Reprinted with permission from ref [43]. (e) Reprinted with permission from ref [46].

hydrogen evolution reaction (HER) (Table 1), oxygen evolution reaction (OER), ORR, nitrogen reduction reaction (NRR), carbon dioxide reduction reaction (CO $_2$ RR), and alcohol oxidation reactions (AORs) (Section 2). Photocatalytically-driven reactions, including HER, CO $_2$ RR, NRR, and pollutant degradation reactions, are then considered (Section 3). Next, the use of MXene-based catalysts for other reactions, including hydrogenation and dehydrogenation, methanol (CH $_3$ OH) conversion, dry reforming of methane (DRM), and carbon monoxide (CO) oxidation are covered (Section 4). The article finally ends with a conclusion and perspectives on MXene-based heterogeneous catalysts.

Table 1Recent reports regarding the application of MXene-based materials for the electrocatalytic hydrogen evolution reaction.

| MXene | Electrolyte | Overpotential (mV) | Ref. |
|--|--|--------------------|------|
| $Nb_4C_3T_x$ | 1.0 M KOH | 398 | [55] |
| $Ti_3C_2T_xNF^as$ | 0.5 M H ₂ SO ₄ | 169 | [56] |
| MoS_2 - $Ti_3C_2T_x$ | 0.5 M H ₂ SO ₄ | 98 | [57] |
| Mo ₂ CT _x /2 H-MoS ₂ | 0.5 M H ₂ SO ₄ | 119 | [58] |
| MD ^b -Ti ₃ C ₂ T _x /MoS _x | $0.5 \text{ M H}_2\text{SO}_4$ | 196 | [59] |
| Pd/Nb ₂ C-HF | $0.5 \text{ M H}_2\text{SO}_4$ | 34 | [60] |
| $CoP/Ti_3C_2T_x$ | $0.5 \text{ M H}_2\text{SO}_4$ | 71 | [61] |
| Ti_2CT_x | 0.5 M H ₂ SO ₄ | 609 | [62] |
| Mo_2CT_x | 0.5 M H ₂ SO ₄ | 283 | [62] |
| $V_4C_3T_x$ | 0.5 M H ₂ SO ₄ | 200 | [63] |
| F-Ti ₂ CT _x | 0.5 M H ₂ SO ₄ | 170 | [64] |
| $Ti_3C_2O_x$ | $0.5 \text{ M H}_2\text{SO}_4$ | 190 | [65] |
| P-Mo ₂ CT _x | $0.5 \text{ M} \text{ H}_2\text{SO}_4$ | 186 | [66] |

a NF = nanofiber

2. Electrocatalysis reactions

MXene-based catalysts have been widely studied for electrocatalysis due to their good hydrophilicity, high electrical conductivity owing to lamellar spacing, large surface area, and tunable properties [67–69]. To boost the catalytic activity of MXenes and MXene-based catalysts, strategies including heteroatom doping, structural engineering of defects, interfaces, strain, lateral size, and thickness have been proposed and studied. Also, efforts have been made to tune surface functional groups of MXenes to increase the electrocatalytic reaction rate. For instance, the rates of HER and NRR can be enhanced by increasing the concentrations of O and F functional groups on the surface of MXenes, respectively [70, 71]. MXenes functional groups act as sites for the adsorption of various reactants, thus accelerating electrocatalytic reactions [72,73].

MXenes' electrocatalytic performance can also be boosted by incorporating them with transition metals, metal oxides, metal-free substrates, and other 2D materials because MXenes and these materials display synergic effects, improving the overall electrocatalytic efficiency [67,74,75]. In this section, we aim to describe the general trend and recent developments in electrocatalysis, including water splitting (HER and the OER), ORR, NRR, CO_2RR , and alcohol oxidization reaction (MOR).

2.1. Water splitting

Industrialization and global population growth have compelled societies to utilize massive levels of fossil fuels to meet their energy demands, which in turn have caused severe and alarming issues, most importantly air pollution [76]. Consequently, unprecedented attention has been paid to developing renewable and environmentally friendly energy sources [77]. During the past few years, some alternatives have been proposed, one of which is the water-splitting system, which

 $^{^{\}rm b}$ MD = modified

decomposes water directly into hydrogen and oxygen [78,79]. Water splitting progresses within two half-reactions: HER at the cathode and OER at the anode. However, the slow rates of HER and OER result in a slow overall water-splitting reaction, which is a roadblock in the production of hydrogen from water via electrocatalysis [80,81]. The widely known water-splitting electrocatalysts are Pt and Ru/Ir-based noblemetal oxides [82–84]. However, these catalysts are scarce in nature, are expensive, and have low stability, which has impeded their applications on large scales. So, finding and producing better electrocatalysts for water-splitting reactions have invariably been a challenge [85–87].

With the discovery of MXenes, the use of MXenes as electrocatalysts or platforms for other catalysts in the water-splitting reaction has been investigated. Due to their exceptional characteristics, MXene-based catalysts have proven efficient in water-splitting reactions. Conducting DFT calculations, Gouveia *et al.* studied water bonding and dissociation on a set of eighteen M_2X MXenes. They concluded that the MXenes can favorably adsorb water in an exothermic reaction, with adsorption energies ranging from 1.43 to -2.94 eV. Additionally, these catalysts can greatly facilitate water splitting with energy barriers below 0.44 eV [88]. As pointed out, water splitting consists of HER and OER, meaning its overall efficiency depends on the respective HER and OER [86]. So, in the following two sub-sections, we will elucidate the HER and OER performance of MXene-based catalysts and summarize recent advances in the use of MXenes as either electrocatalysts or supports.

2.1.1. Hydrogen evolution reaction

Renewable and sustainable energy sources are of primary importance as alternatives to fossil fuels [89]. Hydrogen is an attractive fuel, which can be generated via multifarious reactions known as hydrogen evolution reactions (HERs) [90–97].

In the past few years, several materials, such as noble metals, have been experimented on as catalysts for HER since they can facilitate the low overpotential and increase the rate of H₂-production reactions owing to the fact that these reactions are usually slow. Nonetheless, these metals lack high efficiency, limiting their applications in HER and other catalytically driven reactions associated with producing renewable substances on industrial scales [98–101]. MXenes have shown catalytic activity in HER, attributed to their exceptional structures and transition metals, which are inexpensive and earth-abundance [102]. The Gibbs free energy of atomic hydrogen adsorption describes the catalytic activity of MXenes in HER. The closer the Gibbs free energy to zero, the higher the activity of MXene catalysts [103]. In this respect, Gao calculated the HER catalytic performance of five oxygen-terminated MXenes, all of which showed a Gibbs free energy of near zero (Fig. 3) [71]. It should be noted that, according to the Sabatier principle, the

binding strength of hydrogen absorption on MXene catalysts should be "just right,"— meaning it should not be either too strong or too weak [104]. The HER is:

$$H^*\bigg(aq) + e^- {\to} \frac{1}{2} H_2(g) \eqno(1)$$

where H* is active hydrogen adsorbed on the catalyst surface [71]. It is worth mentioning that an acidic medium is better than an alkaline one for HER progression due to the fact that, in contrast to alkaline media, acidic media require lower overpotentials to begin the catalysis, which is imperative for HER initiation [105].

HER kinetics was found to involve two intermediate steps with three possible pathways, the Volmer, and the Heyrovsky or Tafel (Fig. 4). The first step of HER is called the Volmer reaction, in which a water molecule is adsorbed onto the catalyst surface (in an alkaline media). The second step depends on the concentration of active sites on the catalyst surface, meaning surfaces with low and high concentrations of active sites follow the Heyrovsky or Tafel pathway, respectively. Likewise, the same would happen in an acidic solution [106].

Employing Pourbaix diagrams, Meng and coworkers [107] investigated the effect of mixed surface terminations on the HER performance of MXenes. They considered nearly 450 topologically various surface terminations, encompassing $Ti_3C_2T_x$ with no terminations, full –O, -OH, -F, and –H terminations, and their different compositions. Based on realistic models derived from Pourbaix diagrams, they concluded that models close to HER equilibrium line, namely $O_{2/3}OH_{1/3}, F_{1/3}O_{1/3}OH_{1/3},$ and $F_{3/9}O_{4/9}OH_{2/9}$, demand a negligible overpotential of 0.01 V, showing their potential for use on the surfaces of MXenes for electrocatalytic HER.

Although the HER catalytic performance of MXene-based substances is typically satisfactory, efforts have been made to further boost their catalytic activity in HER. Some progress has been made in this regard, among which controlling surface functional groups [71,108,109], tailoring the structures [110–112], doping with other materials [113–115], and hybridization [102] have proved to be effective (Fig. 5). Recent research on MXenes and their nanocomposites for utilization in HER are summarized in Table 1.

2.1.2. Oxygen evolution reaction

Oxygen evolution reaction (OER) is a reaction by which oxygen molecules are generated through water electrolysis [117]. OER is conducted via two commonly plausible mechanisms, *i.e.*, adsorbate evolution reaction (AER) and lattice-oxygen mediated reaction (LOM) (Fig. 6) [118–121]. In the former, an alkaline medium is preferable over an acidic one since OER suffers from sluggish kinetics in acidic media [86].

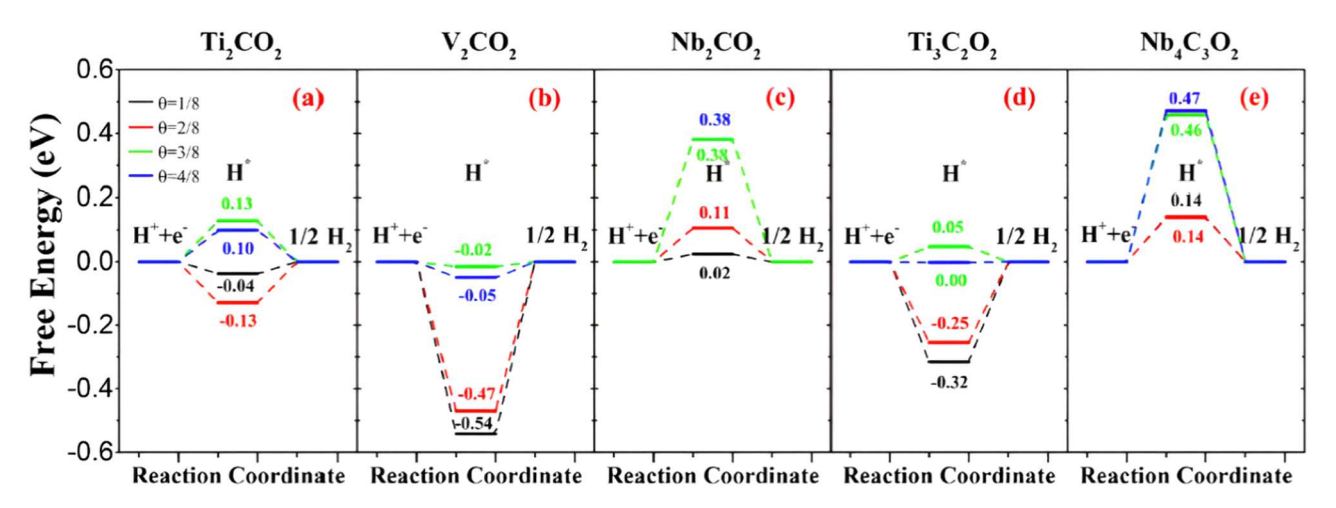


Fig. 3. Free energy diagram of HER on five MXenes (Ti_2CO_2 , V_2CO_2 , Nb_2CO_2 , $Ti_3C_2O_2$, and $Nb_4C_3O_2$) under standard conditions [pH = 0, p(H₂) = 1 bar, U = 0 V] vs. a standard hydrogen electrode. θ denotes the hydrogen coverage in H* adsorption. Reprinted with permission from [71].

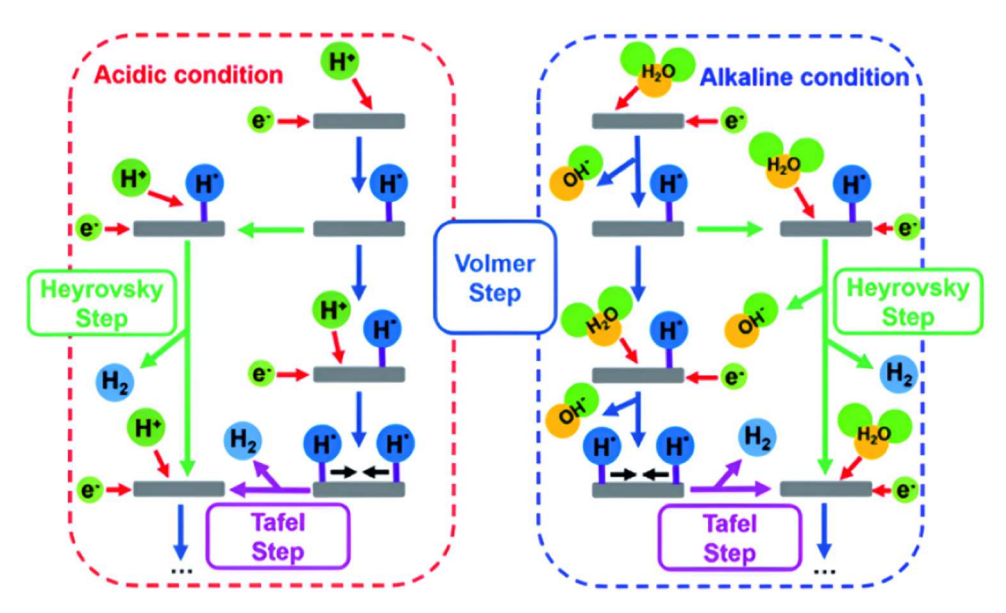


Fig. 4. HER mechanism in acidic and alkaline conditions with the Volmer (blue), Heyrovsky (green), and Tafel (purple) reaction steps. There are two well-defined pathways for HER: Volmer-Heyrovsky and Volmer-Tafel. In an alkaline condition, the reaction begins with the adsorption of a water molecule (Volmer step). If the catalyst surface contains low concentrations of active sites, the Heyrovsky step occurs where another water molecule is adsorbed, followed by OH^- and H_2 desorption. Otherwise, the Tafel step takes place where the desorption of H_2 is provoked by two active sites close to each other. The distance between the two active sites should not exceed the van der Waals radius of two adsorbed hydrogen atoms. Reprinted with permission from [106].

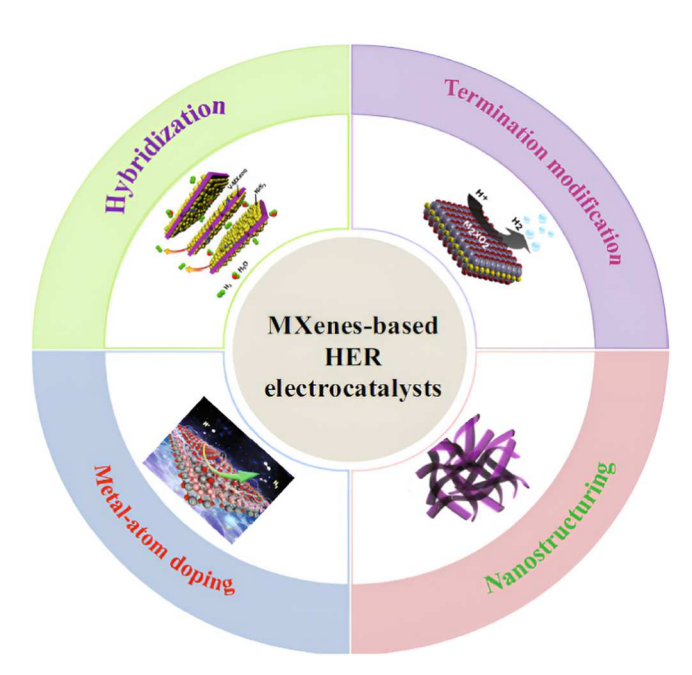


Fig. 5. Approaches for optimizing HER electrocatalytic performance of MXene-based materials. The optimization of MXene surface terminations positively affects the electronic structure and electron transfer (top right). The hybridization of MXenes with other active materials has been demonstrated to synergistically promote HER activity, such as chalcogenides, layered hydroxides, phosphides, metal nanoparticles/alloys, carbides, and even metal-free black phosphorus (top left). The doping of metal atoms can establish new active sites for the adsorption of hydrogen molecules to further drive HER (down left). Nanostructuring is another solution for improving MXenes' HER activity by accelerating the electrochemical response, creating more special electronic properties, and providing abundant active sites (down right). Reprinted with permission from [116].

It should be noted that although LOM is a potential pathway for OER, only a few investigations have assessed this mechanism so far [122,123].

Similar to HER, OER suffers from sluggish kinetics, so

electrocatalysts, such as Ru, Ir-based catalysts, metal oxides, metal sulfides, and metal phosphides, are imperative to boost the reaction rate [122,124-127]. However, the activities or stabilities of these catalysts usually deteriorate due to OER's harsh operating conditions and catalyst particles agglomerate, compelling the incorporation of support materials to immobilize catalyst particles [128]. Doing so prevents particle agglomeration and improves catalyst activity and stability, leading to the production of more efficient electrocatalysts for OER [129-132]. Due to their unique properties, MXenes seem to be paramount electrocatalyst supports for OER. For instance, Liu et al. [133] synthesized MXene-supported NiMn-LDHs through a simple hydrothermal pathway (Fig. 7). Aberration-corrected scanning transmission electron microscopy (Ac-STEM) confirmed the construction of 2D NiMn-LDHs and 2D Ti₃C₂T_x. The results demonstrated that although poor electrical conductivity of LDHs hampers their applications in OERs, their deposition on MXenes can substantially improve their overall performance in electrolysis. The reason for boosting the electrocatalytic performance is the coupling effect between the utilized MXene (Ti₃C₂T_r) and NiMn-LDHs, which effectively narrowed the bandgap of NiMn-LDHs and regulated their electronic structures, thus ameliorating the OER efficiency and reaction kinetics.

MXenes as catalyst supports should have several important properties. For example, they should prevent the catalysts from being agglomerated, ensuring high specific surface areas (SSAs) of the catalysts [134]. For example, Zhao et al. [75] synthesized a 2D porous ${\rm Ti}_3{\rm C}_2{\rm T}_x$ -supported cobalt 1,4-benzene dicarboxylate (CoBDC) catalyst as an effective OER catalysis. The outcomes showed that ${\rm Ti}_3{\rm C}_2{\rm T}_x$ could greatly enhance SSA (from 106.6 to 199.1 ${\rm m}^2{\rm g}^{-1}$) by preventing CoBDC particles from being agglomerated, exposing more nanocatalysts. In another research, Han and coworkers [135] investigated the effect of ${\rm CoS}_2$ introduction between ${\rm Ti}_3{\rm C}_2{\rm T}_x$ sheets. They concluded that not only can the MXene hinder the agglomeration of ${\rm CoS}_2$ particles, but also ${\rm CoS}_2$ prevents the restacking of the MXene nanosheets, improving the overall SSA (from 6.4 to 46.2 ${\rm m}^2{\rm g}^{-1}$). Hao et al. [136] fabricated a vertical array structure of CoFe-LDH on ${\rm Ti}_3{\rm C}_2{\rm T}_x$ support and discovered that the MXene could significantly enhance SSA.

Another pivotal characteristic that MXene supports should contain is the ability to improve electrical conductivity. It is evident that MXenes with the most efficient and optimal conductivity are promising options

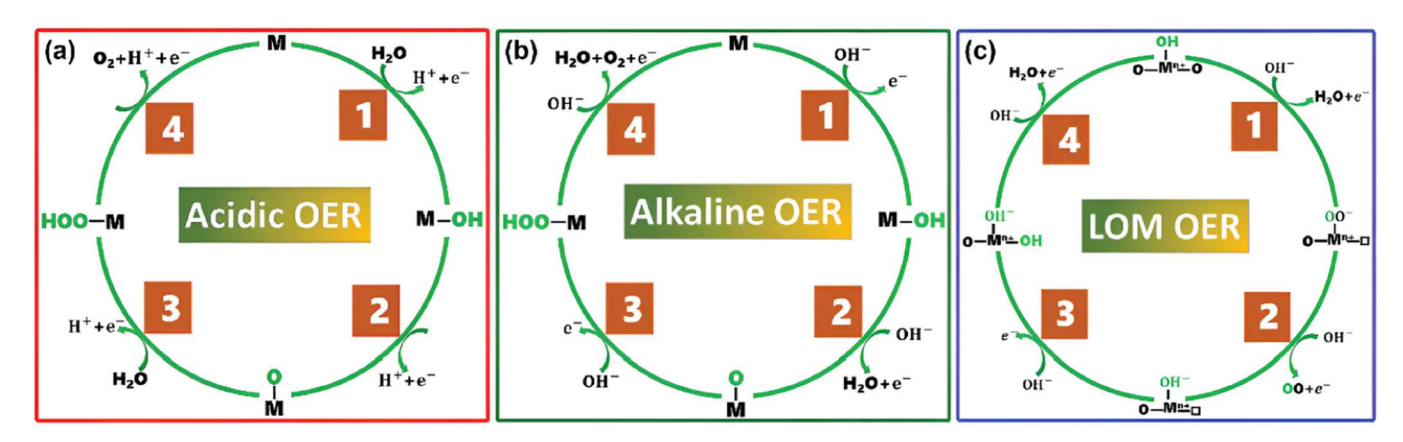


Fig. 6. Adsorbate evolution mechanism (AEM) of OER in an (a) acidic and (b) alkaline medium. (c) Lattice-oxygen mediated mechanism (LOM) of OER. M and □ denote an active site and an oxygen vacancy, respectively. The release of the lattice oxygen ligand from the catalyst is accompanied by the formation of oxygen vacancy, which is replenished and then acts as a new active center. Reprinted with permission from [117].

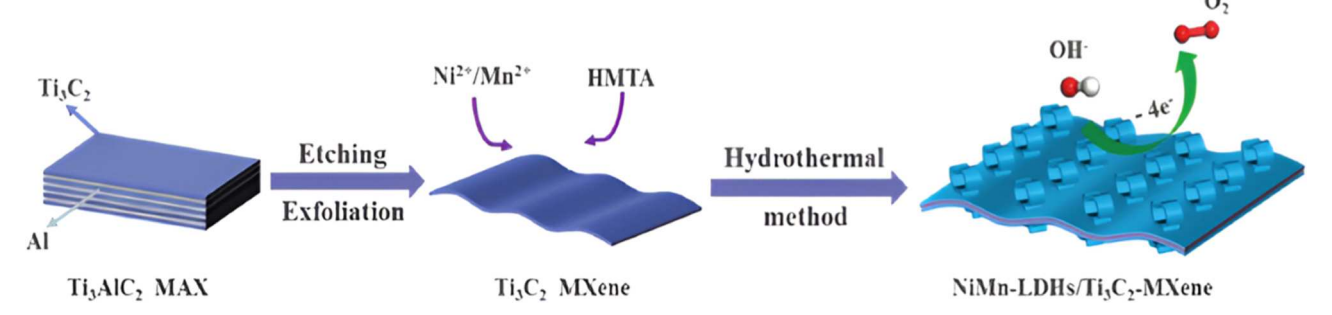


Fig. 7. An illustration of the hydrothermal method for NiMn-LDHs/Ti₃C₂T_x-MXene hybrids preparation. Reprinted with permission from [133].

as supports for OER catalysts owing to the fact that they can facilitate charge transfer across the catalysts [117]. For example, Yu and coworkers [137] reported that the addition of ${\rm Ti}_3{\rm C}_2{\rm T}_x$ to FeNi-LDH reduced the charge transfer resistances (Rct) of FeNi-LDH from 24.7 to 5.1 Ω . OER overpotentials associated with/without the harness of MXenes as supports for layered triple hydroxides (LTH) and LDH are summarized in Table 2. Metal-support solid interaction (SMSI) also plays a crucial role in boosting electron transfer from the catalyst to the MXene. The surface functionality of MXenes changes the electronic structure of catalysts, establishing strong interfacial interactions between catalysts and MXenes. As MXenes can attract electrons quickly, they can quickly transfer them to the supported catalyst [138].

Another attractive property of MXene-supported catalysts is their hydrophilic behavior, which benefits OER. This property is rooted in MXenes' abundant functional groups (F/O/OH/Cl), which can interact with water molecules. Recent research has concluded that MXene-catalyst compounds possess substantial hydrophilicity [117]. To illustrate, Si *et al.* [145] measured the contact angle (CA) of the

 $\label{eq:continuous} \textbf{Table 2} \\ \text{OER performance of LDH/LTH electrocatalysts with/without Ti}_3C_2T_x \, \text{support.}$

| Catalyst | OER overpotential [r | OER overpotential [mV] at 10 mA cm ⁻² | |
|--|--|--|-------|
| | -Without Ti ₃ C ₂ T _x | With Ti ₃ C ₂ T _x | |
| NiFe-LDH | - | 235 | [139] |
| Co ₄ MnFe ₃ -LTH | 370 | 263 | [140] |
| NiFeCe-LDH | 302 | 260 | [141] |
| RuCo-LDH | - | 330 | [142] |
| Co-LDH | 390 | 340 | [128] |
| NiMn-LDH | 356 | 294 | [133] |
| Cr-Fe-Ni-LDH | 280 | 232 | [143] |
| NiCo-LDH | 600 | 300 | [144] |

NiFe-LDH/Ti $_3$ C $_2$ T $_x$ /nickel foam (NF) compound. The outcomes showed that NiFe-LDH/Ti $_3$ C $_2$ T $_x$ /NF had a contact angle $\approx 0^o$ (Fig. 8a), demonstrating its hydrophilic behavior. On the contrary, the CA of NF and NiFe-LDH/NF were 119.7° (Fig. 8b) and 86.2° (Fig. 8c), respectively. Intense interactions between MXene and water molecules can result in more oxygen adsorption, eventually augmenting OER activity [146]. Furthermore, MXene supports can make electrolysis catalysts more chemically stable and corrosive resistant than those not deposited on MXenes [147]. It should be noted that C-containing MXenes are more chemically stable than those containing N atoms [147].

2.2. Oxygen reduction reaction

Oxygen reduction reaction (ORR) is one of the most vital processes in clean energy industries, specifically in fuel cells. ORR is feasible through two main, *i.e.*, the following four-electron and two-electron pathways [148], both of which can be progressed and accelerated by various kinds of catalysts [149]:

$$O_2 + 4H^+ + 4e^- \rightarrow 2H_2O$$
 (2)

$$O_2 + 2H^+ + 2e^- \rightarrow H_2O_2$$
 (3)

It is worth mentioning that a direct reaction between H_2 and O_2 can produce hydrogen peroxide (H_2O_2). Nevertheless, this reaction route has a high risk of explosion and lacks an appropriate level of selectivity owing to the dilution to reduce safety ventures [150,151].

Carbon-supported electrocatalysts utilized in ORR usually suffer from carrier corrosion, leading to the instability of catalysts [152–154]. In the past few years, several studies have been conducted on the corrosion resistance of MXenes as promising candidates in ORR. Having anti-corrosive properties, MXenes have been proven to prevent their

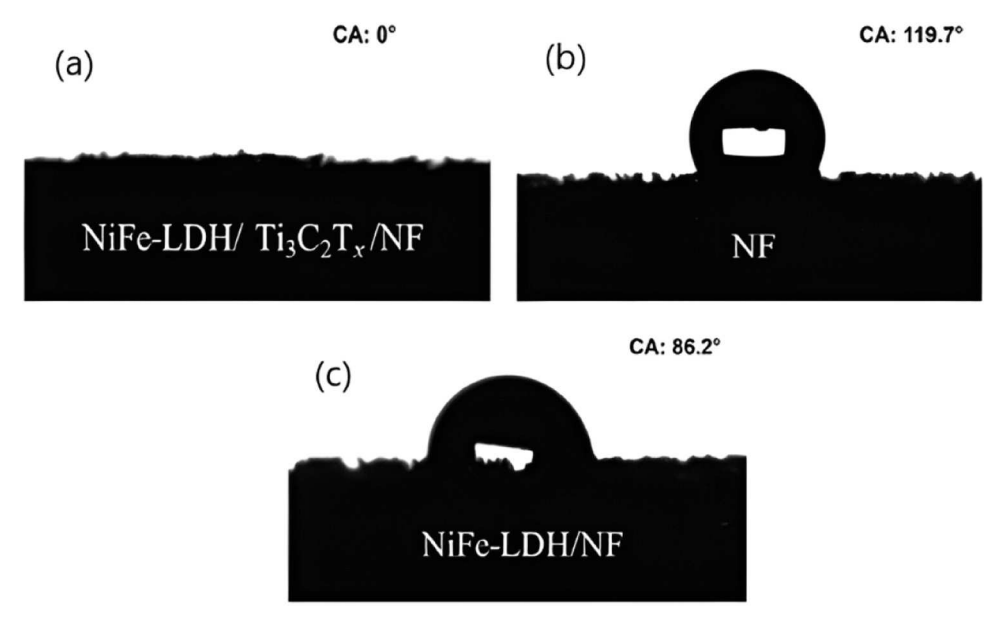


Fig. 8. The contact angle of (a) NiFe-LDH/Ti₃C₂T_x/NF, (b) NF, and (c) NiFe-LDH/NF electrodes. Reprinted with permission from [145].

supported catalysts from being unstable [155]. Moreover, MXenes can diminish the potential barrier for driving electrons across the catalysts and improve charge transfer, thereby making the catalytic activity more efficient [131]. Lastly, despite possessing favorable activity, Pt-based catalysts are not cost-effective and accessible, calling for less costly and more abundant catalysts like MXenes [156,157]. There have been several articles reviewing recent trends and developments in the field of MXene-based materials for ORR. For example, Lin and coworkers [158] assessed the ORR catalytic performance of 2D single-layered (SL) Ti₃C₂T_x nanosheets. They found that the ORR onset potential associated with SL Ti₃C₂T_x was much more than the reversible hydrogen electrode (RHE). Moreover, the charge transfer resistance of SL Ti₃C₂T_x on the electrode surface measured via electrochemical impedance spectroscopy (EIS) was found to be higher than those of multilayered (ML) Ti₃C₂T_x and Ti₃AlC₂, supporting the improved ORR catalytic activity of SL Ti₃C₂T_x. Furthermore, in the possession of their large surface area, 2D MXenes can adsorb many oxygen molecules to accelerate ORR.

Pt-based electrocatalysts are among the most paramount candidates in ORR. However, Pt is expensive and has low accessibility and relatively low stability. As a result, fabricating inexpensive, earth-abundant, and stable catalysts is desirable in clean energy industries [159]. Metal-nitrogen/carbon nanocomposites (M-N/C, which M stands for Fe, Co, Ni, and Cu) are among the most promising alternatives to Pt-based

catalysts for ORR due to their beneficial characteristics, including high nature-abundance, high efficiency, and low cost [160,161]. Despite these merits, the performance of M-N/C substances is unsatisfactory, necessitating the development of novel materials that meet the requirements for ORR [162].

In recent years, MXene supports for M-C/N in ORR have been investigated [163,164]. A case in point is a report by Chen et al. [165], who developed Ti₃C₂T_x-supported-non-precious-metal iron-cobalt (Fe-Co) nanoparticles. This study unraveled the role of ${\rm Ti_3O_2}$ as a hindrance to Co-Fe nanoparticles' agglomeration, resulting in higher catalytic performance owing to the higher exposed surface area. In another study, Zhang et al. [166] investigated the ORR and OER catalytic efficacy of nitrogen-doped multi-walled carbon nanotubes incorporated with Co (Co/N-CNTs) with a Ti₃C₂T_x support. The linear sweep voltammogram (LSV) curve (Fig. 9 a) suggests that (Co/N-CNTs) @Ti₃C₂T_x can outperform the catalyst lacking Ti₃C₂T_x due to its improved electron transfer characteristics. As the LSV curve demonstrates, the (Co/N-CNTs)@Ti₃C₂T_r composite possesses significantly enhanced ORR activity due to the synergetic effect between Co/N-CNTs and Ti₃C₂T_r MXene. Chen et al. [167] prepared cobalt-tipped carbon nanotubes integrated with Ti₃C₂T_x (Co-CNT/Ti₃C₂T_x), in which zeolitic imidazolate framework-67 (ZIF-67) nanoparticles were in-situ grown and exposed to a pyrolysis reaction. Their findings indicate that Co-CNT/Ti₃C₂T_x was

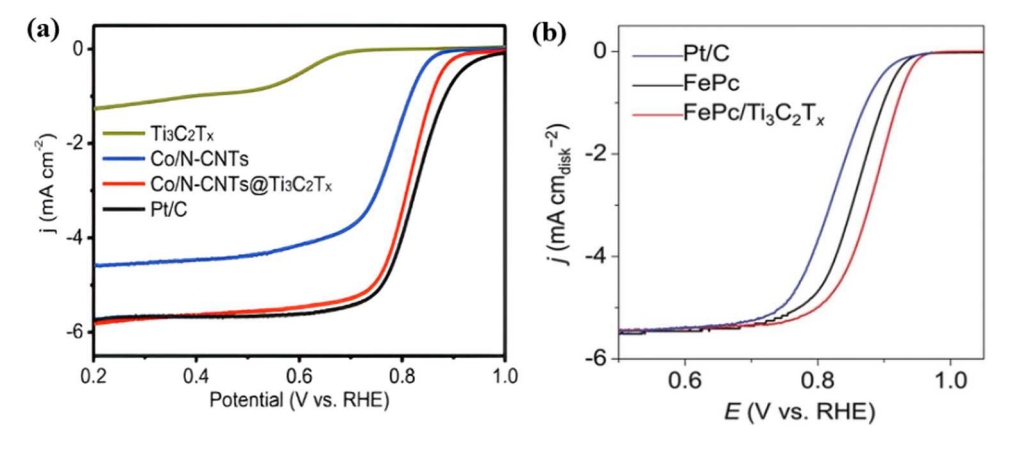


Fig. 9. LSV curves of (a) pristine $Ti_3C_2T_x$, CO/N-CNTs, CO/N-CNTs@ $Ti_3C_2T_x$, and the Pt/C benchmark, and (b) Pt/C, FePc, and FePc/ $Ti_3C_2T_x$. (a) Reprinted with permission from [166]. (b) reprinted with permission from [168].

highly active as an electrocatalyst for ORR. This enhancement was attributed to Co-CNT/Ti $_3$ C $_2$ T $_x$ high surface area, abundant Co-C/N site on the tips of CNTs, and virtually high graphitization of carbon. While Co-CNT/Ti $_3$ C $_2$ T $_x$ represented relatively analogous ORR activity, it had superior stability than Pt/C-based catalysts. In another study, Li *et al.* [168] investigated the ORR activity of a pristine iron phthalocyanine (FePc) catalyst (an early Fe–N–C prototype with typical FeN4 moiety and very Pt-like ORR activity) following the introduction of Ti $_3$ C $_2$ T $_x$ as a support. This coupling caused remarkable Fe 3d electron delocalization and spin configuration changes, which made the active FeC $_4$ sites more readily adsorb reaction species involved, therefore improving the ORR performance. Their LSV results (Fig. 9b) suggested a positive shift of \approx 26 mV compared to that of 0.86 V vs. RHE for pure FePc.

Several research studies have reported the utilization of MXeneassisted catalysts to accelerate OER and ORR. However, only a few studies have mentioned the potential instability of MXenes in oxidative environments of OER and ORR. For instance, Kuznetsov et al. [169] experimentally studied the substitution of Mo sites on Mo₂CT_x MXene by Fe single atoms (Mo₂CT_x:Fe) to verify increased stability and activity following the incorporation of Fe atoms. Characterization results unraveled the in-situ evolution of Mo₂CT_x:Fe to Fe oxyhydroxide (ferrihydrite, Fh) species distributed on a graphitic carbon framework (Fh/C), acting as the main active parts. As a result of the difference between the stability of Mo and Fe, Mo was selectively etched out of Mo₂CT_x, which led to the fabrication of graphitic carbon onto which Fh clusters were distributed, affirming poor stability of pure Mo₂CT_x in the oxidative situations of OER and ORR in basic conditions. Computational calculations have also been conducted to scrutinize the stability of MXenes under electrocatalytic reaction conditions [170]. Tsounis et al. [171] plotted the Pourbaix diagrams of Mo₂CO₂ and V₂CO₂ to assess the (in)stability window of these MXenes in electrochemical reactions, namely OER and ORR. They reported that these pristine MXenes (and possibly other counterparts) are stable at "negative" potentials and high pH. Therefore, Pourbaix diagrams highlight the effect of anodic potentials on the stability of MXenes. Furthermore, the largest window in which the oxidative decomposition of MXenes takes place is in solutions with high pH. As a result, caution must be taken when using MXenes at high pH and high anodic potentials, since the oxidative decomposition is still likely. Therefore, pristine MXenes are potentially appropriate as sole catalysts when used in reactions that occur at potentials near that of HER or lower (e.g., those of N2, CO2 and NO3 reduction); i.e., near or below 0 V vs. RHE, and at a low pH.

2.3. Nitrogen reduction reaction

N₂, as one of the most paramount components of the atmosphere, serves as a pivotal molecule for a sustainable and environmentally friendly pathway of producing ammonia (NH₃) [172]. From a common industrial point of view, NH₃ can be produced through a conventional reaction called the Harber-Bosch (HB) process, in which N₂ and H₂ are the correspondent feedstock, with metals being the reaction catalysts. Nonetheless, this process necessitates tremendous energy (a temperature above 350 °C and a pressure above 150 atm). Furthermore, the raw materials employed in the HB process are derived from petroleum, leading to their accumulation in the atmosphere and contributing to the generation of CO₂ [173]. Consequently, a renewable pathway of NH₃ generation has always been a preoccupation for researchers in the past few decades. In the natural process of NH3 synthesis, N2 and water undergo an electrocatalytic reaction under mild conditions, in which H2 molecules and electrons are derived from H2O and electricity sources, respectively [174]. However, this route results in low yield and selectivity of NH₃ [175]. In this regard, 2D materials have gained significant attention as alternatives to noble metal catalysts for efficient N2 fixation and then N₂ conversion to NH₃. This significance is owing to their large surface area and dispersed active sites that they potentially offer for N2 adsorption and activation [79].

MXenes, as the most promising 2D substances, have proven to be efficient for clean NRR due to their previously mentioned characteristics, for which some review papers have been published in the past few years [176]. From a computational viewpoint, Azofra and coworkers [177] investigated the NRR performance of MXenes. Utilizing DFT, they concluded that MXenes bring about a spontaneous Gibbs free binding energy for N₂ fixation and further activation. Wet-lab research has also been conducted along with computational ones to confirm the NRR efficacy of MXenes. For example, Zhao et al. [178] assessed 2D Ti₃C₂T_x (T = F, OH) MXene performance of NRR and attained an NH3 yield rate of $\approx 20.4 \ \mu g \bullet m g_{cat}^{-1} \bullet h^{-1}$. MXene-assisted NRRs proceed through three consecutive steps, namely adsorption and activation, hydrogenation, and desorption. The electrocatalytic-driven mechanisms associated with N₂ reduction to NH₃ fall into two generally accepted pathways of dissociative and associative routes, which differ in their hydrogenation order [179]. The dissociative pathway correlates to the cleavage of the N₂ triple bond in the adsorption stage, which requires an immense level of energy. Subsequently, each separated N atom goes through independent hydrogenation reactions, followed by desorption from the catalyst surface (Fig. 10a). The requisite harsh condition (high temperature and pressure) in the HB process is due to this mechanism (for breaking the N₂ triple bond). On the other hand, the associative takes place so that the N2 triple bond is not dissociated during adsorption but happens at a particular stage in hydrogenation. This pathway is divided into three distinctive sub-pathways called alternating, distal, and enzymatic (Fig. 10b) [180].

While there is no general rule for predicting the precise pathway by which NRR progresses, research studies have demonstrated that different MXenes follow different NRR mechanisms. For instance, Xia et al. [181] studied the NRR electrocatalytic performance of V₂CT_x. Via DFT calculations, they discovered that this MXene could result in the NH_3 rate of 12.6 μ g h^{-1} mg_{cat}^{-1} and Faradaic efficiency (FE) of 4% at -0.7 V in the M Na₂SO₄ media through a distal mechanism. Lastly, it is noteworthy that various parameters, including morphology [182], surface terminations [183], and incorporation of other materials [184–187], affect the electrocatalytic efficacy of MXenes. MXenes-doped with nanomaterials have also enhanced NRR electrocatalytic activity compared to pristine MXenes. In a case DFT study, Zheng and coworkers [188] incorporated Boron (B) sites as doping agents onto Mo₂CO₂ and W2CO2 MXene surfaces, resulting in a remarkably increased catalytic performance and improved selectivity in NRR. The modeled B-doped Mo₂CO₂ and W₂CO₂ MXenes showed limiting potentials of -0.20 and -0.24 V, respectively. Previous research results associated with the electrocatalytic NRR application of MXenes and MXene-based materials are summarized in Table 3.

2.4. Carbon dioxide reduction reaction

The greenhouse effect caused by industrialization has resulted in the accumulation of contaminant gases, on top of which is CO_2 . Therefore, researchers have been endeavoring to diminish the CO_2 level by integrating various methods, like recycling, energy recovery, biomass utilization, and carbon capture and utilization [194]. During the past few decades, some research has been conducted on the plausibility of CO_2 conversion into valuable substances through the electrolytic $\mathrm{CO}_2\mathrm{RR}$. Nonetheless, the effectiveness of this reaction strongly depends on developing potential and cutting-edge catalysts to ensure the long-run feasibility of $\mathrm{CO}_2\mathrm{RR}$ on industrial scales [195].

In the possession of exceptional properties mentioned in the previous paragraphs, 2D materials hold promise as potential catalysts for CO_2RR . MXenes are among those 2D electrocatalysts whose CO_2RR efficiency has been investigated within the past few years. Not many studies have been conducted on the CO_2RR performance of MXenes since their potential as heterogeneous catalysts is still in its infancy, so preliminary computational research on this topic was done by Li *et al.* [196]. In this study, they discovered that Cr_3C_2 and Mo_3C_2 MXenes are capable of

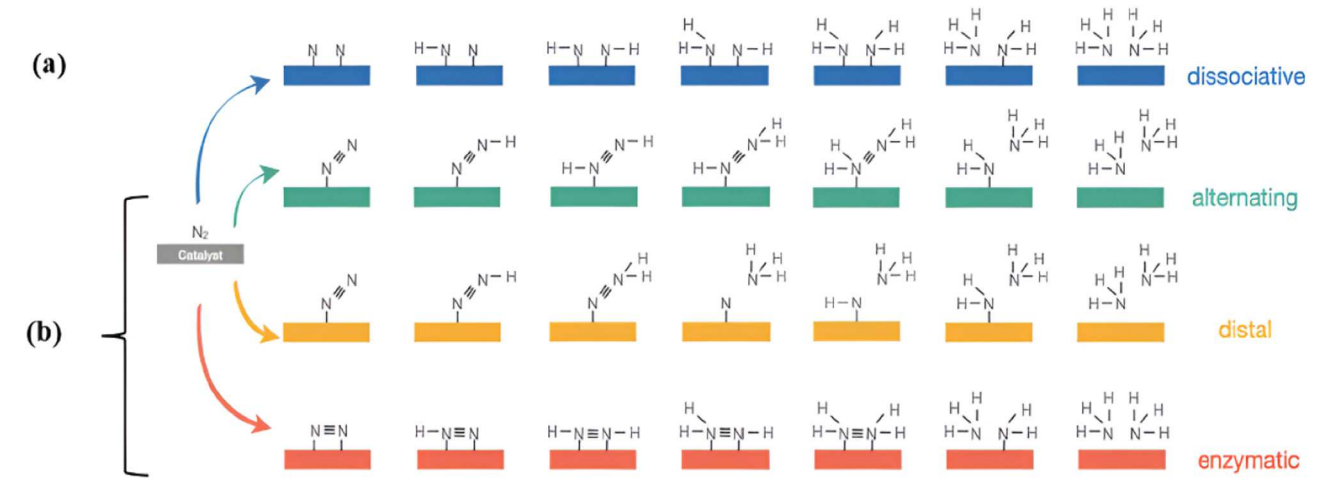


Fig. 10. Schematics of NRR on catalysts via (a) the dissociative and (b) associative pathways. Reprinted with permission from [180].

Table 3Recent research regarding the electrocatalytic ability of MXenes and MXenebased materials towards NRR.

| Catalyst | NH ₃ yield rate | FE (%), potential vs. RHE | N ₂ reduction mechanism | Ref |
|---|--|---------------------------------|---------------------------------------|-------|
| F-terminated Ti ₃ C ₂ T _x | 0.1 μmol•cm ⁻ ² •h ⁻¹ | 7.4% at -0.55 V | NR ^a | [189] |
| Cu/Ti ₃ C ₂ T _x | 3.04 µmol•cm ⁻ ² •h ⁻¹ | 7.31% at -0.5 V | Distal | [184] |
| $\text{Au/Ti}_3\text{C}_2\text{T}_x$ | 30.06 µg∙mg ⁻ ¹ _{cat} •h ⁻¹ | 18.34% at -0.2 V | Alternating | [190] |
| Surface- engineered $Ti_3C_2T_x$ | 1.71 µg•cm ⁻² •h ⁻¹ | 7.01% at -0.2 V | Alternating | [191] |
| $Ti_3C_2T_x$ (T= F, OH) | 20.4 μg•mg ⁻ 1 _{cat} •h ⁻¹ | 9.3% at -0.4 V | Distal | [178] |
| Ru@ Ti ₃ C ₂ T _x | 2.3 μmol•cm ⁻ ² •h ⁻¹ | 13.13% at -0.4 V | Distal | [192] |
| V_2CT_x | 12.6 μg•mg ⁻ ¹ _{cat} •h ⁻¹ | 4% at -0.7 V | Distal | [181] |
| N-S-doped $Ti_3C_2T_x$ | 34.23 μg•mg ⁻¹ cat•h ⁻¹ | 6.6% at -0.55 V | NR ^a | [193] |

 $^{^{\}rm a}$ NR = Not reported

converting CO2 to CH4, which is a vital energy-generating gas in industries. Other theoretical investigations have also been concentrated on employing MXenes to produce CH₄ [197]. Conversely, in 2020, Handoko et al. [198] embarked on an experimental study to explore titanium and molybdenum carbide MXenes for CO2RR in an effort to expand horizons in the emerging field of MXenes. Unlike preceding computational research in which CH₄ was the predominant CO₂RR product, this study discovered formic acid as the dominant product, with an FE of 56.1% for KF-HCl-etched Ti₂CT_x. It is important to note that the synthesis route of MXenes and CO2RR experimental conditions can affect the type of reaction products. In another case, Attanayake and coworkers [199] studied the CO₂RR potential of Mo_2CT_x and $Ti_3C_2T_{\chi^{--}}$ based MXenes in an acetonitrile-based electrolyte mixture with 1-ethyl-3-methylimidazolium tetrafluoroborate. They found CO to be the primary product of this reaction, with an FE of 90% and 65% for Mo₂CT_x and Ti₃C₂T_x, respectively. Meng et al. [200] reviewed the recent advances in DFT calculations on the CO2RR efficacy of MXenes. They divided models into three generations. The first generation of models (2017-2018) revealed the potential application and high activity of clean MXenes in CO2 adsorption, even in harsh operational situations, with a maximum CO₂ capture capacity of 8.25 mol.kg⁻¹. These theoretical findings were later validated experimentally, paving the way for the employment of MXene materials as electrocatalysts in $\rm CO_2RR$. However, these models suffered from oversimplification and overlooked the effects of surface terminations. The second generation of models (2018–2020) studied the effects of surface terminations, such as $\rm -O$, $\rm -OH$, $\rm -S$, and $\rm -F$, on $\rm CO_2$ and other intermediates binding energies. Different intermediates may react with surface groups via the H, C, or O atoms. Nevertheless, interaction with H atoms of the $\rm -OH$ -containing terminations may either simplify proton-couples electron transfers or lead to the stability of intermediates by as-generated surface $\rm -O$ group after $\rm -H$ removal from $\rm -OH$. The third generation of models (2020–present) revealed the significant role of vacancies in modifying intermediate binding energies. They also showed that the vacancies have more paramount influences on the reduction of $\rm H^+$ than the binding of $\rm CO_2$ during the process.

Various techniques have been exploited to tune the activity and selectivity of MXene-based catalysts in CO2RR, such as controlling surface vacancies [201], doping [202], and incorporating multiple components into MXenes [203]. Concerning metal-doped MXenes, Eid et al. [201] investigated the CO₂RR performance of Cu/Ti₃C₂T_x MXene. They found that the Cu/Ti₃C₂T_x catalyst outperformed pristine Ti₃C₂T_x, with a formic acid FE of 58.1% in $Cu/Ti_3C_2T_x$ and $\sim 18.7\%$ in $Ti_3C_2T_x$, respectively (Fig. 11a). In another DFT study, Cheng et al. [204] assessed the CO2RR efficiency of pristine Nb2CO2 and nonmetallic and metallic-doped Nb₂CO₂ (N- and Cu-doped Nb₂CO₂). Their results indicated that N- and Cu-doped specimens possessed lower reaction Gibbs free energy than pure Nb₂CO₂ (Fig. 11(b-d)), demonstrating higher activity towards CO2RR. Kannan et al. [205] also investigated the effect of iron-doped-zinc oxide (ZnO-Fe) on the Ti₃C₂T_x-based electrochemical reduction (eCR) of CO₂. They found the current density of ZnO, Ti₃C₂T_x, ZnO-Fe, ZnO- $Ti_3C_2T_x$, and ZnO-Fe- $Ti_3C_2T_x$ to be 3.439, 6.64, 7.13, 10.21, and 18.745 mA/cm², respectively, under an applied potential of 0.2 V, thus indicating the high activity of ZnO-Fe-Ti₃C₂T_x towards CO2RR.

2.5. Methanol and ethanol oxidization reactions

Direct alcohol fuel cells (DAFCs) have attracted interest in generating electricity from commonly known alcohols, *i.e.*, CH_3OH and ethanol (C_2H_6O) , as they have advantages such as convenient energy transformation, low noise, and high efficiency [14]. In the past few years, Pt-based catalysts supported by carbon have been widely used as potential electrocatalysts in DAFC processes [206,207]. Nonetheless, there are several bottlenecks with Pt, including its high cost, alcohol crossover, long-run instability, and CO poisoning [208]. Furthermore, some carbon supports used to immobilize Pt-based catalysts usually suffer from corrosion-induced degradation and low graphitization. Therefore,

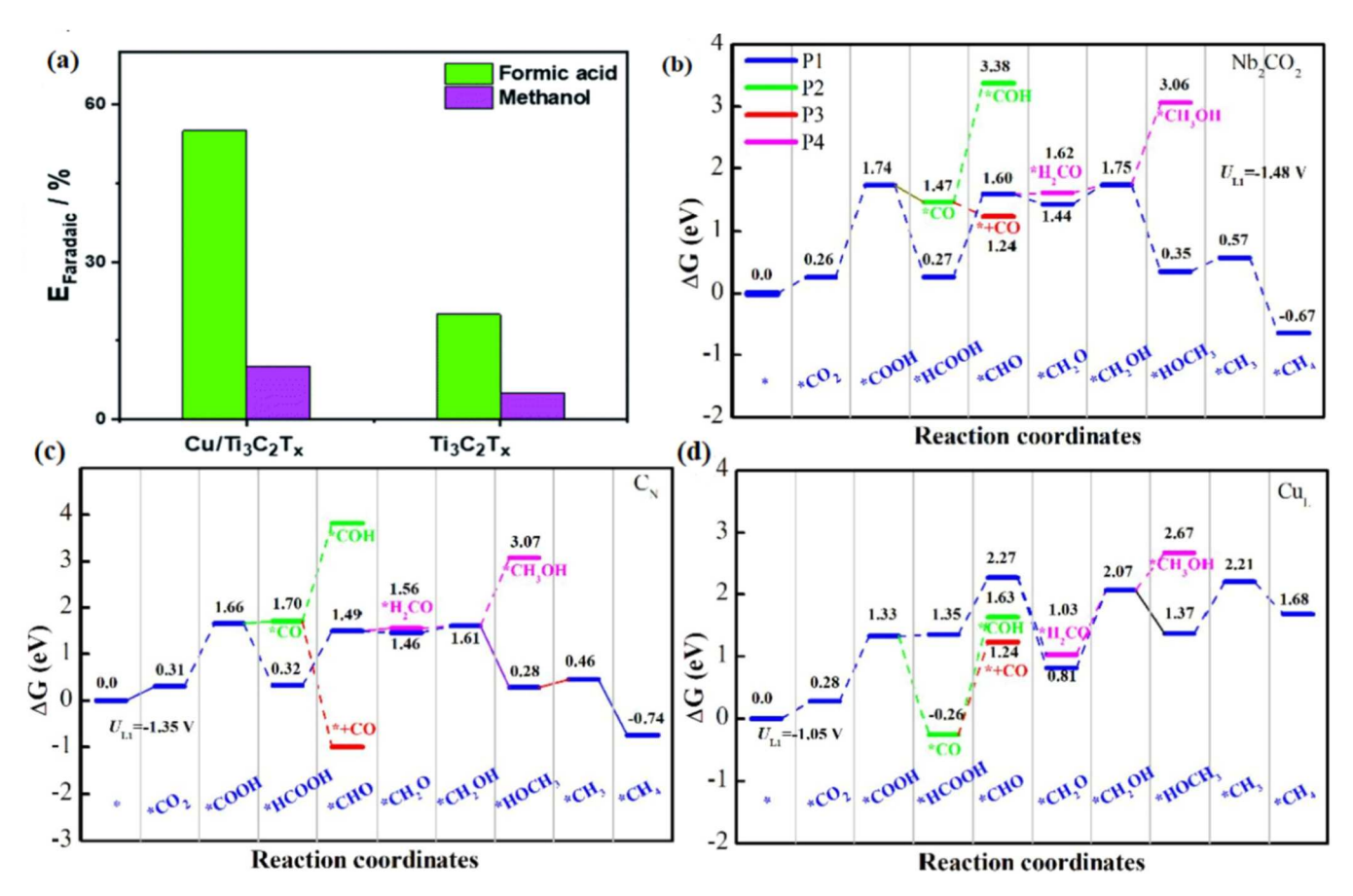


Fig. 11. (a) Comparison of the FE products between pristine $Ti_3C_2T_x$ and Cu-doped- $Ti_3C_2T_x$. (b) Reaction Gibbs free energy plots of CO_2RR on (b) pure Nb_2CO_2 , (c) N-doped- Nb_2CO_2 , and (d) Cu-doped- Nb_2CO_2 surfaces. Note that P1, P2, P3, and P4 illustrate different pathways of CO_2RR on Nb_2CO_2 -based catalysts, corresponding to different Gibbs free energies.

(a) Reprinted with permission from [201]. (b) B-d: Reprinted with permission from [204].

efforts have been made to harness carbon supports with superior characteristics beneficial to DAFC or develop strategies to mitigate their corrosion. For example, Zhao et al. [209] investigated different methods to reduce carbon corrosion. However, they discovered that carbon corrosion and degradation remain significant challenges despite these corrosion diminishment strategies. Considering these challenges, researchers have fabricated low-carbon or free-carbon supports, such as metal dioxides (TiO2, IrO2, WO3, and SnO2) [210], nitrates, and carbides (SiC, TiC, and B₄C) [211]. Apart from these materials, MXenes have also gained particular interest because of their well-defined characteristics. DFT calculations showed that MXene supports, specifically Ti-based ones, can establish favorable adsorption energy for depositing necessary noble metals and other catalysts [212,213]. Experimental investigations revealed that Ti-based MXenes are highly efficient for MOR and that Ti₃C₂T_x MXene enriched Ti-O terminals exhibit a high electrical conductivity and a large specific area, leading to improved electrochemical performance in MOR. The prepared specimen demonstrated an onset potential of -0.51 V, with long-term stability and durability toward MOR [214].

To date, several review articles have represented the potential of harnessing metal and non-metal-supported MXenes. However, as mentioned in the previously elucidated paragraphs, the utilization of MXenes in catalytic reactions is still at the nascent stage [79,215–218]. As a result, in this paper, we review some of the most novel updates on MXenes MOR and EOR performance, whose valuable outcomes have been represented in Table 4. As pointed out, Pt is among the widely used electrocatalysts for MOR and EOR purposes. However, due to the issues mentioned at the beginning of this section, they should be immobilized into 2D substances to ensure their stability and durability. MXenes have

been shown to hold promises as support for Pt and many other catalysts. A few studies have focused on MXenes-supported Pt, the first of which conducted by Wang *et al.* [219] reported a peak current density for Pt/Ti $_3$ C $_2$ T $_x$ three times higher than a conventional carbon-supported Pt (Fig. 12a and b), indicating that Pt/Ti $_3$ C $_2$ T $_x$ is a promising candidate for MOR. Furthermore, transmission electron microscopy (TEM) and high-resolution transmission electron microscopy (HRTEM) analyses illustrated that Pt nanoparticles were successfully deposited and distributed on the Ti $_3$ C $_2$ T $_x$ surface, guaranteeing a high surface area for adsorption and activation (Fig. 12c and d). In terms of stability of the Ti $_3$ C $_2$ T $_x$ support, the calculated electrochemical surface area (ECSA) Pt/Ti $_3$ C $_2$ T $_x$ was $_3$ 0.2 m $_2$ /g, and it lost only 15% of its surface electrochemical stability toward Pt immobilization. In contrast, the correspondent loss was 47% for Pt/C.

2.6. Nitrate reduction reaction

With the rapid discharge of industrial wastewater, a vast amount of nitrate (NO $_3$) enters water grounds, calling for urgent actions to remove them to provide global populations with drinking water and prevent individuals from getting fatal diseases such as liver cancer and gastric cancer [230–233]. Currently, two leading technologies exist for the removal of NO $_3$ from water: reverse osmosis and biological denitrification. However, the former suffers from high expenses and the latter from creating byproducts caused by the metabolism of microorganisms, leading to secondary pollution to the water body [234,235].

Electrocatalytic nitrate reduction has garnered substantial interest in converting NO_3^- into harmless substances, including N_2 and NH_3 , as industrial raw materials, which demands low energy consumption and

Table 4Recent studies on the electrochemical performance of MXene support for MOR/FOR

| Catalyst | ECSA (m ² /g) | Specific activity (mA cm ⁻²) | Methanol oxidation peak current (mA cm ⁻²) | Stability (Retention rate) | Ref |
|---|-----------------------------|--|---|---|----------------|
| Ni(3%wt) MoS ₂ / Ti ₃ C ₂ T _r | 1.17 ^a | NR ^b | 7.7 | 78.4%/ 500 cycles | [220] |
| $Pt/Ti_3C_2T_x$ | 30.2 | NR ^b | 1.137 | 85%/ 1000 cycles | [219] |
| $Pd/Ti_3C_2T_{x^-}$ rGO (1:1) | 97.97 | 25.47 | NR ^b | NR ^a | [221] |
| Pt/(RGO) ₃ - $Ti_3C_2T_x$ | 90.1 | NR ^b | NR ^b | 24.4%/ 1000 cycles | [222] |
| Pd/Ti ₃ C ₂ T _x @NG° | 34.5 | 6.56 | NR ^b | 31.4%/ 500 cycles | [223] |
| NiCu-LDH/ $Ti_3C_2T_x$ (45%wt) | 7.625 ^a | 11.39 | 86.9 | 77.8%/ 500 cycles | [224] |
| Pt NW ^d / PDDA ^e - Ti ₃ C ₂ T _r | 61 | NR ^b | 17.2 | NR ^b | [225] |
| $Pt_{69}Rh_8Fe_{23}$ $PNS^f@$ $Ti_3C_2T_x$ | 46.4 | NR ^b | NR ^b | 72.8%/ 1000 cycles | [226] |
| Pt-on-Pd/ $Ti_3C_2T_x$ | 157.3 | 0.93 | NR ^b | 62.9%/ 200 cycles | [227] |
| PtRu/Ti ₃ C ₂ T _x Pd/GO ₅ - Ti ₃ C ₂ T _x -PS | 54.91 89.9 | NR ^b NR ^b | 22.9 NR ^b | NR ^a 55.4%/ 800 cycles | [228] [229] |

 $a = unit: cm^2$

diminished environmental pollution [236]. Nonetheless, owing to the lack of high selectivity for nitrate reduction reaction (NITRR) to NH $_3$, harnessing electrocatalysts is vital to ensure the long-term feasibility of this reaction on industrial scales [237]. Moreover, one of the challenges in NITRR is the competence with HER and the production of byproducts like H $_2$, which decreases the efficiency of this reaction [238].

Given the extraordinary characteristics mentioned in the previous sections, 2D MXenes have attracted attention in NITRR [239]. For instance, Hu et al. [240] assessed the potential use of MXenes as electrocatalysts in NITRR (converting NO₃ to NH₃) via DTF calculations. They concluded that MXenes could drive NITRR through their basal planes, where NO₃ was readily deoxygenated, while the subsequent hydrogenation was challenging. Combining MXenes and NITRR bimetallic catalysts, such as Fe-Mo [241], Cu-Rh [242], and Cu-Fe [243], can improve charge transfer and exposure of active sites, thus increasing overall catalytic performance. In another research, Zhang et al. [244] incorporated highly dispersed Bi₂O₃ electrocatalyst on Ti₃C₂T_x nanosheets, in which oxygen vacancies facilitated electron transfer and exposed more active sites. Meanwhile, Bi₂O₃ inhibited HER, further boosting the overall NITRR efficiency (NH $_3$ yield rate of \sim 7.0 mg•cm⁻²•h⁻¹). Nevertheless, these catalysts might lose their stability on the surface of MXenes due to the insufficiency of MXene surface functional groups (-F, -OH, etc.), which necessitates the application of negatively charged surface functional groups of MXenes to establish robust interactions with cationic metals, or the solid interfacial polarization of MXenes to catalyze the breaking of N-O bonds [245-247]. Additionally, MXenes themselves suffer from issues such as collapsing, causing decreased electron transfers and catalytic performance. This shortcoming can be partially addressed though adjusting the interfacial states, functional groups, and defect states, utilizing confinement effects to load single atoms, constructing heterogeneous structures, and creating interfacial polarization [245].

3. Photocatalysis reactions

Photo-induced reactions (harnessing sunlight) hold promise as alternative routes to developing and producing clean energies [248]. More specifically, photocatalytic reactions are crucial in water splitting, CO_2RR , NRR, and pollutant degradation. MXenes are promising candidates for this purpose owing to their superior properties over other catalysts [54,249–251]. This section describes different MXenes photocatalytic applications in the pertinent reactions, including water splitting, CO_2RR , NRR, and pollutant degradation.

3.1. Water splitting

There are various technologies for hydrogen and oxygen clean production, among which the water splitting innovation offers more benefits such as inexpensiveness, convenience, and being environmentally friendly [252]. A photo-driven water splitting reaction follows these three preliminary steps: 1) light absorption by the semiconductor photocatalyst and generation of photogenerated charge carriers, meaning electrons (e') and holes (h⁺), 2) migration of electrons and holes from the bulk to the surface of the photocatalyst, and 3) the contribution of electrons and holes to the redox reactions directed into $\rm H_2$ and $\rm O_2$ generation [253]. Unlike computational research investigating the "excited states," namely excitons of traditional photocatalysts like rutile $\rm TiO_2$ (110), the assessment of MXenes for their photocatalytic activity is often based on their band gap size and alignment [254–256]. This section describes recent investigations and advances in the area of $\rm H_2$ generation using MXene photocatalytic HER.

3.1.1. Hydrogen evolution reaction

Hydrogen is the primary molecule for the production of ammonia and a vital substance in petrochemical industries. However, there are some challenges with its production by conventional methods like exploiting fossil fuels. The water-splitting reaction has shown promise in H_2 generation to meet global demands. This reaction occurs in the presence of a semiconductor photocatalyst and sunlight illumination, proceeding a reaction independent of hazardous fossil fuels. The reaction mechanism is the same as described previously, *i.e.*, Volmer—Tafel or Volmer—Heyrovsky pathways [257]. Nonetheless, photocatalytic water splitting lacks high efficiency on industrial scales. Therefore, efforts have been made to enhance the reaction performance using cocatalysts [253,258]. Cocatalysts extract charge carriers from the correspondent photocatalyst surface and hinder their recombination, improving HER rate and yield [259].

MXenes have attracted prominent attraction as HER cocatalysts owing to their high electrical conductivity, which is beneficial to electron transport to the surface of the photocatalysts [71]. DFT calculations have proven MXenes' co-catalytic performance. For instance, Ran and coworkers [260] investigated the co-catalytic activity of $\rm Ti_3C_2O_2$ MXene deposited on a CdS photo-absorber. They discovered that the $\Delta G_{\rm H^{\prime}}$ of this MXene was close to zero at ½ H* coverage (Fig. 13a), thus boosting the HER performance compared to traditional catalysts, namely Pt, MoS₂, and WS₂ (Fig. 13b).

MXenes can also be employed as direct HER photocatalysts with suitable valence band (VB) and conduction band (CB) potentials [85]. To illustrate, $\mathrm{Ti}_3\mathrm{C}_2\mathrm{T}_x$ MXene is applicable as an HER photocatalyst since it offers advantages like a hydrophilic surface and a Gibbs-free adsorption energy close to zero [261]. Using DFT calculations, Ontiveros *et al.* studied the bandgap of a wide array of MXenes by their structure, composition, and oxygen surface termination to determine appropriate MXenes for photocatalytic water splitting. Their study indicated that C-MXenes possessed more cases with bandgap favorable for water splitting compared to N counterparts. Moreover, the effects of factors such as stacking and specific oxygen-termination hollow sites were

 $^{^{\}rm b}$ NR = Not reported

^c NG = nitrogen-doped grapheme

 $^{^{\}rm d}$ NW = worm-shaped nanocrystals

^e PDDA = poly(diallyldimethyl-ammonium chloride)

f PNS = porous ternary nanosphere.

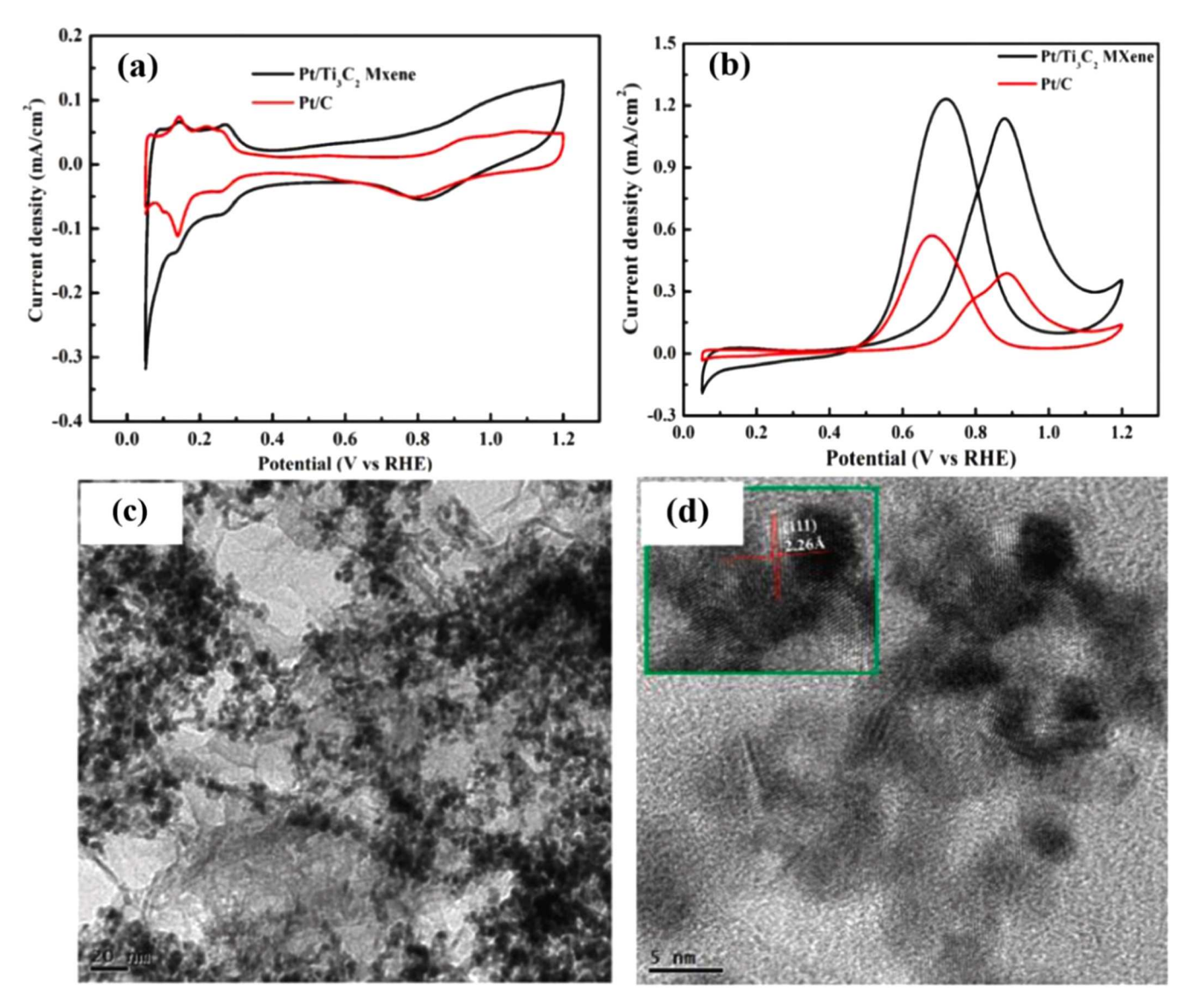


Fig. 12. (a) Cyclic voltammogram (CV) curves of $Pt/Ti_3C_2T_x$ MXene and commercial Pt/C in N_2 -saturated 0.5 M H_2SO_4 solution, (b) CV curves of MOR on $Pt/Ti_3C_2T_x$ MXene and commercial Pt/C in 0.5 M $H_2SO_4 + 0.5$ M CH_3OH solution at a scan rate of 50 mV/s, (c) TEM, and (d) HRTEM of $Pt/Ti_3C_2T_x$ MXene surface. Reprinted with permission from [219].

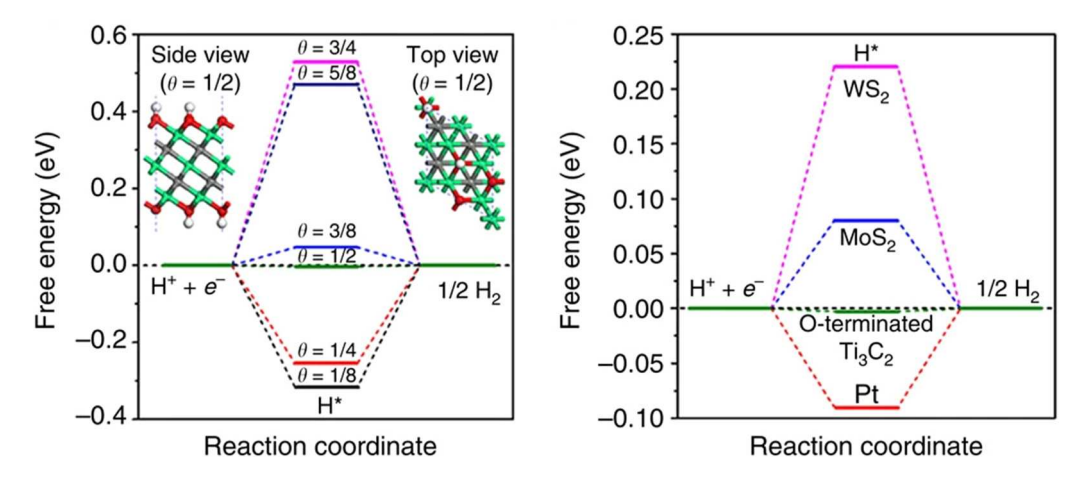


Fig. 13. Calculated free energy for HER, for (a) $Ti_3C_2T_x$ at various H^* coverage (1/8, 1/4, 3/8, 1/2, 5/8 and 3/4) and (b) Pt, Mo_2 , and WS_2 at $\frac{1}{2}$ H^* coverage. Reprinted with permission from [260].

found to be irregular and circumstantial. DFT calculations demonstrated that for all possible cases with a bandgap larger than 1.23 eV, the minimum required in order for the water-splitting reaction to occur, $\rm Zr_2CO_2$ was a promising photocatalyst candidate in water splitting [256].

Utilizing *ab initio* calculations, Guo and coworkers assessed 48 MXenes to unravel their photocatalytic properties. Their outcomes revealed that $2D \, Zr_2CO_2$ and Hf_2CO_2 , whose band gaps and band edges positions substantially met initial requirements for photocatalytic water splitting, possess incredibly high and directionally anisotropic carrier mobility, meaning that they likely facilitate the migration and

separation of photo-generated e'-h⁺ pairs. Regarding sunlight absorption, these two MXenes were proved to be effective in optical absorption in the wavelength ranging from 300 to 500 nm. Additionally, these 2D MXenes were potentially stable in a liquid water medium based on *ab initio* molecular dynamic simulations. Eventually, the absorption and decomposition of a water molecule and the formation process of H_2 on concerned MXenes were investigated, which demonstrated to be energetically feasible [85].

The results associated with other research are presented in Table 5, which opens up a novel trend into developing MXene-based HER catalysts or cocatalysts in water-splitting applications.

Table 5
Recent research associated with the development of MXenes as cocatalysts in photocatalytic HER.

| MXene cocatalyst | Final catalyst | Sacrificial agent | H_2 production (µmol $h^{-1}g^{-1}$) | Activity improvement following MXene cocatalyst addition | Ref |
|---|---|--|---|--|-------|
| Ti ₃ C ₂ T _x - monolayer nanosheets | $CdLa_2S_4/Ti_3C_2T_x$ | 0.25 M Na ₂ SO ₃ , 0.35 M Na ₂ S | 11182.4 | 13.4 times | [262] |
| | $TiO_2/$ $Ti_3C_2T_x$ | 25% methanol | 17.8 | 4 times | [263] |
| | g- $C_3N_4^a/Ti_3C_2T_x$ / TiO_2 | 10% triethanolamine | 1620.0 | 2.41 times (compared to g-C ₃ N ₄) | [264] |
| | $g-C_3N_4/Ti_3C_2T_x$ | 10% triethanolamine | 72.3 | 10.18 times | [265] |
| | CdS/Ti ₃ C ₂ T _x | 10% lactic acid | 2407.0 | 6.68 times | [266] |
| | P-doped tubular g-C ₃ N ₄ /Ti ₃ C ₂ T _x | 20% methanol | 565.0 | 3.07 times | [267] |
| | heptazine-based g-C ₃ N ₄ /Ti ₃ C ₂ T _x | 10% triethanolamine | 4225.0 | 1.84 times | [268] |
| | $\text{CuS/Ti}_3\text{C}_2\text{T}_x$ | $0.25 \text{ M Na}_2\text{SO}_3,$ $0.35 \text{ M Na}_2\text{S}$ | 4.2 | 1.42 times | [269] |
| | Black phosphorus/ultrathin g-C ₃ N ₄ / Ti ₃ C ₂ T _x | 10% triethanolamine | 18420.0 | 19.4 times | [270] |
| | Protonated g-C ₃ N ₄ / Ti ₃ C ₂ T _x / hollow spheres | 10% triethanolamine | 982.8 | 3.5 times | [271] |
| MXene cocatalyst | Final catalyst | Sacrificial agent | H_2 production (µmol $h^{-1}g^{-1}$) | Activity improvement following MXene cocatalyst addition | Ref |
| Ti ₃ C ₂ T _x - multilayer nanosheets | $Zn_2In_2S_5/Ti_3C_2T_x$ | 0.25 M Na ₂ SO ₃ , 0.35 M Na ₂ S | 2596.8 | 1.97 times | [272] |
| | $g-C_3N_4/Ti_3C_2T_x$ | 20% triethanolamine | 26.7 | 2.13 times | [273] |
| | $TiO_2/Ti_3C_2T_x$ | Ascorbic acid | 33.4 | NR^{b} | [274] |
| | /amorphous carbon/ Eosin Y | | | | |
| | ZnIn ₂ S ₄ /TiO ₂ / | 0.25 M Na ₂ SO ₃ , | 1185.8 | 5.61 times (compared to ZnIn ₂ S ₄) | [275] |
| | $Ti_3C_2T_x$ | 0.35 M Na ₂ S·9 H ₂ O | | | |
| | $ZnS/Ti_3C_2T_x$ microspheres | 25% lactic acid | 502.6 | 4 times | [276] |
| | $MoS_2/Ti_3C_2T_x/$ TiO_2 | Triethanolamine | 6425.3 | NR^{b} | [277] |
| | $Ti_3C_2T_x(TiO_2)$ @CdS/MoS ₂ | 20% lactic acid | 8470.0 | 3.06 times | [278] |
| | Black phosphorus/ TiO ₂ /Ti ₃ C ₂ T _x | 25% triethanolamine | 684.5 | NR^{b} | [279] |
| | g-C ₃ N ₄ /Ti ₃ C ₂ T _x | 10% triethanolamine | 88.0 | NR ^b | [280] |
| | O-doped g-C ₃ N ₄ / Ti ₃ C ₂ T _x | Triethanolamine | 25124.0 | 1.82 times | [281] |
| | BiOBr/Ti ₃ C ₂ T _x | 0.25 M aqueous methanol | 1.3 | 3.88 times | [282] |
| | $WS_2/TiO_2/Ti_3C_2T_x$ | 15% acetone, 5% triethanolamine | 3409.8 | NR^{b} | [283] |
| MXene cocatalyst | Final catalyst | Sacrificial agent | H_2 production (μ mol $h^{-1}g^{-1}$) | Activity improvement following MXene cocatalyst addition | Ref |
| Ti ₃ C ₂ T _x – few layered nanosheets | $ZnIn_2S_4/Ti_3C_2T_x$ | 10% triethanolamine | 3475.0 | 6.6 times | [284] |
| | $SnNb_2O_6$ $/Ti_3C_2T_x$ | 20% methanol | 43.8 | 1.95 times | [285] |
| Ti ₃ C ₂ T _x quantum dots | $BiVO_4/ZnIn_2S_4/$ $Ti_3C_2T_x$ | NR ^a | 102.7 | ≈1.42 times | [286] |
| | g-C ₃ N ₄ /Ti ₃ C ₂ T _x | 15% triethanolamine | 5111.8 | 25.97 times | [287] |
| $Ti_3C_2T_x$ nanoparticles | CdS-Ti ₃ C ₂ T _x cauliflower-like submicron spheres | 18% lactic acid | 14342.0 | 136.59 times | [260] |
| | g-C ₃ N ₄ /Ti ₃ C ₂ T _x /Pt | 10% triethanolamine | 5100.0 | 5 times | [288] |
| | UiO-66-NH ₂ / | 0.1 M Na ₂ S, 0.1 M | 204.0 | 7.96 times | [289] |
| | Ti ₃ C ₂ T _x | Na ₂ SO ₃ | | | 2 2 |
| Mo ₂ C - nanoparticles (Mo ₂ C/C) | g-C ₃ N ₄ /Mo ₂ C nanorods | 10% triethanolamine | 507.0 | 2.34 times | [290] |
| | $Mo_2C/C/g-C_3N_4$ | 10% triethanolamine | 2269.5 | 333.74 times | [291] |
| Mo ₂ C- nanosheets | Mo ₂ C/CdS | 20% lactic acid | 7700.0 | 16.38 times | [292] |

 $^{^{}a}\ g\text{-}C_{3}N_{4}=graphitic\ carbon\ nitride$

b NR = Not reported

3.2. Carbon dioxide reduction reaction

Massive CO_2 emissions resulting from burning high levels of fossil fuels have been among the threatening problems of industrialization in the past century. As such, there is strong interest in converting this gas, via CO_2RR , to high value-added and clean products (CO, CH₄, CH₃OH, etc.) [293,294]. In this regard, photocatalytic reactions have shown promise in mimicking the natural photosynthesis of green plants, driving CO_2 conversion via solar radiation [295].

Recently, photocatalysts, such as metal oxides [296], nitrides [297], and sulfides [298], have been found to possess photocatalytic activity toward CO₂RR. However, these materials suffer from low efficiency in practical applications due to their poor ability to hinder the recombination of electron-hole pairs during their transfer [299]. To address this problem, noble metals (e.g., Au, Pd, Pt, Ru) have been combined with conventional catalysts to boost CO₂RR efficiency. However, the high cost of this strategy has hindered the industrial-scale use of these catalysts. Hence, affordable and efficient catalysts or cocatalysts to meet industrial demands are needed [300].

Solar-driven MXenes have attracted substantial interest as emerging CO_2RR photocatalysts owing to their improved performance in the separation and transformation of charge carriers. Several review articles have comprehensively investigated the potential of MXenes in CO_2RR for producing environmentally friendly products [249,253,301–303]. As mentioned earlier, MXene-based photocatalysts promote the conversion of CO_2 to substances like CO, CH_3OH , and CH_4 . CO_2RR proceeds within two main steps: 1) the incident light collides onto the photocatalyst surface and separates electrons (e⁻) and holes (h⁺) only if the energy of the incident light is equal to or greater than the bandgap of the photocatalyst, thereby transferring e⁻ to the photocatalytic surface, 2) CO_2 captures e⁻ and protons (H^+) , and corresponding products are generated. Simultaneously, water is oxidized into O_2 (Fig. 14) [304].

The reactions by which CO_2 is converted into CH_3OH , CO, and CH_4 are as follows [305]:

$$CO_2 + 2H^+ + 2e^- \rightarrow CO + H_2O$$
 (4)

$$CO_2 + 6H^+ + 6e^- \rightarrow CH_3OH + H_2O$$
 (5)

$$CO_2 + 8H^+ + 8e^- \rightarrow CH_4 + 2H_2O$$
 (6)

Several studies have demonstrated the paramount influence of MXenes on CO_2 reduction. As an illustration, Chen *et al.* [306] investigated the in-situ growth of TiO_2 on $Ti_3C_2T_x$, which established a Schottky junction between these materials. They discovered that the optimal $Ti_2O/Ti_3C_2T_x$ structure resulted in 2.8 and 4 times higher production rates than pristine TiO_2 for CO and CH_4 , respectively. This improvement in CO_2RR performance was due to forming an intimate

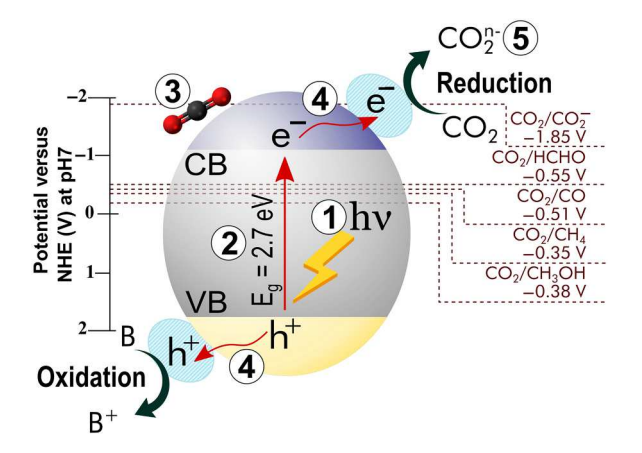


Fig. 14. Schematic illustration of the mechanism of photocatalytically-driven CO_2RR . Reprinted with permission from [304].

interface between TiO₂ and Ti₃C₂T_x via Schottky heterojunctions, which encouraged the separation of e-h+ pairs. It seems Schottky heterojunctions have more positive effects on the e⁻-h⁺ separation and electron mobility than when MXene and the second substance are mechanically mixed. In a study carried out by Wang et al. [307], a heterojunction 2D/2D was constructed by combining La₂Ti₂O₇ and few-layered Ti₃C₂T_r. The outcomes indicated that the La₂Ti₂O₇/Ti₃C₂T_r possessed Schottky heterojunctions and yielded more CO and CH₄, whose production rates were 4.6 and 11.4 times more than the La₂Ti₂O₇/Ti₃C₂T_x fabricated by a facile mechanical mixing method. Zhang et al. [308] prepared a Cu₂O/Ti₃C₂T_x heterojunction composite through an in situ hydrothermal growth procedure with 2, 5, 10, 20, and 30 percent of Ti₃C₂T_r. According to their results, the as-prepared composite with 10% Ti₃C₂T_x exhibited the highest photocatalytic CO₂RR performance, with 3.1 and 4.0 times greater CO and CH₄ yield rates (17.55 µmol·g⁻¹·h⁻¹ and $0.96 \,\mu\text{mol}\cdot\text{g}^{-1}\cdot\text{h}^{-1}$, respectively) than pristine Cu_2O (5.73 $\mu\text{mol}\cdot\text{g}^{-1}\cdot\text{h}^{-1}$ for CO and 0.24 µmol·g⁻¹·h⁻¹ for CH₄). This CO₂RR enhancement was attributed to the formation of a heterojunction contact surface between Cu₂O and Ti₃C₂T_x, which improved the separation of photogenerated e⁻h⁺ pairs. From prior research, Table 6 represents the effect of MXene incorporation into photocatalysts on overall CO₂RR yield rate or yield.

3.3. Nitrogen reduction reaction

Ammonia (NH₃) is widely used in many applications, including refrigeration [324], textiles [325], plastics, pesticides, and dyes [326]. As mentioned, NH₃ is usually produced industrially using the Haber-Bosch (HB) process, which requires harsh processing conditions [327]. These extreme conditions are due to the high dissociation energy of the N₂ triple bond, the thermodynamically forbidden addition of the H atom to N₂, and the high chemical stability of N₂ [328]. Moreover, the HB process contributes to CO₂ generation [329], which has motivated the research community to develop sustainable alternative processes.

Photocatalytic N_2 reduction has been found to be an attractive way of NH_3 fabrication. Recently, various photocatalysts have been exploited as potential NRR photocatalysts for driving solar energy and promoting N_2 conversion [330]. There are fundamental differences between the HB process and photocatalytically-based NRR regarding their hydrogen source, processing conditions, catalysts, and energy source (Table 7) [331]. Photocatalyst-assisted NRRs follow these three steps: (1) Solar radiation is absorbed by the photocatalyst and excites electrons (e') to move from the VB to the CB provided that the visible light energy (h_{ν}) is greater than the forbidden band width (E_g) of the catalyst, leaving positively-charged holes (h^+) in the VB. (2) Some e^-h^+ pairs recombine, and the rest diffuse into the catalyst surface. (3) Electrons react with H^+ and N_2 to produce NH_3 , and holes combine with H_2O to yield O_2 and H^+ (Fig. 15) [332].

Like electrocatalytic NRR, the photocatalytic reaction proceeds via four well-defined pathways: dissociative, distal associative, alternative associative, and enzymatic (Fig. 10) [330,331]. Concerning N_2 immobilization and activation, some roadblocks in NRR involve the slow kinetics of N_2 reduction due to the six-electron transfer procedure, the combination of e-h⁺ pairs, the potential reduction, and the light absorption range. Consequently, using an appropriate photocatalyst with acceptable VB-CB potentials is imperative for the suitable activation of N_2 and reduction to NH₃ [333]. Potential NRR photocatalysts have been extensively investigated, encompassing single atoms [334], transition metal oxides [335], transition metal sulfides [336], bismuth oxide (oxyhalides) [337], graphitic C_3N_4 [338,339], and bionic materials [340].

MXenes have attracted paramount interest in N_2 fixation during the past decade. The attractiveness of MXenes in photocatalytic reaction applications is due to their high surface area, which provides extensive active sites for concerned reactants, and the creation of the Schottky barrier to hamper the recombination of charge carriers [341]. In view of the photocatalytic activity, MXenes favor photocatalytic NRR

 $\begin{tabular}{ll} \textbf{Table 6}\\ A summary of the CO_2RR performance of various photocatalysts after adding a MXene component. \end{tabular}$

| Photocatalyst | Product (s) | Light source | Yield rate or yield | Ref |
|---|---------------------------|------------------------------------|---|-------|
| $\mathrm{Ti}_{3}\mathrm{C}_{2}\mathrm{T}_{x}$ | CH ₄ and CO | 300 W high- pressure Xe lamp | CH_4 , 0.88 μ mol·g ⁻¹ ·h ⁻¹ | [309] |
| | | | CO, 3.10 μmol·g ⁻ ¹ ·h ⁻¹ | |
| $g-C_3N_4/Ti_3C_2T_x$ | | | CH_4 , $2.12 \mu \text{mol} \cdot \text{g}^{\text{-}}$ $^1 \cdot \text{h}^{\text{-}1}$ | |
| | | | CO, 3.98 μmol·g ⁻ ·h ⁻¹ | |
| TiO ₂ | CH ₄ | 300 W Xe lamp | $\sim 0.059~\mu mol \cdot h^{\text{-}1}$ | [310] |
| $TiO_2/Ti_3C_2T_x$ g- C_3N_4 | CH ₄ and | Xe lamp | 0.220 μmol·h ⁻¹ CH ₄ , 0.20 μmol·g ⁻¹ ·h ⁻¹ | [311] |
| | | | CO, 0.79 µmol·g ⁻ ·h ⁻¹ | |
| ZnO | | | CH ₄ , 0.17 μmol·g ⁻ ·h ⁻¹ | |
| | | | CO, 0.52 μmol·g ⁻ ¹ ·h ⁻¹ | |
| g-C ₃ N ₄ /ZnO | | | CH ₄ , 0.27 μ mol·g ⁻ ·h ⁻¹ | |
| | | | CO, 1.41 μmol·g ⁻ ·h ⁻¹ | |
| g-C ₃ N ₄ /ZnO/Ti ₃ C ₂ T _x | | | CH ₄ , 0.26 μ mol·g ⁻¹ ·h ⁻¹ | |
| | | | CO, 6.41 μmol·g ⁻ ¹ ·h ⁻¹ | |
| PCN ^a | CH ₄ and CO | 35 W HID Car lamp | CH_4 , 23.4 μ mol·g ⁻ | [312] |
| TiC-48/PCN | | | CO, 63.5 μmol·g ⁻¹ CH ₄ , 157.1 | |
| | | | μmol·g ⁻¹ CO, 634.8 | |
| Photocatalyst | Product | Light source | μmol·g ⁻¹ Yield rate or | Ref |
| Ni/Nb ₂ O ₅ | (s) CH ₄ | 300 W Xe arc | yield 12.9 mmol·g ⁻¹ ·h ⁻ | [313] |
| Ni/Nb ₂ CT _x | | lamp | 72.5 mmol·g ⁻¹ ·h | |
| CN | CO | Visible light | 4.47 μmol·g ⁻¹ | [314] |
| BCN ^b Ti ₃ C ₂ T _x /BCN ^b | | | 6.42 μmol·g ⁻¹ 14.40 μmol·g ⁻¹ | |
| TiO ₂ (P25) | CO and CH ₄ | 300 W Xe lamp | CH ₄ , ~ 0.06 μ mol·g ⁻¹ ·h ⁻¹ | [315] |
| | | | $CO \sim 3.91$ $\mu mol \cdot g^{-1} \cdot h^{-1}$ | |
| TiO ₂ (P25)/ Ti ₃ C ₂ OH | | | CH ₄ , 16.61 μmol·g ⁻¹ ·h ⁻¹ | |
| | | | CO, 11.74 μmol·g ⁻¹ ·h ⁻¹ | |
| g-C ₃ N ₄ | CO and CH ₄ | 300 W Xe lamp | CH ₄ , NR ^d | [316] |
| g-C ₃ N ₄ /Ti ₃ C ₂ OH | | | CO, 1.88 µmol·g ⁻¹ CH ₄ , NR ^d | |
| | | | CO, 11.21 μmol·g ⁻¹ | |
| Bi_2WO_6 | CH₄ and CH₃OH | 300 W Xe lamp | CH ₄ , 0.39 μmol·g ⁻ 1·h ⁻¹ | [317] |
| | | | CH ₃ OH, 0.1 μmol·g ⁻¹ ·h ⁻¹ | |
| $\mathrm{Bi_2WO_6}/\mathrm{Ti_3C_2T_x}$ | | | CH ₄ , 1.78 μmol·g ⁻ ·h ⁻¹ | |
| | | | CH ₃ OH, 0.44 μmol·g ⁻¹ ·h ⁻¹ | |
| Cu ₂ O NWs/Cu | CH ₃ OH | 300 W Xe lamp | 3.12 ppm·cm ⁻² ·h | [318] |
| $Cu_2O/Ti_3C_2T_x$ Sheets/Cu | | - | 11.98 ppm·cm ⁻ ² ·h ⁻¹ | |
| Cu ₂ O/Ti ₃ C ₂ T _x QD ^e s/ | | | 25.77 ppm·cm ⁻² ·h ⁻¹ | |
| | | | | |

Table 6 (continued)

| Photocatalyst | Product (s) | Light source | Yield rate or yield | Ref |
|---|------------------------------|------------------|--|-------|
| NiAl-LDH | CO | 300 W Xe lamp | \sim 247.5 μ mol·g ⁻ 1 ·h ⁻¹ | [319] |
| Ni-LDH/Ti ₃ C ₂ T _x | | | 2128.46 μmol·g ⁻ ¹ ·h ⁻¹ | |
| TiO ₂ | CH ₄ and CO | 300 W Xe lamp | CH ₄ , <0.15 μmol·g ⁻¹ ·h ⁻¹ CO, <1.46 μmol·g ⁻¹ ·h ⁻¹ | [320] |
| g-C ₃ N ₄ | | | CH ₄ , NR ^d CO, <1.46 μmol·g ⁻¹ ·h ⁻¹ | |
| TiO ₂ /g-C ₃ N ₄ | | | CH ₄ , NR ^d CO, 3.14 μmol·g ⁻ ¹ ·h ⁻¹ | |
| TiO_2/g - $C_3N_4/Ti_3C_2T_x$ | | | CH ₄ , 1.20 μmol·g ⁻¹ ·h ⁻¹ CO, 4.39 μmol·g ⁻ | |
| Photocatalyst | Product | Light source | ¹.h⁻¹ Yield rate or | Ref |
| , | (s) | · · | yield | |
| TiO ₂ Ru-Ti ₃ CN-TiO ₂ | CO and CH ₄ | 300 W Xe lamp | CH ₄ , < 0.96 μ mol·g ⁻¹ ·h ⁻¹ CO, < 4.86 μ mol·g ⁻¹ ·h ⁻¹ CH ₄ , 8.97 μ mol·g ⁻¹ | [321 |
| | | | CO, 99.58 | |
| Cd _{0.2} Zn _{0.8} S | CO and CH ₄ | 300 W Xe lamp | μ mol·g ⁻¹ CH ₄ , ~ 0.95 μ mol·g ⁻¹ ·h ⁻¹ CO ~ 0.8 μ mol·g ⁻¹ | [322] |
| $Cd_{0.2}Zn_{0.8}S@Ti_3C_2T_x$ | | | ¹ ·h ⁻¹ CH ₄ , 3.51 μmol·g ⁻¹ ·h ⁻¹ | |
| | | | CO, 3.31 μmol·g ⁻ ¹ ·h ⁻¹ | |
| Bi ₂ O ₂ SiO ₃ | CO and CH ₃ OH | 300 W Xe lamp | CH ₃ OH, 1.80 μmol·g ⁻¹ ·h ⁻¹ CO, 3.45 μmol·g ⁻¹ | [323] |
| ${\rm Bi}_2{\rm O}_2{\rm SiO}_3/{\rm Ti}_3{\rm C}_2{\rm T}_x$ | | | CH ₃ OH, 2.07 μmol·g ⁻¹ ·h ⁻¹ CO, 17.82 μmol·g ⁻¹ ·h ⁻¹ | |

 $^{^{}a}$ PCN = porous g-C₃N₄

Table 7The differences between the HB process and photocatalytic nitrogen reduction. Reprinted with permission from [331].

| | HB process | Photocatalytic nitrogen reduction |
|-----------------|-------------|-----------------------------------|
| Hydrogen source | Natural gas | Water |
| Catalysts | Iron | Semiconductors |
| Temperature | 400–500 °C | Ambient temperature |
| Pressure | 200 atm | 1 atm |
| Energy source | Fossil fuel | Solar energy |

manufacturing NH₃ through an environmentally friendly process. In this respect, several reviews have described the promising contributions of photocatalytic MXenes and their recent developments in photocatalytic NRR [301,342–344]. However, very few articles have been published in this field since it is still in its infancy. To mention in a study by Li *et al.* in 2022 [345], an ultrasonicated Ti₃C₂T_x MXene doped by tungsten (W) atoms (W/Ti₃C₂T_x-U) with regard to its nitrogen photo fixation. The outcomes indicated that bare Ti₃C₂T_x-U and W/Ti₃C₂T_x-U resulted in an NH₃ yield rates of 14.5 and 227.5 μ mol·g⁻¹·h⁻¹, respectively. The better efficiency of W/Ti₃C₂T_x-U than Ti₃C₂T_x-U was associated with active sites created by W, which further promoted electron transfer and N₂

^b Boron- doped g-C₃N₄, ^c: $Ti_2O/C = produced$ by $Ti_3C_2T_x$ calcination

d NR= not reported

e QD: quantum dot.

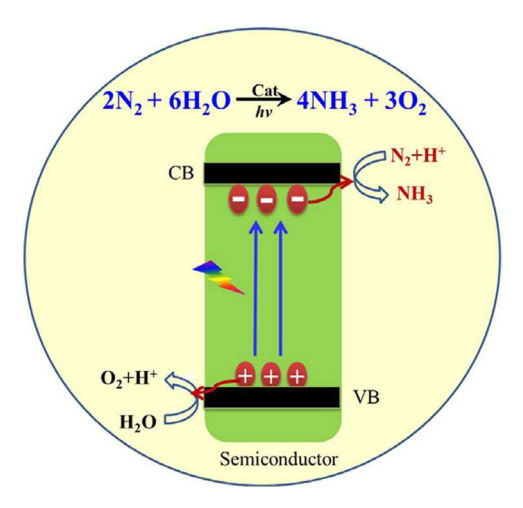


Fig. 15. A general schematic of nitrogen reduction via photocatalysts. Reprinted with permission from [332].

adsorption. In another study, Jiang et al. [346] synthesized a 2D MXene-derived Nb₂O₅/C/Nb₂C/g-C₃N₄ heterojunction via immobilizing Nb₂O₅ on Nb₂C and subsequently, the in-situ formation of g-C₃N₄ nanosheets on Nb₂O₅/C/Nb₂C. The prepared composite showed a 9.1 times greater NH₃ production rate of 0.365 mmol.g⁻¹.h⁻¹ than that of MXene-derived Nb₂O₅/g-C₃N₄. This enhancement was attributed to the close contact between Nb2O5 and Nb2C and the Schottky junction formed at the Nb2O5/Nb2C interface, assisting charge transfer and boosting the overall N₂ fixation efficiency. Chang et al. [347] fabricated a reduced Ti₃C₂T_x MXene embedded with Au nanoparticles (r-Ti₃C₂Tx/Au). r-Ti₃C₂T_x provided more Ti active sites, which can facilitate N₂ adsorption and activation. Moreover, Au nanoparticles donated plasmonic hot electrons to promote the reduction of already activated N2 molecules. The synthesized r-Ti₃C₂T_x/Au composite demonstrated an NH₄⁺ production rate of 12.4 μmol.g⁻¹.h⁻¹ under visible light, approximately 5.9 and 10.3 times those of Ti₃C₂T_x/Au and r-Ti₃C₂T_x, respectively. This effect obviously indicates the synergic influences of increased Ti active sites and accessibility to electrons. Other research regarding the application of MXenes in NRR is briefly represented in Table 8.

Table 8 The efficiency of MXene-based photocatalysts in photo-induced $\rm N_2$ reduction. A 300 W xenon lamp was used in all cases.

| Photocatalysts | NH_3 yield rate | NRR activity improvement following the incorporation of MXene | Ref |
|---|---|---|-------|
| Ti ₃ C ₂ T _x /TiO ₂ | 422.0 μmol•g ⁻ ¹ •h ⁻¹ | NR ^a | [348] |
| 1D/2D CdS nanorod@ $Ti_3C_2T_x$ | 293.1 μmol•L ⁻ ¹ •h ⁻¹ | NR ^a | [349] |
| $0D/2D AgInS_2/$ $Ti_3C_2T_x$ | 38.8 µmol•g⁻ ¹•h⁻¹ | 19.4 times | [350] |
| $\mathrm{Bi_4O_5Br_2/Ti_3C_2T}_x$ | 277.7μmol•g ⁻ ¹ •h ⁻¹ | 5 times | [351] |
| Ti ₃ C ₂ T _x /CuZnInS | 45.6 μmol•g ⁻ 1•h ⁻¹ | 2 times | [352] |
| BiOBr/Ti $_3$ C $_2$ T $_x$ | 234.6 μmol•g ⁻¹ •h ⁻¹ | 48.8 times | [353] |
| ${ m Ti}_3{ m C}_2{ m T}_x$ /TiO ₂ /Co | 69.2 μmol•g⁻ ¹•h⁻¹ | 1.4 times | [354] |
| ${\rm Ti_3C_2T_x/TiO_2}$ | 50.0 μmol.•g ⁻ ¹ •h ⁻¹ | 1.8 times | [354] |
| r-Ti ₃ C ₂ T _x QDs/g- C ₃ N ₄ | 328.9 μmol•g ⁻¹ •h ⁻¹ | NR ^a | [355] |

^a NR = not reported

3.4. Water pollutant degradation

Organic matter released from facilities, chemical plants, transportation systems, and refineries enter lakes, seas, oceans, and other aquatic milieu, posing a severe threat to ecosystems and human health [356]. Hence, it is of great importance to develop materials to remove water pollutants through various water treatment routes, including adsorption [357], membrane separation [358], and catalytic reactions. However, these methods suffer from low contaminant removal efficacy, rising premiums, and the emission of toxic by-products [359]. Motivated by these, in the past few years, emerging advanced oxidation processes (AOPs), which include electrolysis, ozonation, and photocatalysis, have been introduced to purify aquatic environments [360]. Solar light-driven pollutant degradation is among the most emerging techniques to alleviate water pollution. In a typical photo-assisted degradation, when light collides with the catalyst surface, the VB electrons are excited and transferred to the CB, forming holes in the corresponding CB. Subsequently, these electron-hole pairs bring about redox reactions in which electrons reduce existing O2 molecules, and holes function as active sites to oxidize H_2O molecules, thereby creating. O_2^- and $OH^$ reactive species. Lastly, these will interact with pollutants and convert them to benign products. The diagrammatic illustration of a typical photo-induced pollutant degradation is depicted in Fig. 16 [361].

Photocatalysts fall into multifarious categories, most of which were mentioned in the prior section. Nevertheless, these catalysts represent vital challenges, such as charge carrier recombination and low chemical stability, diminishing the overall performance of photocatalytic pollutant degradation. Accordingly, producing highly efficient materials as alternatives to traditional photocatalysts is crucial [362].

MXenes with high surface area and negatively charged surface enable the intercalation of positively charged cations (e.g., Na⁺, K⁺, and Li⁺) and organic molecules (e.g., dimethyl sulfoxide (DMSO) and urea) in between MXenes layers, thereby promoting the removal of contaminants from water [363]. Moreover, with their surface functional groups (e.g., F, O, and OH), MXenes can be potential hosts for other catalysts to form potent photocatalysts for the spontaneous depletion of contaminants [364]. So, MXenes are usually employed with other materials in the form of composites because MXenes alone lack proper semiconducting characteristics [365]. Several investigations have been conducted on the performance of MXenes incorporating photocatalysts toward eliminating a wide array of contaminants. For example, in a study by Shahzad and coworkers [366], a hybrid Ti₃C₂T_y/TiO₂ photocatalyst was fabricated via a facile hydrothermal method. The heterostructure of the as-synthesized photocatalyst was attained by the Schottky junction formed between the Ti₃C₂T_x and TiO₂ interfaces. The fabricated photocatalyst was investigated regarding its potential photocatalytic application in the degradation of antiepileptic drug carbamazepine (CBZ). The resulting degradation stage rate of Ti₃C₂T_x/TiO₂ (10.0 mg) was 0.0304 min⁻¹ under ultraviolet radiation, higher than that under solar light (Fig. 17a and b). Furthermore, the percent decomposition of CBZ by pristine Ti₃C₂T_x and Ti₃C₂T_x/TiO₂ was 60% and 98.67%, respectively, clearly showcasing the effect of TiO2 incorporation. The mechanism through which the degradation occurs is illustrated in Fig. 17(c). As this figure shows, when light radiates onto the $Ti_3C_2T_x/TiO_2$ surface, the VB electrons (e⁻) are excited and leave the VB to CB, forming respective holes (h^+) in CB. The e^-h^+ pairs then react with dissolved oxygen to generate reactive OH radicals, which decompose CBZ to produce CO2 and H2O. The remarkable photocatalytic activity of $Ti_3C_2T_x/TiO_2$ was ascribed to the extra e^-h^+ pairs generated by {0 0 1} facets of TiO2 along with the formation of the Schottky junction. In another research, Chen et al. [367] constructed bismuth oxychloride (BiOCl)/Ti₃C₂T_x MXene heterostructures through a simple electrostatic self-assembly pathway (Fig. 18a). This MXene-based substance resulted in up to 90% photodegradation of ciprofloxacin (CIP), a fluoroquinolone antibiotic, in only 30 min under sunlight irradiation. This enhancement in degradation was correlated with the

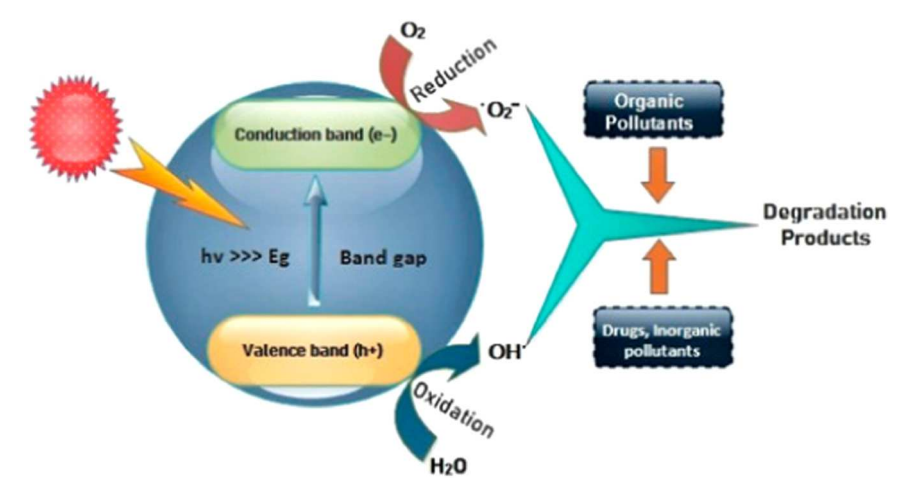


Fig. 16. The diagrammatic representation of a general solar light-assisted pollutants degradation Reprinted with permission from [361].

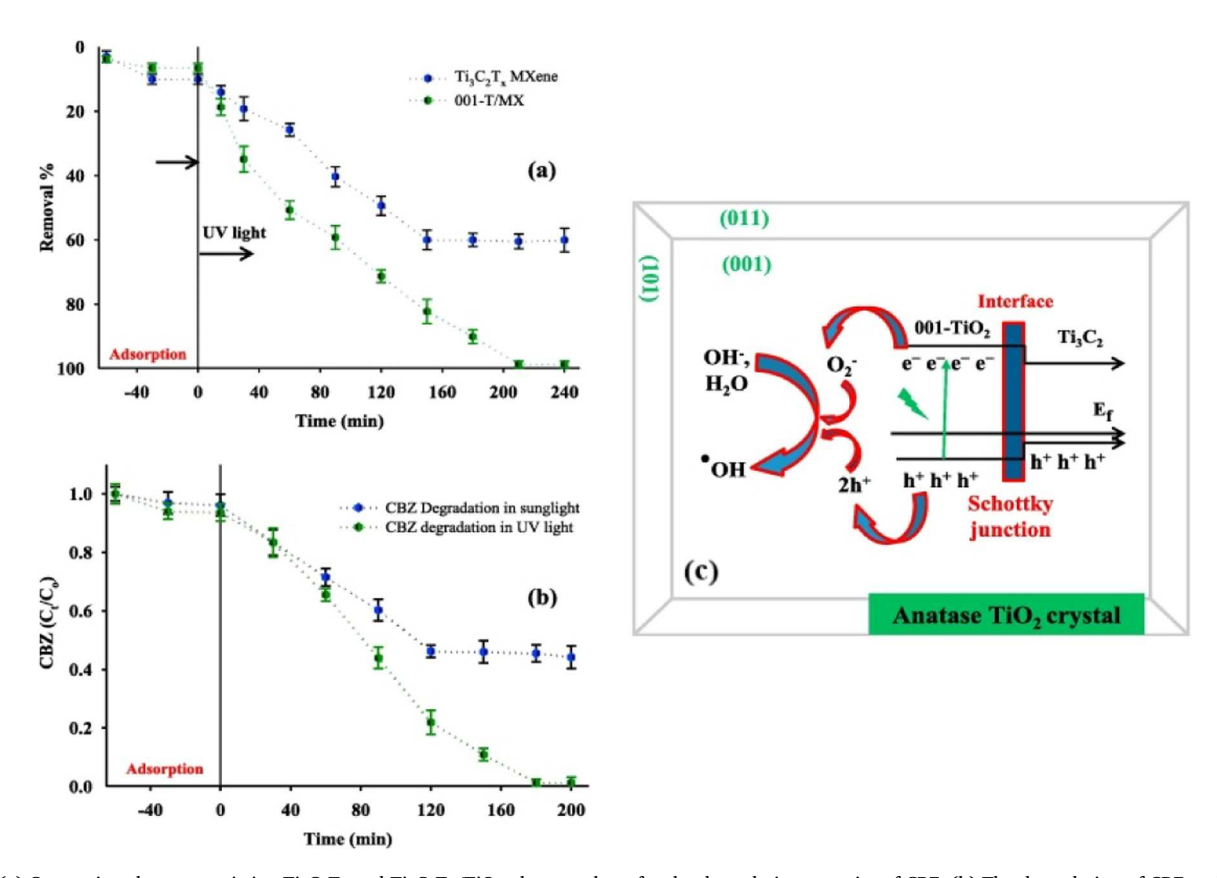


Fig. 17. (a) Comparison between pristine $Ti_3C_2T_x$ and $Ti_3C_2T_x/TiO_2$ photocatalysts for the degradation capacity of CBZ. (b) The degradation of CBZ under UV and solar light irradiation utilizing $Ti_3C_2T_x/TiO_2$ photocatalyst. (c) Schematic illustration of CBZ degradation mechanism by $Ti_3C_2T_x/TiO_2$. Reprinted with permission from [366].

hindrance of e^-h^+ pairs recombination and the improved light absorption capacity. The influence of adding different amounts of $Ti_3C_2T_x$ on the photocatalytic performance of as-prepared catalysts is depicted in Fig. 18(b). First, a 30 min of physical blending between BiOCl and $Ti_3C_2T_x$ occurred. Subsequently, the stimulated sunlight source was switched on.

Grzegórska *et al.* [368] prepared a hybrid Zn/Ti LDH photocatalyst integrated with ${\rm Ti_3C_2T_x}$ MXene. They assessed its improved ability for acetaminophen and ibuprofen, both commonly present in the aquatic milieu. They discovered that the LDH/MXene sample containing 2.5%wt of MXene reached the highest degradation of 100% (within 40 min) and 99.7% (within 60 min) for acetaminophen and ibuprofen, respectively

(Fig. 19a and b). With regard to the activity of reactive species, O_2^- had the main contribution to photocatalytic degradation of acetaminophen, whereas 'OH and h⁺ were more reactive toward ibuprofen. More importantly, characterization analyses revealed the outstanding stability and reusability of the LDH/Ti₃C₂T_x photocatalyst after four subsequent cycles of degradation (Fig. 19c). After the fourth cycle, the photocatalytic efficacy of the synthesized Zn/Ti LDH-Ti₃C₂T_x in acetaminophen degradation remained 100% within 40 min. In another study, tetracycline hydrochloride (TC-HCl), a common antibiotic found in pharmaceutical wastewater, was degraded by BiOBr/Ti₃C₂T_x/g-C₃N₄. Their outcomes indicated 99% degradation of TC-HCl within 30 min, which was 12 times higher than the degradation efficacy of pure g-C₃N₄

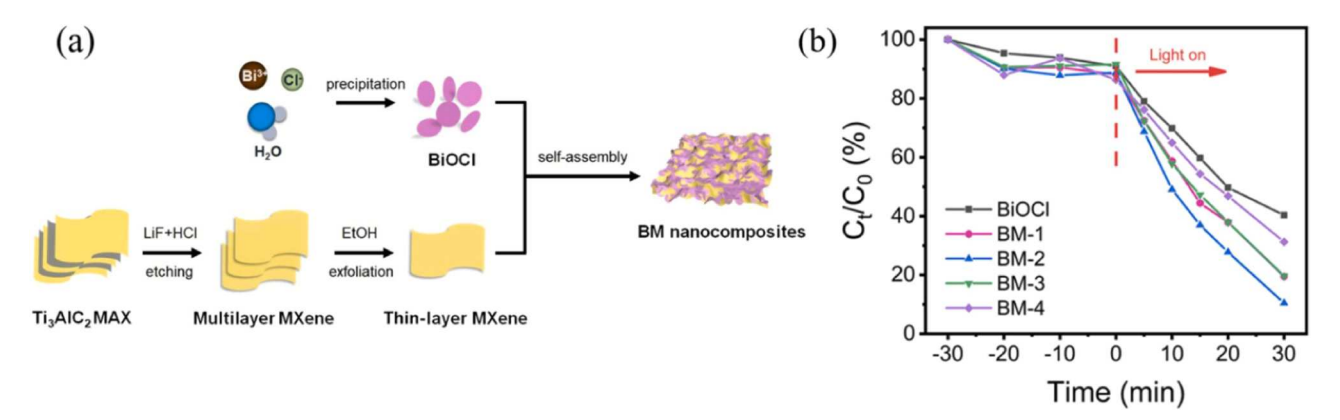


Fig. 18. (a) The preparation route of the BiOCl/ $Ti_3C_2T_x$ photocatalyst via a self-assembly strategy. (b) The photocatalytic activity of BiOCl/ $Ti_3C_2T_x$ in the degradation of CIP. Reprinted with permission from [367].

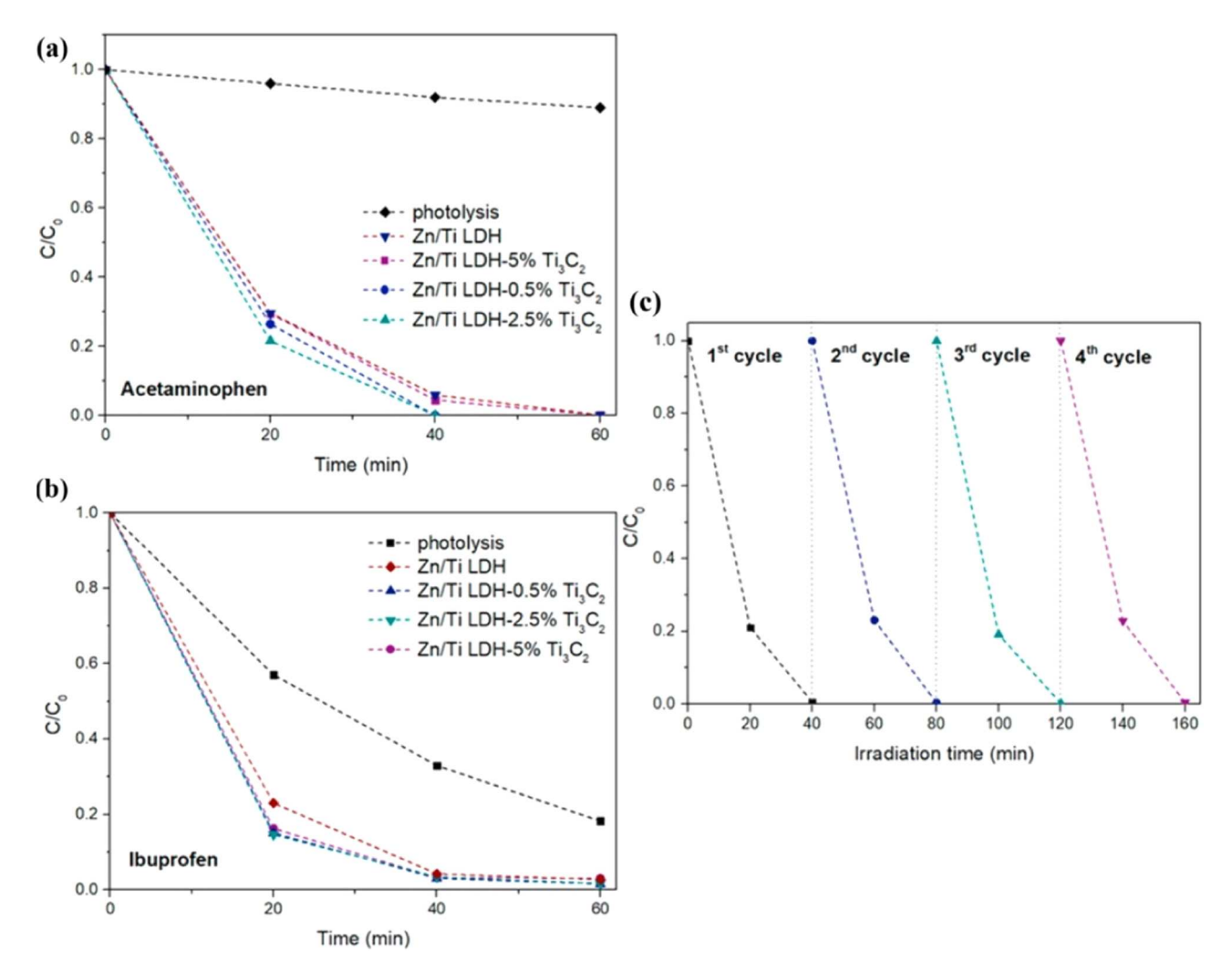


Fig. 19. The performance of Zn/Ti LDH coupled with $Ti_3C_2T_x$ in photocatalytic degradation of (a) acetaminophen and (b) ibuprofen. (c) The stability of fabricated Zn/Ti LDH- $Ti_3C_2T_x$ in acetaminophen degradation after four successive cycles. Reprinted with permission from [368].

(Fig. 20(a)). This improvement was brought about by the increased number of exposed active sites, increased formation of adsorbed oxygen, avoidance of recombination of electron-hole pairs, and efficient production of reactive ${}^{\bullet}O_2^-$, h^+ , and ${}^{1}O_2$ (singlet oxygen generated by superoxide radical reactions) [369].

Due to their severe threat to aquatic environments, organic dyes must be removed and degraded via various degradation routes [370].

Fig. 20(b) depicts the MXene-induced photocatalytic degradation of a detrimental organic dye called methylene blue (MB). The MXene used in this research was ${\rm Ti}_3{\rm C}_2{\rm T}_x$ oxidized with ${\rm Ti}{\rm O}_2$ and decorated with Ag and Pd NPs. The results showed the superior performance of AgNPs (PdNPs)/ ${\rm Ti}{\rm O}_2/{\rm Ti}_3{\rm C}_2{\rm T}_x$ compared to pristine, which was mainly ascribed to the significant role of ${\rm Ti}{\rm O}_2$ and Ag(Pd) in augmenting light harvesting, dye adsorption, and charge separation capability [370]. Fig. 20(c)

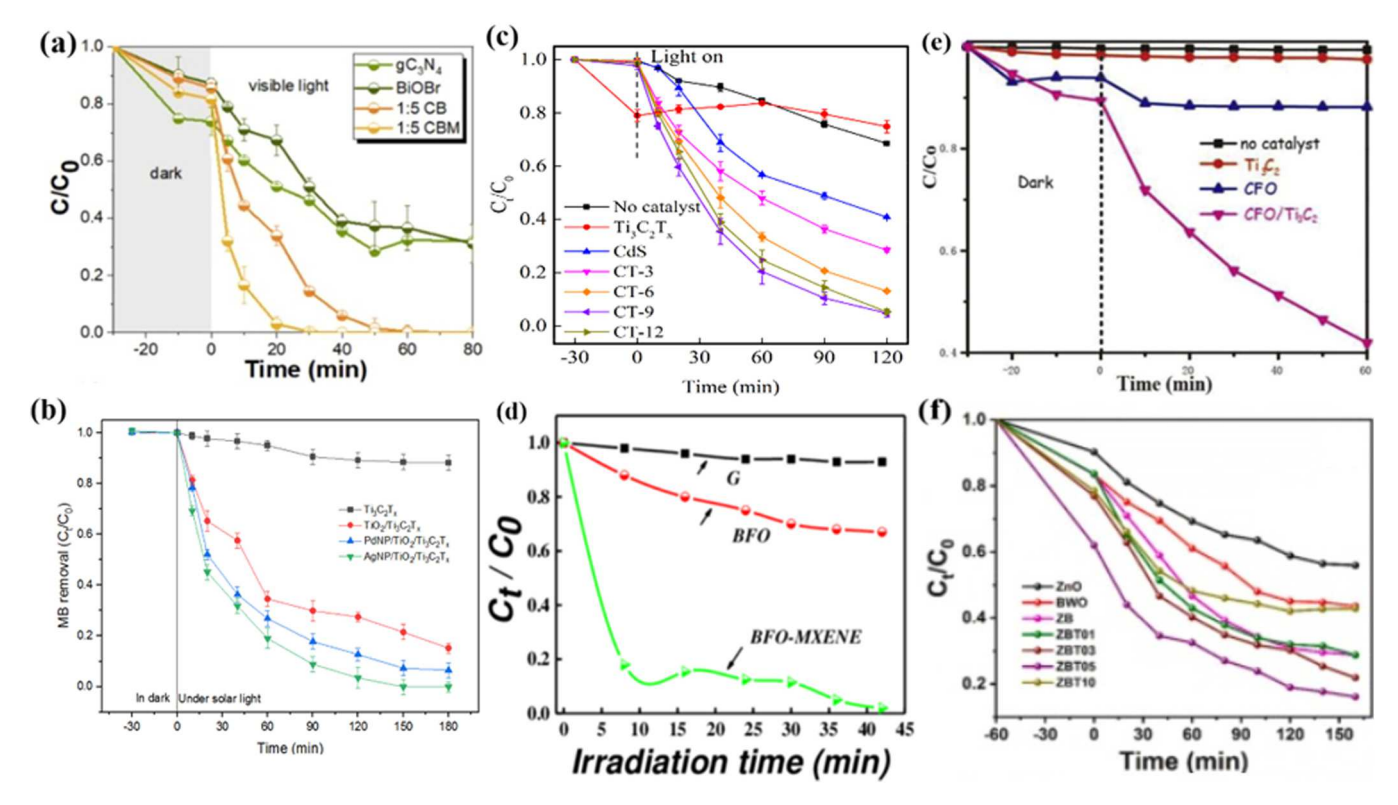


Fig. 20. The photocatalytic degradation of (a) TC-HCl by BiOBr/MXene/g- C_3N_4 , (b) MB by AgNPs(PdNPs)/TiO₂/Ti₃C₂T_x, (c) CBZ by CdS QDs/ Ti₃C₂T_x, (d) CR by BiFeO₃/Ti₃C₂T_x, (e) SMZ by CuFe₂O₄/Ti₃C₂T_x, and (f) CFX by ZnO-Bi₂WO₆-Ti₃C₂T_x. (a) reprinted with permission from [369], (b) reprinted with permission from [370], (c) reprinted with permission from [371], (d) reprinted with permission from [372], (e) reprinted with permission from [375].

illustrates the effect of CdS QDs/ $Ti_3C_2T_x$ photocatalyst on the degradation of CBZ. In this research, CdS QDs were intimately grafted onto the surface of Ti₃C₂T_x MXene. Therefore, the interface between CdS QDs and Ti₃C₂T_x substantially improved the generation of charge carriers, their separation, and their transfer from CdS. As for the reactive intermediates involved in the removal of CBZ, ${}^{\bullet}O_2^-$, H_2O_2 , 1O_2 , and ${}^{\bullet}H$ were the main active superoxide radicals, with ${}^{\bullet}O_2^-$ possessing the primary contribution [371]. In another similar study, Iqbal et al. [372] reported the removal of Congo Red (CR) contaminant from water utilizing a nanohybrid system composed of bismuth ferrite nanoparticles with two-dimensional (2D) MXene sheets, namely, the BiFeO₃ (BFO)/ $Ti_3C_2T_r$ (MXene) (Fig. 20(d)). 100% of CR was discovered to be degraded from water in 42 min, indicating the paramount effect of the fabricated nanohybrid structure attributed to its light-harvesting ability for photocatalysis. Moreover, the rapid and efficient removal of CR was caused by the low recombination rate of (e⁻, h⁺) pairs and the large surface area of the nanohybrid. Rhodamine B (RhB) is another water pollutant found to be hazardous to aquatic milieu [373]. To tackle this issue, Liu et al. [373] conducted a study on the degradation of RhB by TiO2/Ti3C2Tx MXene. They found that TiO₂/Ti₃C₂T_x can remove RhB from water by 44% in 150 min, which was more effective than $Ti_3C_2T_x$ (30%) . This improvement stemmed from better separation of charge carriers and increased light adsorption compared to pristine Ti₃C₂T_x. Cao and coworkers [374] employed CuFe₂O₄/Ti₃C₂T_x MXene hierarchical heterostructures as photocatalysts for improved degradation of Sulfamethazine (SMZ), which causes serious contamination of aquatic media (Fig. 20(e)). Transient surface photovoltage (TPV) spectroscopy was conducted to assess charge carrier lifetimes, indicating that the lifetime of the (e-, h+) pair was prolonged by incorporating Ti₃C₂T_x due to the inhibition of charge carrier recombination. Lastly, Sharma et al. [375] assessed the photocatalytic degradation of a colorless pharmaceutical pollutant, ciprofloxacin (CFX), using a novel 2D-2D-2D ternary photocatalyst ZnO-Bi₂WO₆-Ti₃C₂T_x. Their results showcased the highest degradation

of CFX, \sim 77% in 160 min, for a sample containing 5 wt% of ${\rm Ti_3C_2T_x}$ (Fig. 20(f)). This performance was brought about by the efficient separation of photogenerated charge carriers due to the ternary interface established between individual components.

The results associated with other studies conducted in recent years are represented in Table 9.

4. Other reactions

4.1. Hydrogenation reactions

4.1.1. CO₂ hydrogenation to methanol

As previously mentioned, CO_2 has contributed to climate change substantially, increasing the global temperature during the past few decades. Therefore, CO_2 conversion to non-hazardous substances has attracted much attention in recent decades. Photocatalytically and electrochemically-driven strategies for the conversion of CO_2 were covered in the previous sections. In this regard, DFT calculations have shown that surface termination affects the adsorption energies of reaction intermediates [183]

 Table 9

 Recent studies on the photocatalytic performance of MXene-based materials in contaminant degradation.

| Photocatalyst | Pollutant(s) | Light source | Degradation efficiency (%) | Remark(s) | Ref |
|--|----------------------------------|--|---------------------------------------|--|------|
| BiOBr/Ti ₃ C ₂ T _x /g- C ₃ N ₄ | TC-HCl | 300 W Xenon lamp | 99.00 | -13 intermediates and possible degradation pathways - the photocatalyst can produce an antibacterial effect following radiation | [369 |
| CdS QDs/ Ti ₃ C ₂ T _x | CBZ | Simulated solar light | Up to 95.2 | degradation efficiency reached its maximum level after nine cycles of CdS QD deposition. | [371 |
| CdS/Ti ₃ C ₂ T _x / TiO ₂ | sulfachloropyridazine (SCP) | 300 W Xenon lamp | 100 for all contaminants | degradation was progressed via the pseudo-first-order model The catalyst was stable after four consecutive cycles SCP degradation efficiency had a direct relation with the reaction | [373 |
| | MB RhB | | | temperature. | |
| ZnO/Bi ₂ WO ₆ / Ti ₃ C ₂ T _x | ciprofloxacin (CFX) | 300 W Xenon lamp | 77 | - ${\rm Ti}_3{\rm C}_2{\rm T}_x$ facilitated the separation of e-h ⁺ pairs | [375 |
| Γi ₃ C ₂ T _x /TiO ₂ /Ag | -TC-HCl | 300 W Xenon lamp | 79.5 | Degradation took place in 15 min under light radiation, followed by 45 min under darkness since the enhanced electron storage caused more degradation activity during darkness | [370 |
| | Oxytetracycline (OTC) RhB | | 81.4 98.9 | | |
| | Methyl orange (MO) | | 99.1 | | |
| Bi ₂ WO ₆ /Nb ₂ CT _x | MB RhB | Visible light (λ > 420) | 99.2 99.8 | - Photodegradation rate constant of BN-2 for RhB and MB was 2.8 times and 2 times higher than | [37 |
| | MB | | 92.7 | pristine Bi ₂ WO ₆ , respectively | |
| Photocatalyst | TC-HCl Pollutant(s) | Light source | 83.1 Degradation efficiency (%) | Remark(s) | Ref |
| AgNPs(PdNPs)/ TiO_2 / $Ti_3C_2T_x$ | MB | UV light | 85 | - Improved photocatalytic degradation efficiency was ascribed to the formation of anatase ${\rm TiO_2}$ and the plasmonic resonance effect of noble metals, which further enhance charge separation | [37 |
| BiFeO ₃ /Ti ₃ C ₂ T _x | CR | Visible light | 100 for both | - Low $e^{\boldsymbol{\cdot}}\text{-}h^+$ recombination rate according to the photoluminescence spectra | [37 |
| | | | | - The hybrid photocatalyst had a larger surface area of 147 $\rm m^2.g^{-1}$, conducive to the improved degradation | |
| ΓiO ₂ /Ti ₃ C ₂ T _x | Acetaminophen RhB | Visible light (λ~554 nm) | 50 | Reusable after five cycles | [37 |
| $CuFe_2O_4/Ti_3C_2T_x$ | SMZ | Visible light | 59.4 | - Lifetime of photo-induced carriers increased after loading ${\rm Ti_3C_2T_x}$ - Semi-stable after three cycles | [37 |
| Ti ₃ C ₂ T _x /NiFe ₂ O ₄ / V ₂ O ₅ | RhB | 150 W visible light (λ >400 nm) | 88.7 | Hydroxyl and superoxide anion radicals played the most crucial roles in photodegradation | |
| Ti ₃ C ₂ T _x /TiO ₂ | perfluorooctanoic acid (PFOA) | UV | 100 | - Almost complete stability after four cycling runs - Photocatalyst was synthesized through the deep eutectic solvents (DESs) method, which expanded the interlayer space between ${\rm Ti_3C_2T_x}$ | |
| Photocatalyst | Pollutant(s) | Light source | Degradation | nanosheets, augmenting the growth of ${\rm TiO_2}$ molecules Remark(s) | Ref |
| Ti ₃ C ₂ T _x /TiO ₂ | MB | UV | efficiency (%) 96.44 | - | [38 |
| BiOIO ₃ /Ti ₃ C ₂ T _x | TC-HCl | 500 W Xenon lamp | 93.4 | Excellent recyclability after the fourth cycle (72.4% of TC-HCl was degraded) | [38 |
| | Levofloxacin hydrochloride | | 77.4 | | |
| g-C ₃ N ₄ /Ti ₃ C ₂ T _x / black phosphorus | 4-nitrophenol CIP | visible light (λ >420 nm) | 43.3 99 | - P-bridging effect caused by reactions between the active P atom in the black phosphorus nanosheet and as-fabricated g-C_3N_4 improved | [38 |
| (BP) Γi ₃ C ₂ QDs/SiC | NO ^a | 300 W Xenon lamp | 74.6 | photocatalytic degradation efficiency - Extraordinary stability following four successive cycles | [38 |
| $Ag/g-C_3N_4/Ti_3C_2T_x$ | RhB | $(\lambda > 420 \text{ nm})$ visible light $(\lambda > 420 \text{ nm})$ | 99.2 | - The incorporation of Ag nanoparticles resulted in the localized surface plasmon resonance, accelerating photo-driven degradation | [38 |
| | TC | 120 11111) | 92.1 | phonon resonance, accelerating photo arriver degradation | |
| Fe ₂ O ₃ /Ti ₃ C ₂ T _x | RhB | 500 W Xe Lamp | 98 | - | [38 |
| g-C ₃ N ₄ /BiOCl/ Ti ₃ C ₂ T _x | TC | visible light ($\lambda >$ 420 nm) | 97 | The photocatalyst was reusable after five consecutive cycles | [38 |
| Γi ₃ C ₂ T _x /Bi ₄ Ti ₃ O ₁₂ | тс-он | 500 W Xe Lamp | 100 for all contaminants | High stability after four cycles | [38 |
| | RhB MO | | | | |
| Ti ₃ C ₂ T _x /TiO ₂ /BiOCl | RhB | 500 W Xe Lamp | 78.36 | - | [38 |
| La-doped bismuth ferrite/Ti ₃ C ₂ T _x | CR | 500 W Xe Lamp | 93 | - High stability after four cycles | [389 |

 $^{^{\}rm a}\,$ NO = nitrogen oxide

subsequently, increased Lewis acidic Cu^+ sites, improving the overall methanol formation rate. Their results demonstrated that the optimum synthesized catalyst ($\mathrm{Cu/MoCT_x/SiO_{2-6h}}$) possessed a higher intrinsic methanol formation rate than $\mathrm{Cu/SiO_{2-2h}}$ (2.49 versus 0.41 gh⁻¹ gcll), with a methanol selectivity of 52% (Fig. 21a). Furthermore, at the constant $\mathrm{CO_2}$ conversion of 1.0%, the methanol selectivity of $\mathrm{Cu/Mo_2CT_x/SiO_{2-6h}}$ was more than that of $\mathrm{Cu/SiO_{2-2h}}$ (Fig. 21b).

4.1.2. Reverse water-gas shift reaction

The reverse water-gas shift reaction (RWGS) is a pathway for converting hazardous CO₂ to CO (a constituent of syngas), which itself can be further used in methanol synthesis and other procedures. To accelerate this reaction, MXene-based substances are valuable and have shown promise. For example, Salvador et al. [393] conducted computational studies, including DFT calculations and kinetic phase diagrams, to verify the capability of MXenes in catalyzing the RWGS reaction. They discovered that CO2 could be dissociated conveniently on a set of 18 carbides and nitride MXene catalysts with super-low CO2 dissociation energy (E_b^{dis}) values of 0.14 eV for Ti₂C and below the chemical accuracy of 0.04 eV for Mo_2N . The (E_b^{dis}) on Mo_2C MXene is 0.31, which is suitable for CO2 facile dissociation. The outcomes indicated that the RWGS catalysis occurs in a two-step process because the hydrogenation step is essential to regenerate the MXene catalysis. When CO₂ is adsorbed on the MXene surface, it becomes O-covered, demanding an additional step to restore the employed catalyst. Hence, surface termination type and concentration influence the catalytic activity of MXenes in CO2 hydrogenation. H2-treatment of MXenes with surface terminations can significantly change their catalytic performance for CO₂ hydrogenation. For example, a T_x-free, Mo-terminated 2D-Mo₂C is catalytically more active than Mo₂CT_x, β- Mo₂C, and Cu-ZnO-Al₂O₃ [394].

4.1.3. Hydrogenation of nitro derivative compounds

Hydrogenation of nitro-substituted materials into amines is vital in industrial applications. However, selective hydrogenation, meaning targeting a given functional group (in the case of nitro derivatives, $-\mathrm{NO}_2$ group), is formidable, calling for developing novel materials to progress the hydrogenation reaction toward desirable products [395]. Thanks to their chemoselective properties and paramount activity due to the presence of dispersed particles, heterogeneous metal-based catalysts hold promise for selective catalytic hydrogenation of nitro derivatives to fabricate favorable materials [396]. Several reports have been published on the potential application of MXene-based catalysts in the progression of nitro compounds' reduction reactions. For instance, Li and coworkers [397] synthesized functionalized core-shell MXene composites through the layer-by-layer (LBL) self-assembly procedure by amine-containing polyethyleneimine (PEI) and carboxyl-containing polyacrylic acid

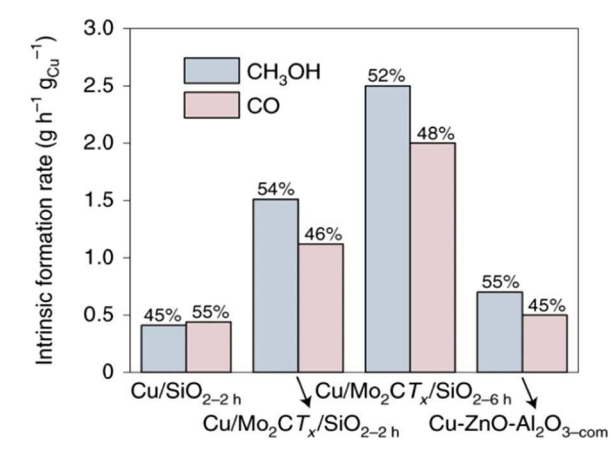
(PAA), with the final chemical formula of MXene-COOH@(PEI/PAA)n@AuNPs ("n" denotes the number of shell structures) and for the hydrogenation of 2- and 4-nitrophenol (2- and 4-NP). Their results indicated that the optimum composition MXene-COOH@(PEI/-PAA)₁₀@AuNPs possessed the best stability and repeatability after nine successive cycles of deployment (~90% conversion). Fan et al. [398] carried out a study in 2018 where PdNPs were uniformly dispersed onto the surface of an alk-Ti₃C₂T_r MXene (alk = alkaline) to fabricate a catalyst for the reduction of 4-NP to 4-aminophenol (4-AP). The well-dispersed PdNPs endowed the catalyst with available active sites to promote the complete conversion and selective hydrogenation of 4-NP to 4-AP in 70 min. Moreover, the resultant catalyst demonstrated no substantial loss in efficiency after seven cycles, showcasing its capability to be a promising candidate for multifarious catalytic reactions. Table 10 summarizes recent research studies on the use of MXene and MAX-based catalysts in the reduction of nitro derivatives.

4.1.4. Furfural hydrogenation

Harnessing novel non-fossil substances is a crucial step to producing fuel in energy areas. Furural is a bio-based material derived from lignocellulose, which can be employed to manufacture various products through the hydrogenation reaction. In particular, ~62% of this hydrogenation product is furfuryl alcohol, which further converts into tetrahydro furfuryl alcohol (THFA), 2-methylfuran (MF), and 2-methyltetrahydrofuran (MTHF) [402]. Naguib et al. [403] have reported the utilization of Ti₃C₂T_x and Ti₃CNT_x MXenes for hydrogenation of furfural to furfuryl alcohol. Despite their similar activities (72 mmol.g⁻¹.h⁻¹ for Ti₃CNT_x and 88 mmol.g⁻¹.h⁻¹ for Ti₃C₂T_x) and selectivities (49% for Ti₃CNT_x and 52% for Ti₃C₂T_x), Ti₃CNT_x was more stable than Ti₃C₂T_x, which was justified by the fact that Ti₃C₂T_x was enriched with abundant OH surface terminations, leading to the intercalation reactions between the layers and faster deactivation. In contrast, the N atom in Ti₃CNT_x outstandingly diminished OH terminations, resulting in a decrease in the intercalation reactions.

4.1.5. Selective hydrogenation of butadiene to butene

Selective hydrogenation is crucial in industrial processes, albeit challenging due to the potential hydrogenation of various functional groups [395,404]. Yan et al. [405] have demonstrated the capability of ${\rm Ti}_3{\rm C}_2{\rm T}_x$ MXene to serve as a support for atomically dispersed Pt/Pd nanoparticles, owing to its ability to provide vacancies for single atoms. ${\rm Ti}_3{\rm C}_2{\rm T}_x/{\rm Pt}$ -Pd catalysts have proven effective in the selective hydrogenation of butadiene, a process important for generating butenes, key monomers in the polymer industry. This study investigates the effect of different etching methods on the catalytic hydrogenation of butadiene. It was found that the LiF-HCl method is preferable to the HF method due



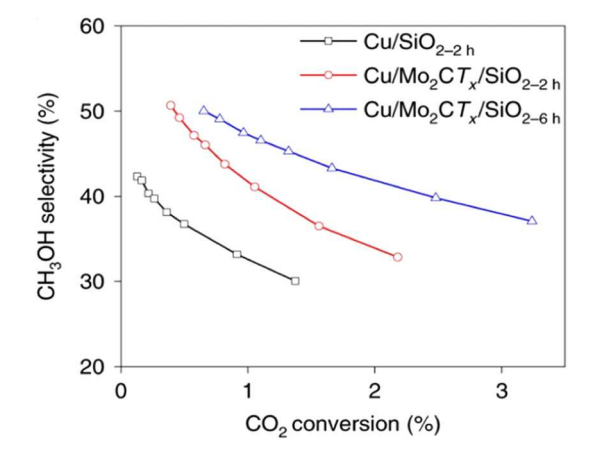


Fig. 21. Comparison of Cu/SiO_2 containing Mo_2CT_x MXene and pristine Cu/SiO_2 regarding (a) performance in intrinsic methanol formation rate and (b) methanol selectivity. Reprinted with permission from [392].

Table 10
Catalytic performance of MXene and MAX-based catalysts in hydrogenation reactions of nitro derivatives.

| Catalyst | Reactant | Conversion (%) | Reaction time | Ref. |
|--|--------------------------|----------------|---------------|-------|
| Pd/Ti ₃ C ₂ T _x ⊂graphene hydrogels | 4-Nitroaniline | 91 | 1 min | [399] |
| | 4- Chloronitrobenzene | ~15 | 1 min | |
| | 4-Bromonitrobenzene | ~48 | 1 min | |
| | 4-Nitrotoluene | ~63 | 1 min | |
| | 4-Nitrophenol | ~70 | 1 min | |
| 0.0005 wt% Pd/Ti ₃ SiC ₂ DP | 4-Nitrostyrene | 100 | - | [400] |
| $Pt/Ti_3C_2T_x-D^a-AB^b$ | 4- Chloronitrobenzene | 100 | 1 h | [401] |
| 021 | 2- Chloronitrobenzene | 100 | 1.5 h | |
| | 3- Chloronitrobenzene | 100 | 2 h | |
| | 4-Nitrotoluene | 100 | - | |
| | 2-Nitrotoluene | 100 | - | |
| | 2-Methoxi-1-nitrobenzene | 100 | 3 h | |
| | 4-Nitrophenol | 100 | 1.5 h | |
| | 2-Fluoronitrobenzene | 100 | - | |
| | Nitrobenzene | 100 | 1 h | |
| $Pt/Ti_3C_2T_{x}-D^a-SB^c$ | 4- Chloronitrobenzene | 40.4 | - | |

^a D=decorated on

to its safer nature and efficient delamination, resulting in enhanced metal dispersion and facile unstacking with solid substrates. These two factors contribute significantly to notable hydrogenation performances.

4.1.6. Fischer-Tropsch process

The Fischer–Tropsch (F-T) process has long been used to produce chemicals and fuels through the hydrogenation of CO [406]. The F-T

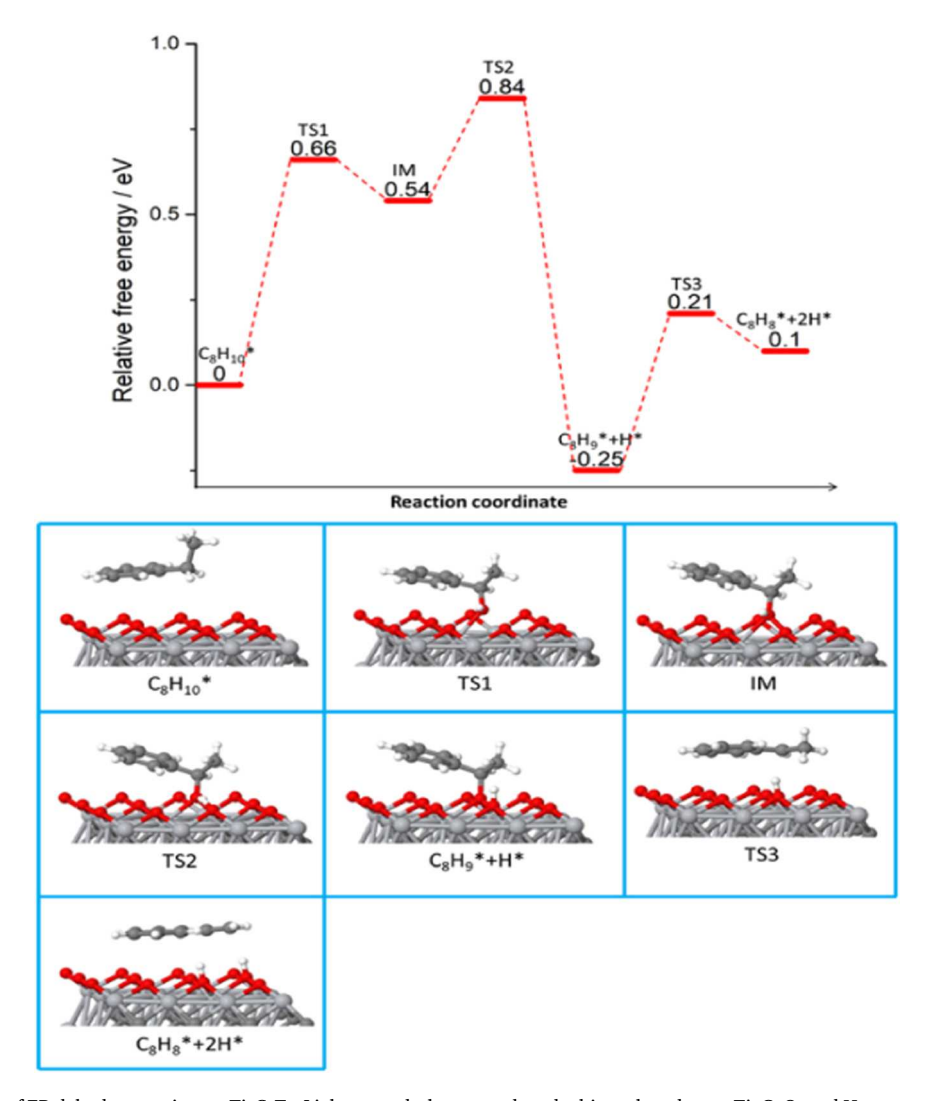


Fig. 22. Reaction pathway of EB dehydrogenation on $Ti_3C_2T_x$. Light gray, dark gray, red, and white colors denote Ti, C, O, and H atoms, respectively. Reprinted with permission from [409].

^b AB= ammonia borane (reducing agent)

^c SB= sodium borohydride

reaction is [407]:

$$(2n+1)H_2 + nCO \rightarrow C_nH_{(2n+2)} + nH_2O$$
 (7)

Kountoupi et al. [408] found that Mo₂CT_x-derived catalysts can be employed for this reaction. Their results indicated that the selectivity of the F-T reaction is contingent upon the coverage of surface oxygen and carbide content. In this regard, Mo₂CT_x pretreated at 500 °C (Mo₂CT_{x-500}) in undiluted H₂ is more active than Mo₂CT_x pretreated at 400 °C (Mo₂CT_{x-400}), which is ascribed to the oxygen content. Moreover, the study revealed that these two catalysts differ in selectivity at ca. 90% CO conversion. Specifically, Mo₂CT_{x-400} is more selective towards C₅₊ alkanes and Mo₂CT_{x-500} to methane (55 and 61%, respectively). This discrepancy is related to the differences in the structure (and the active sites) and, in particular, the substoichiometric carbidic carbon content in Mo₂CT_{x-400}. Also, DFT calculations indicated substantial differences between the reaction barriers and the stability of intermediates on 2D-Mo₂C and those achieved for 3D-Mo₂C, with H-assisted CO dissociation pathway (leading to HCO* and COH* intermediates) being dominant in the latter and carbidic chain growth mechanism in the former.

4.2. Dehydrogenation reactions

The production of alkene monomers from hydrocarbons is of great importance, specifically in the polymer industry. However, these reactions require high temperatures (~600 °C) and high levels of steam, and the lack of stability of their catalysts due to coke formation is a major issue. MXenes have been found to serve as catalysts or supports for direct dehydrogenation (DDH) of oxidative dehydrogenation (ODH) reactions [55]. One of the DDH applications of MXenes is the synthesis of styrene, a pivotal monomeric compound, from ethylbenzene (EB). Specifically, Diao et al. [409] conducted research associated with Ti₃C₂T_x MXene-catalyzed EB dehydrogenation. They prepared a Ti₃C₂T_x MXene terminated with O groups through an etching method, the dehydrogenation pathway of which is depicted in Fig. 22. The as-synthesized Ti₃C₂T_x MXene led to an EB conversion rate of 92 μmol m⁻² h⁻¹, whereas those of graphene, nanodiamond, and TiC-derived carbon (TiC-CDC) were 12, 7, and 0.8 μmol m⁻² h⁻¹, respectively. Furthermore, the styrene selectivity of the MXene-based catalyst was as high as 97.5%, which was comparable to other mentioned carbon catalysts (Fig. 23A). A long-run stability test was also conducted to confirm the long-term activity of the Ti₃C₂T_x catalyst. Interestingly, the outcomes indicated that EB conversion rate (%) remained at 21% for nearly 40 h, demonstrating no deactivation and coke formation (Fig. 23B).

4.3. Oxidation of CH4 and CO

Methane (CH₄) is considered one of the most critical fuel gases in a myriad of industrial applications. Nonetheless, CH₄ can be converted into methanol in a stepped manner because it is challenging to stop the product selectively after the first C-H activation without deactivating the catalyst [410]. Consequently, potential catalysts are necessary for directly converting methane to methanol. In this regard, MXenes have proven efficient as applicable supports for SACs. For instance, Sun and coworkers [411] modeled Mo₂CO₂-supported Pd monomer and dimer (Pd₂) and compared their abilities in methane conversion to methanol. The electronic and geometrical configurations results showed that Mo₂CO₂ can support anchor Pd dimer. Additionally, calculations illustrated the suitable adsorption of CH₄ and O₂ onto the Pd₂/Mo₂CO₂ surface due to its multiple active sites.

The seemingly facile CO oxidation reaction:

$$CO + \frac{1}{2}O_2 \rightarrow CO_2 \tag{8}$$

is of great significance in controlling pollution and the separation of CO from H_2 fuel [412]. In this regard, heterogeneous catalysts like Pd

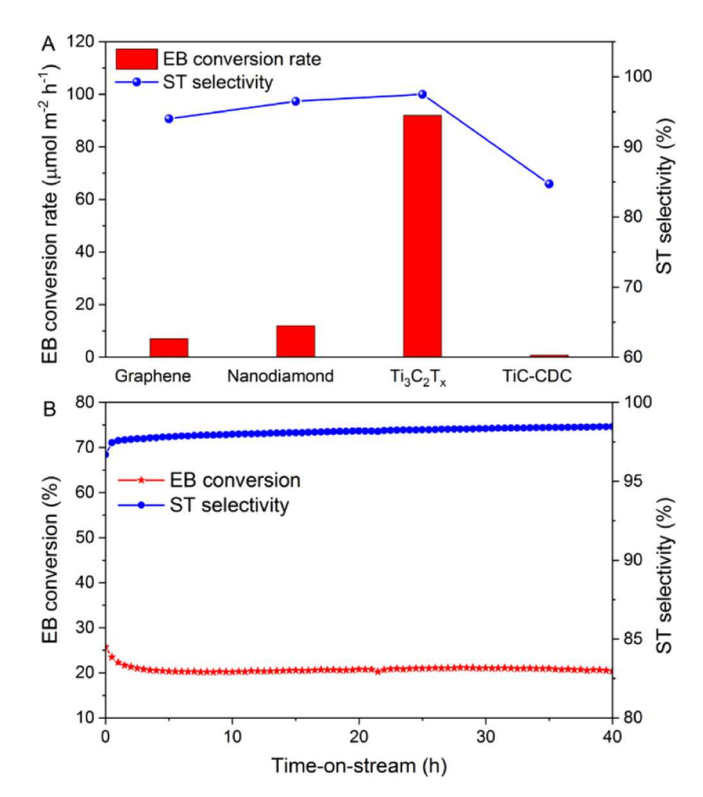


Fig. 23. (A) Comparison of EB conversion rate and styrene (ST) selectivity between $Ti_3C_2T_x$ MXene and three carbon-based catalysts and (B) the stability test of $Ti_3C_2T_x$ MXene on dehydrogenation of EB. Reprinted with permission from [409].

and Cu can be potentially harnessed to accelerate this reaction [413]. From a theoretical standpoint, MXenes can be potentially utilized as heterogeneous catalysts for CO oxidation, for which three possible reaction pathways are plausible: the Langmuir—Hinshelwood (LH), the traditional Eley-Rideal (ER), and the trimolecular Eley-Rideal (TER) mechanisms [414]. Among these pathways, the LH mechanism is the most feasible, although the occurrence of the appropriate pathway generally depends on the level of the rate-determining energy barrier [415]. Schematics of CO oxidation through LH and ER mechanisms on Ag(111) surfaces are depicted in Fig. 24.

Computational methods such as ab initio molecular dynamics have shown dynamic and thermal stabilities of Mo₂CS₂ monolayer [417]. Peng and coworkers [418] modeled a Ti₂CN₂ MXene-supported Zn catalyst and investigated its performance in CO oxidation. DFT calculations revealed that ER is the most probable mechanism for CO oxidation with a tiny barrier (only 0.06 eV), allowing the reaction to progress at low temperatures. In the ER mechanism, CO reacts with already pre-adsorbed O_2 and proceeds as follows: $CO + O_2^* \rightarrow CO_2 + O^*$ and $CO + O^* \rightarrow CO_2$. Based on the density of states, Bader charge, and other electronic structure analysis, the high catalytic activity of Ti₂CN₂/Zn was attributed to the structure of single atom Zn, which instigates the activation of O-O bond. In a comparative study, Cai et al. [419] computationally assessed the catalytic activity of Sc and Ti-anchored Zr₂CO₂ (MXene) in CO oxidation in incomplete combustion gas (O2, CO, N2, and CO2). Due to its high barrier energy, the Ti/Zr2CO2 catalyst was more efficacious than Sc/Zr₂CO₂. According to DFT studies, they concluded that CO oxidation can progress by both LH and ER mechanisms. In addition, after O2 was adsorbed, it remarkably remained to replace other pre-adsorbed gases, showcasing that both catalysts could resist the disturbance of the major gases so that a CO oxidation reaction was possible. A systematic DFT investigation of the catalytic activity of Ti₂CO₂ MXene-supported single atom catalysts M₁/Ti₂CO₂ (M = Fe, Co, Ni, Cu Ru, Rh, Pd, Ag Os, Ir, Pt, Au) by Zhu et al. [420]

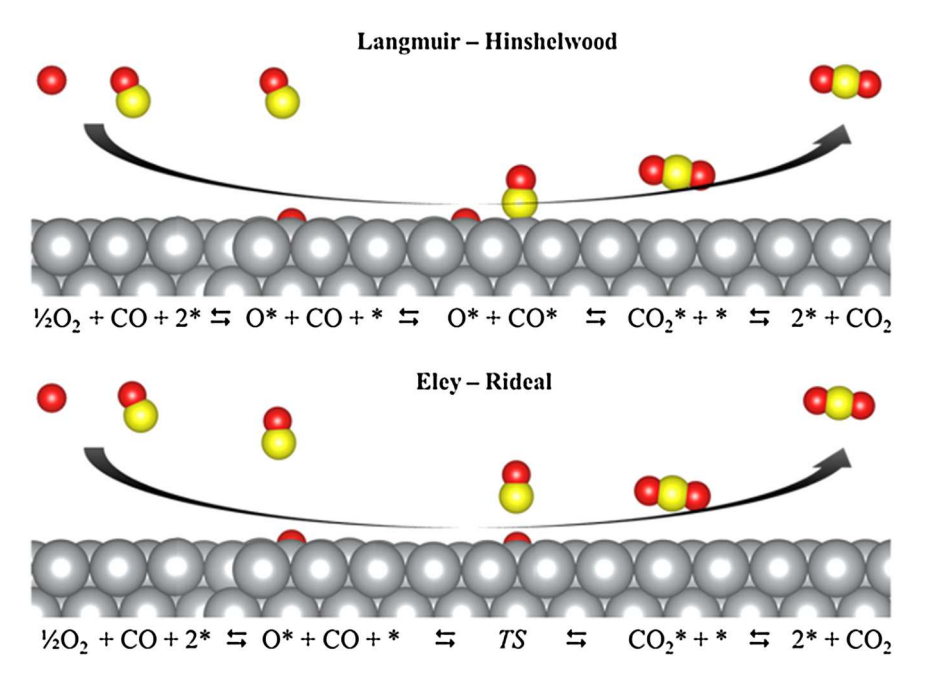


Fig. 24. Different mechanisms of CO oxidation on Ag(111) surface: (a) Langmuir– Hinshelwood mechanism of CO and O₂ co-adsorption and (b) Eley–Rideal mechanism of just O₂ adsorption. TS denotes the transition state. Reprinted with permission from [416].

relvealed that the Fe-containing catalyst, with a distinct low-energy barrier (0.2 eV), has the most favorable catalytic performance.

4.4. Dry reforming of methane

DRM reaction is the reaction of CH_4 and CO_2 that generates CO and H_2 , which in turn allows to alleviate CH_4 and CO_2 concentrations as greenhouse gases [421]:

$$CH_4 + CO_2 \rightarrow CO + 2H_2 \tag{9}$$

Thakur et al. [422] investigated the catalytic performance of V₂O₃-V₈C₇. In this research, an m-V₂CT_x MXene was utilized as a precursor to the 3D V₂O₃-V₈C₇ phases since, like other multilayered thin MXenes, m-V₂CT_x MXene is unstable at high temperatures [423]. Therefore, the m-V₂CT_x phase was initially pre-treated in N₂ at 800 °C, decomposing m-V₂CT_r to V₂O₃-V₈C₇, which was then utilized as a catalyst. The study showed that the DRM activity of V2O3-V8C7 (converting 78% CH₄ and 82% CO₂) is comparable to that of the nickel catalyst supported on zeolite Socony Mobil-5 (ZSM-5). Furthermore, it was discovered that stability in high temperatures, anti-oxidation characteristics under mild oxidative situations, and the ability to participate in oxidation-carburization cycles are pivotal properties in the dry reforming of methane and other hydrocarbons. Although a MXene was not used as a direct catalyst in DRM, it was employed as a precursor for the leading catalysts. In another research, Kurlov et al. [424] dispersed Mo₂CO₂ MXene on silica, showing high catalytic activity and stability in the dry reforming of CH₄. DFT calculations verified CH₄ activation on oxygen sites to form *OCH₃ and *OH. It is worth mentioning that the idea of depositing Mo₂CO₂ on the surface of silica was to hinder the thermal transformation into bulk Mo₂C, augmenting the accessibility of Mo sites and hampering catalyst deactivation. The results indicated that the consumption rate of CH₄ using Mo₂CO₂/SiO₂ was ~10-200 times higher compared to the bulk counterpart. Huang et al. [425] also conducted research on a sintered V₂C-V₂O₃ (m-V₂C-V₂O₃)-supported Ni as a potential heterogeneous catalyst for DRM. The synthesized catalyst showed high stability and activity in a 90-hour cycle of utilization. Ni/m-V₂C-V₂O₃ led to optimal CH₄ and CO₂ conversion rates of 94% and 89%, respectively.

5. Conclusion and perspectives

In conclusion, the versatile and remarkable properties exhibited by MXenes underscore their potential across a spectrum of applications, ranging from electromagnetic interference shielding to flexible opto-electronics, sensors, thermal heaters, and nanocomposites. The recent surge in exploring MXenes as heterogeneous catalysts for diverse reactions reflects a strategic response to the challenges posed by the scarcity and elevated costs of noble metals inherent in traditional catalysts. MXenes, with their abundance and cost-effectiveness, present a viable alternative that has garnered significant research attention.

This review has provided a summary of recent advances in leveraging MXenes for catalytic activities, emphasizing their efficacy in reactions such as hydrogen evolution, oxygen evolution, oxygen reduction, nitrogen reduction, carbon dioxide reduction, alcohol oxidation, hydrogenation, dehydrogenation, methanol conversion, dry reforming of methane, and Fischer-Tropsch synthesis. The exploration of these catalytic applications has opened new avenues for MXenes, expanding their role beyond traditional material applications.

Despite these promising developments, challenges persist, and further research is required to address issues such as scalability, stability, and optimization of catalytic performance. As the field continues to evolve, this review serves as a valuable resource for researchers, offering insights into the current state of MXene-based catalysis, highlighting challenges, and outlining prospective directions for future investigations. The inexhaustible potential of MXenes in catalysis positions them as pivotal contributors to the ongoing evolution of advanced materials and catalytic technologies.

Declaration of Competing Interest

The authors declare the following financial interests/personal relationships which may be considered as potential competing interests: Masoud Soroush reports financial support was provided by National Science Foundation. Masoud Soroush reports a relationship with National Science Foundation that includes: funding grants. If there are other authors, they declare that they have no known competing financial interests or personal relationships that could have appeared to influence the work reported in this paper.

Acknowledgments

M.S. would like to acknowledge financial support from the U.S. National Science Foundation under Grant No. CMMI-2134607. Any opinions, findings, and conclusions or recommendations expressed in this material are those of the authors and do not necessarily reflect the views of the National Science Foundation. The authors would also like to thank the anynomous reviewers for their careful constructive comments.

References

- [1] Y. Yan, P. Zhang, Z. Qu, M. Tong, S. Zhao, Z. Li, M. Liu, Zhiqun Lin, Carbon/sulfur aerogel with adequate mesoporous channels as robust polysulfide confinement matrix for highly stable lithium–sulfur battery, Nano Lett. 20 (2020) 7662–7669, https://doi.org/10.1021/acs.nanolett.0c03203.
- [2] M. Liu, P. Zhang, Z. Qu, Y. Yan, C. Lai, T. Liu, S. Zhang, Conductive carbon nanofiber interpenetrated graphene architecture for ultra-stable sodium ion battery, Nat. Commun. 10 (2019), https://doi.org/10.1038/s41467-019-11925-
- [3] Y. Wang, J. Mao, X. Meng, L. Yu, D. Deng, X. Bao, Catalysis with two-dimensional materials confining single atoms: concept, design, and applications, Chem. Rev. 119 (2019) 1806–1854, https://doi.org/10.1021/acs.chemrev.8b00501.
- [4] Y. Xue, G. Zhao, R. Yang, F. Chu, J. Chen, L. Wanga, X. Huang, 2D metal-organic framework-based materials for electrocatalytic, photocatalytic and thermocatalytic applications, Nanoscale 13 (2021) 3911–3936, https://doi.org/ 10.1039/D0NR09064F
- [5] X. Cai, Y. Luo, B. Liu, H.M. Cheng, Preparation of 2D material dispersions and their applications, Chem. Soc. Rev. 47 (2018) 6224–6266, https://doi.org/ 10.1030/CRCS00254A
- [6] Y. Chen, Z. Fan, Z. Zhang, W. Niu, C. Li, N. Yang, B. Chen, H. Zhang, Twodimensional metal nanomaterials: synthesis, properties, and applications, Chem. Rev. 105 (2005) 185–212, https://doi.org/10.1021/cr0204606.
- [7] D. Geng, X. Zhao, Z. Chen, W. Sun, W. Fu, J. Chen, W. Liu, W. Zhou, K.P. Loh, Adv. Mater. 29 (2017), https://doi.org/10.1002/adma.201700072.
- [8] L. Jiang, D. Zhou, J. Yang, S. Zhou, H. Wang, X. Yuan, J. Liang, X. Li, Y. Chen, H. Li, 2D Single- and few-layered mxenes: synthesis, applications and perspectives, Mater. Chem. A. 10 (2022) 13651–13672, https://doi.org/ 10.1007/DXTAST2P.
- [9] M. Malaki, X. Jiang, H. Wang, R. Podila, H. Zhang, P. Samorì, R.S. Varma, MXenes: from past to future perspectives, J. Chem. Eng. 463 (2023), https://doi. org/10.1016/j.cej.2023.142351.
- [10] Y. Yang, Y. Xu, Q. Li, Y. Zhanga, H. Zhou, Two-dimensional carbide/nitride (MXene) materials in thermal catalysis, Mater. Chem. A. 10 (2022) 19444–19465, https://doi.org/10.1039/D2TA03481F.
- [11] Z. Xie, Y. Duo, Z. Lin, T. Fan, C. Xing, L. Yu, R. Wang, M. Qiu, Y. Zhang, Y. Zhao, X. Yan, H. Zhang, The Rise of 2D photothermal materials beyond graphene for clean water production, Adv. Sci. 7 (2020), https://doi.org/10.1002/advs.201902236.
- [12] Two-Dimensional Nanomaterials for Photothermal Therapy, Angew. Chem. Int. Ed. 59 (15) (2020) 5890–5900.
- [13] V.Hiep Nguyen, R. Tabassian, S. Oh, S. Nam, M. Mahato, P. Thangasamy, A. Rajabi-Abhari, W.Jun Hwang, A.Kamal Taseer, I.Kwon Oh, Stimuli-responsive mxene-based actuators, Adv. Funct. Mater. 30 (2020), https://doi.org/10.1002/ adfm.201909504.
- [14] C. Lamy, A. Lima, V. LeRhun, F. Delime, C. Coutanceau, J.Michel Léger, Recent advances in the development of direct alcohol fuel cells (DAFC), J. Power Sources 105 (2002) 283–296, https://doi.org/10.1016/S0378-7753(01)00954-5.
- [15] A. Ghaffarkhah, M. Kamkar, Z.Azimi Dijvejin, H. Riazi, S. Ghaderi, K. Golovin, M. Soroush, M. Arjmand, High-Resolution Extrusion Printing of Ti₃C₂-based inks for wearable human motion monitoring and electromagnetic interference shielding, Carbon 191 (2022) 277–289, https://doi.org/10.1016/j.carbon.2022.02.003.
- [16] A. Ghaffarkhah, S.Alireza Hashemi, S. Rostami, M. Amini, F. Ahmadijokani, A. Pournaghshband Isfahani, S.E. Mhatre, O.J. Rojas, M. Kamkar, S. Wuttke, M. Soroush, M. Arjmand, Ultra-Flyweight Cryogels of MXene/graphene oxide for electromagnetic interference shielding, Adv. Funct. Mater. 33 (2023) 2304748, https://doi.org/10.1002/adfm.202304748.
- [17] M.J. Ledoux, C.Pram Huu, J. Guille, H. Dunlop, Compared ACtivities of Platinum and High Specific Surface Area Mo₂C and WC catalysts for reforming reactions: i. catalyst activation and stabilization: reaction of n-Hexane, J. Catal. 134 (1992) 383–398, https://doi.org/10.1016/0021-9517(92)90329-G.
- [18] R.B. Levy, M. Boudart, Platinum-like behavior of tungsten carbide in surface catalysis, J. Sci. 181 (1973), https://doi.org/10.1126/science.181.4099.547.
- [19] A. Michaelides, P. Hu, Catalytic water formation on platinum: a first-principles study, J. Am. Chem. Soc. 123 (2001) 4235–4242, https://doi.org/10.1021/ ia003576x.
- [20] A.W. Aldag, L.D. Schmidt, Interaction of hydrogen with palladium, J. Catal. 22 (1971) 260–265, https://doi.org/10.1016/0021-9517(71)90193-X.
- [21] T. Paryjczak, W.K. Jóźwiak, J. Góralski, Interactions between oxygen, hydrogen and supported rhodium over a wide temperature range: i. oxygen and hydrogen adsorption, J. Chromatogr. A. 166 (1978) 65–74, https://doi.org/10.1016/ S0021-9673(00)92250-7.

- [22] M. Naguib, V.N. Mochalin, M.W. Barsoum, Y. Gogotsi, 25th anniversary article: mxenes: a new family of two-dimensional materials, Adv. Mater. 26 (2014) 992–1005, https://doi.org/10.1002/adma.201304138.
- [23] R. Gautam, N. Marriwala, R. Devi, A review: study of mxene and graphene together, Meas. Sens. 25 (2023), https://doi.org/10.1016/j. measen.2022.100592.
- [24] D.D.V. Dhinakaran, B. Hun-Soo, MXenes: an emerging 2d material, Carbon 192 (2022) 366–383, https://doi.org/10.1016/j.carbon.2022.03.004.
- [25] Y. Gogotsi, B. Anasori, The rise of MXenes, ACS Nano 13 (2019) 8491–8494, https://doi.org/10.1021/acsnano.9b06394.
- [26] M. Naguib, M. Kurtoglu, V. Presser, J. Lu, J. Niu, M. Heon, L. Hultman, Y. Gogotsi, M.W. Barsoum, Two-dimensional nanocrystals produced by exfoliation of Ti₃AlC₂, Adv. Mater. 23 (2011) 4248–4253, https://doi.org/ 10.1002/adma.201102306.
- [27] W. Hong, B.C. Wyatt, S.Kartik Nemani, B. Anasori, Double Transition-Metal MXenes: atomistic design of two-dimensional carbides and nitrides, MRS Bull. 45 (2020) 850–861, https://doi.org/10.1557/mrs.2020.251.
- [28] B. Anasori, Y. Gogotsi, MXenes: trends, growth, and future directions, Graph. 2D Mater. 7 (2022) 75–79, https://doi.org/10.1007/s41127-022-00053-z.
- [29] X. Xiao, H. Wang, P. Urbankowski, Y. Gogotsi, Topochemical synthesis of 2d materials, Chem. Soc. Rev. 7 (2019) 8744–8765, https://doi.org/10.1039/ C8CS00649K.
- [30] M. Malaki, A. Malekib, R.S. Varma, MXenes and ultrasonication, Mater. Chem. A. 7 (2019) 10843–10857, https://doi.org/10.1039/C9TA01850F.
- [31] A. VahidMohammadi, J. Rosen, Y. Gogotsi, The world of two-dimensional carbides and nitrides (MXenes), J. Sci. 372 (2021) 10843–10857, https://doi.org/ 10.1126/science.abf1581.
- [32] K.A. Papadopoulou, A. Chroneos, D. Parfitt, S.Richard G. Christopoulos, A perspective on mxenes: their synthesis, properties, and recent applications, J. Appl. Phys. 128 (2020), https://doi.org/10.1063/5.0021485.
- [33] L. Verger, V. Natu, M. Carey, M.W. Barsoum, MXenes: an introduction of their synthesis, select properties, and applications, Trends Chem. 1 (2019) 656–669, https://doi.org/10.1016/j.trechm.2019.04.006.
- [34] P. Huang, W.Qiang Han, Recent advances and perspectives of lewis acidic etching route: an emerging preparation strategy for MXenes, Nano-Micro Lett. 15 (2023), https://doi.org/10.1007/s40820-023-01039-z.
- [35] S. Siddique, A. Waheed, M. Iftikhar, M.Taqi Mehran, M.Zafar Zarif, H.A. Arafat, S. Hussain, F. Shahzad, Fluorine-free mxenes via molten salt lewis acidic etching: applications, challenges, and future outlook, Prog. Mater. Sci. 132 (2023), https://doi.org/10.1016/j.pmatsci.2023.101183.
- [36] L. Liu, M. Orbay, S. Luo, S. Duluard, H. Shao, J. Harmel, P. Rozier, P. Louis Taberna, P. Simon, Exfoliation and Delamination of Ti₃C₂T_x MXene prepared via molten salt etching route, ACS Nano 16 (2022) 111–118, https://doi.org/10.1021/acsnano.1c08498.
- [37] W. Hu, M. Yang, T. Fan, Z. Li, Y. Wang, H. Li, G. Zhu, J. Li, H. Jin, L. Yu, A Simple, Efficient, Fluorine-Free Synthesis Method of MXene/Ti₃C₂T_x anode through molten salt etching for sodium-ion batteries, Battery Energy 2 (2023), https://doi.org/10.22541/au.168665406.61851863/v1
- [38] Y. Wei, P. Zhang, R.A. Soomro, Q. Zhu, B. Xu, Advances in the synthesis of 2D MXenes, Adv. Mater. 33 (2021), https://doi.org/10.1002/adma.202103148.
- [39] U. Khan, B. Gao, L.Bing Kong, Z. Chen, W. Que, Green synthesis of fluorine-free mxene via hydrothermal process: a sustainable approach for proton supercapacitor electrodes, Electrochim. Acta 475 (2024) 1242–1247, https://doi. org/10.1016/j.electacta.2023.143651.
- [40] D. Wang, C. Zhou, A.S. Filatov, W. Cho, F. Lagunas, M. Wang, S. Vaikuntanathan, C. Liu, R.F. Klie, D.V. Talapin, Direct synthesis and chemical vapor deposition of 2d carbide and nitride mXenes, J. Sci. 379 (2023) 1242–1247, https://doi.org/ 10.1126/science.add9204.
- [41] Y. Zhu, J. Liu, T. Guo, J. Jing Wang, X. Tang, V. Nicolosi, Multifunctional Ti3C2Tx MXene composite hydrogels with strain sensitivity toward absorptiondominated electromagnetic-interference shielding, ACS Nano 15 (2021) 1465–1474, https://doi.org/10.1021/acsnano.0c08830.
- [42] J. Halim, M.R. Lukatskaya, K.M. Cook, J. Lu, C.R. Smith, L.Åke Näslund, S.J. May, L. Hultman, Y. Gogotsi, P. Eklund, M.W. Barsoum, Transparent conductive twodimensional titanium carbide epitaxial thin films, Chem. Mater. 26 (2014) 2374–2381, https://doi.org/10.1021/cm500641a.
- [43] S. Yang, P. Zhang, F. Wang, A.Gaetano Ricciardulli, M.R. Lohe, P.W.M. Blom, X. Feng, Fluoride-free synthesis of two-dimensional titanium carbide (MXene) using a binary aqueous system, Angew. Chem. Int Ed. Engl. 57 (2018) 15491–15495, https://doi.org/10.1002/ange.201809662.
- [44] X. Xie, Y. Xue, L. Li, S. Chen, Y. Nie, W. Dinga, Z. Wei, Surface Al Leached Ti3AlC2 as a Substitute for carbon for use as a catalyst support in a harsh corrosive electrochemical system, Nanoscale 6 (2014) 11035–11040, https://doi. org/10.1039/C4NR02080D.
- [45] M. Li, J. Lu, K. Luo, Y. Li, K. Chang, K. Chen, J. Zhou, J. Rosen, L. Hultman, P. Eklund, P.O.Å. Persson, S. Du, Z. Chai, Z. Huang, Q. Huang, Element replacement approach by reaction with lewis acidic molten salts to synthesize nanolaminated MAX phases and MXenes, J. Am. Chem. Soc. 141 (2019) 4730–4737, https://doi.org/10.1021/jacs.9b00574.
- [46] J. Mei, G.A. Ayoko, C. Hu, J.M. Bell, Z. Sun, Two-dimensional fluorine-free mesoporous Mo₂C MXene via UV-induced selective etching of Mo₂Ga₂C for Energy Storage, SMT 25 (2020), https://doi.org/10.1016/j.susmat.2020.e00156.
- [47] F. Shahzad, A. Iqbal, H. Kim, C.Min Koo, 2D Transition metal carbides (MXenes): applications as an electrically conducting material, Adv. Mater. 32 (2020), https://doi.org/10.1002/adma.202002159.

- [48] S.-Y. Pang, Y.-T. Wong, S. Yuan, Y. Liu, M.-K. Tsang, Z. Yang, H. Huang, W. T. Wong, J. Hao, Universal Strategy for HF-free facile and rapid synthesis of two-dimensional mxenes as multifunctional energy materials, J. Am. Chem. Soc. 141 (2019) 9610–9616, https://doi.org/10.1021/jacs.9b02578.
- [49] V. Kamysbayev, A.S. Filatov, H. Hu, X. Rui, F. Lagunas, D. Wang, R.F. Klie, D. V. Talapin, Covalent surface modifications and superconductivity of two-dimensional metal carbide MXenes, J. Sci. 369 (2020) 979–983, https://doi.org/10.1126/science.aba8311.
- [50] Y. Li, H. Shao, Z. Lin, J. Lu, L. Liu, B. Duployer, P.O.Å. Persson, P. Eklund, L. Hultman, M. Li, K. Chen, X.H. Zha, S. Du, P. Rozier, Z. Chai, E. Raymundo-Piñero, P.L. Taberna, P. Simon, Q. Huang, A General Lewis Acidic Etching Route for Preparing MXenes with enhanced electrochemical performance in nonaqueous electrolyte, Nat. Mater. 19 (2020) 894–899, https://doi.org/10.1038/ s41563-020-0657-0.
- [51] J.D. Gouveia, Á. Morales-García, F. Viñes, J.R.B. Gomes, F. Illas, MXenes à la Carte: Tailoring the epitaxial growth alternating nitrogen and transition metal layers, ACS Nano 16 (2020) 12541–12552, https://doi.org/10.1126/science. aba8311
- [52] Á. Morales-García, F. Calle-Vallejo, F. Illas, MXenes: new horizons in catalysis, ACS Catal. 10 (2020) 13487–13503, https://doi.org/10.1021/acscatal.0c03106.
- [53] I.M. Chirica, A.G. Mirea, Ş. Neaţu, M. Florea, M.W. Barsoum, F. Neaţu, Applications of MAX phases and mxenes as catalysts, Mater. Chem. A 9 (2021) 19589–19612, https://doi.org/10.1039/D1TA04097A.
- [54] K. Li, S. Zhang, Y. Li, J. Fan, K. Lv, MXenes as noble-metal-alternative co-catalysts in photocatalysis, Chin. J. Catal. A 42 (2021) 3–14, https://doi.org/10.1016/ \$1872-2067(20)63630-0
- [55] Y. Tan, Z. Zhu, X. Zhang, J. Zhang, Y. Zhou, H. Li, H. Qin, Y. Bo, Z. Pan, Nb₄C₃T_x (MXene) as a New stable catalyst for the hydrogen evolution reaction, Int. J. Hydrog. Energy 46 (2021) 1955–1966, https://doi.org/10.1016/j.iihydene.2020.10.046.
- [56] W. Yuan, L. Cheng, Y. An, H. Wu, N. Yao, X. Fan, X. Guo, MXene nanofibers as highly active catalysts for hydrogen evolution reaction, J, ACS Sustain Chem. Eng. 6 (2018) 8976–8982. https://doi.org/10.1021/acssuschemeng.8b01348.
- [57] X. Li, X. Lv, X. Sun, C. Yang, Y. -Zhen Zheng, L. Yang, S. Li, X. Tao, Edge-oriented, high-percentage 1T'-phase MoS₂ Nanosheets Stabilize Ti₃C₂ MXene for efficient electrocatalytic hydrogen evolution, Appl. Catal. 284 (2021) 8976–8982, https:// doi.org/10.1016/j.apcatb.2020.119708.
- [58] K.Rui Garrick Lim, A.D. Handoko, L.R. Johnson, X. Meng, M. Lin, G. Sandhya Subramanian, B. Anasori, Y. Gogotsi, A. Vojvodic, Z.Wei Seh, 2H-MoS₂ on Mo₂CT_x MXene nanohybrid for efficient and durable electrocatalytic hydrogen evolution, ACS Nano 14 (2020) 16140–16155, https://doi.org/10.1021/acsnano.0c08671.
- [59] S. Li, X. Que, X. Chen, T. Lin, L. Sheng, J. Peng, J. Li, Ma Zhai, One-Step Synthesis of Modified Ti₃C₂ MXene-supported amorphous molybdenum sulfide electrocatalysts by a facile gamma radiation strategy for efficient hydrogen evolution reaction, ACS Appl. Energy Mater. 3 (2020) 10882–10891, https://doi. org/10.1021/acsaem.0c01900.
- [60] S. Zhang, H. Zhuo, S. Li, Z. Bao, S. Deng, G. Zhuang, X. Zhong, Z. Wei, Z. Yao, J.-guo Wang, Effects of Surface Functionalization of MXene-based nanocatalysts on hydrogen evolution reaction performance, Catal. Today 368 (2021) 187–195, https://doi.org/10.1016/j.cattod.2020.02.002.
- [61] L. Yan, B. Zhang, S. Wub, J. Yub, A General Approach to the Synthesis of Transition Metal Phosphide Nanoarrays on MXene nanosheets for ph-universal hydrogen evolution and alkaline overall water splitting, J. Mater. Chem. 8 (2020) 14234–14242, https://doi.org/10.1039/D0TA05189F.
- [62] Z.Wei Seh, K.D. Fredrickson, B. Anasori, J. Kibsgaard, A.L. Strickler, M. R. Lukatskaya, Y. Gogotsi, T.F. Jaramillo, A. Vojvodic, Two-dimensional molybdenum Carbide (MXene) as an efficient electrocatalyst for hydrogen evolution, ACS Energy Lett. 1 (2016) 589–594, https://doi.org/10.1021/acsenersylett.6b00247.
- [63] M.H. Tran, T. Schäfer, A. Shahraei, M. Dürrschnabel, L. Molina-Luna, U.I. Kramm, Christina S. Birkel, Adding a New Member to the MXene family: synthesis, structure, and electrocatalytic activity for the hydrogen evolution reaction of V₄C₃T_x, ACS Appl. Energy Mater. 1 (2018) 3908–3914, https://doi.org/10.1021/ acsaem.8b00652.
- [64] S. Li, P. Tuo, J. Xie, X. Zhang, J. Xu, J. Bao, B. Pan, Y. Xie, Ultrathin MXene nanosheets with rich fluorine termination groups realizing efficient electrocatalytic hydrogen evolution, ChemSusChem 47 (2018) 512–518, https://doi.org/10.1016/j.nanoen.2018.03.022.
- [65] S. Li, P. Tuo, J. Xie, X. Zhang, J. Xu, J. Bao, B. Pan, Y. Xie, Oxygen-functionalized ultrathin Ti₃C₂T_x MXene for enhanced electrocatalytic hydrogen evolution, ChemSusChem 12 (2019) 1368–1373, https://doi.org/10.1002/cssc.201803032.
- [66] G. Qu, Y. Zhou, T. Wu, G. Zhao, F. Li, Y. Kang, C. Xu, Phosphorized MXene-phase molybdenum carbide as an earth-abundant hydrogen evolution electrocatalyst, ACS Appl. Energy Mater. 1 (2018) 7206–7212, https://doi.org/10.1021/ accept 8b01642
- [67] H. Wang, Y. Wu, X. Yuan, G. Zeng, J. Zhou, X. Wang, J.Wei Chew, Clay-inspired MXene-based electrochemical devices and photo-electrocatalyst: state-of-the-art progresses and challenges, Adv. Mater. 30 (2018), https://doi.org/10.1002/ adma.201704561.
- [68] J. Peng, X. Chen, W. -Jun Ong, X. Zhao, N. Li, Surface and heterointerface engineering of 2d mxenes and their nanocomposites: insights into electro- and photocatalysis, Chem 5 (2019) 18–50, https://doi.org/10.1016/j. chempr.2018.08.037.

- [69] Q. Jiang, N. Kurra, M. Alhabeb, Y. Gogotsi, H.N. Alshareef, All pseudocapacitive MXene-RuO₂ asymmetric supercapacitors, Adv. Energy Mater. 8 (2018), https://doi.org/10.1002/aenm.201703043.
- [70] L.R. Johnson, S. Sridhar, L. Zhang, K.D. Fredrickson, A.S. Raman, J. Jang, C. Leach, A. Padmanabhan, C.C. Price, N.C. Frey, A. Raizada, V. Rajaraman, S. Aparna Saiprasad, X. Tang, A. Vojvodic, MXene materials for the electrochemical nitrogen reduction—functionalized or Not? ACS Catal. 10 (2020) 253–264, https://doi.org/10.1021/acscatal.9b01925.
- [71] G. Gao, A.P. O'MullaneOrcid, A. Du, 2D MXenes: a new family of promising catalysts for the hydrogen evolution reaction, ACS Catal. 7 (2017) 494–500, https://doi.org/10.1021/acscatal.6b02754.
- [72] T. Yu Shuai, Q. -Ni Zhan, H. -Min Xu, C. -Jin Huang, Z. -Jie Zhanga, G. -Ren Li, Recent Advances in the synthesis and electrocatalytic application of mxene materials, Chem. Commun. 59 (2023) 3968–3999, https://doi.org/10.1039/ D2CC06418A.
- [73] H. -Jun Liu, B. Dong, Recent advances and prospects of MXene-based materials for electrocatalysis and energy storage, Mater. Today Phys. 20 (2021), https://doi.org/10.1016/j.mtphys.2021.100469.
- [74] M. Khazaei, A. Ranjbar, M. Arai, T. Sasakib, S. Yunoki, Electronic properties and applications of MXenes: a theoretical review, J. Mater. Chem. C. 5 (2017) 2488–2503, https://doi.org/10.1039/C7TC00140A.
- [75] L. Zhao, B. Dong, S. Li, L. Zhou, L. Lai, Z. Wang, S. Zhao, M. Han, K. Gao, M. Lu, X. Xie, B. Chen, Z. Liu, X. Wang, H. Zhang, H. Li, J. Liu, H. Zhang, X. Huang, W. Huang, Interdiffusion reaction-assisted hybridization of two-dimensional metal-organic frameworks and Ti₃C₂T_x nanosheets for electrocatalytic oxygen evolution, ACS Nano 11 (2017) 5800–5807, https://doi.org/10.1021/acsnano.7b01409.
- [76] S. Chu, A. Majumdar, Opportunities and challenges for a sustainable energy future, ACS Nano 488 (2012) 294–303, https://doi.org/10.1038/nature11475
- [77] B. Dunn, H. Kamath, J.-Marie Tarascon, Electrical energy storage for the grid: a battery of choices, J. Sci. 334 (2011) 928–935, https://doi.org/10.1126/ science.1212741.
- [78] A. Liu, X. Liang, X. Ren, W. Guan, M. Gao, Y. Yang, Q. Yang, L. Gao, Y. Li, T. Ma, Recent Progress in MXene-based materials: potential high-performance electrocatalysts, Adv. Funct. Mater. 30 (2020), https://doi.org/10.1002/ adfm.202003437.
- [79] W.-Jie Jiang, T. Tang, Y. Zhang, J. -Song Hu, Synergistic modulation of non-precious-metal electrocatalysts for advanced water splitting, Acc. Chem. Res 53 (2020) 1111–1123, https://doi.org/10.1021/acs.accounts.0c00127.
- [80] C. Wang, L. Jin, H. Shang, H. Xu, Y. Shiraishi, Y. Du, Advances in engineering RuO₂ electrocatalysts towards oxygen evolution reaction, Chin. Chem. Lett. 32 (2021) 2108–2116, https://doi.org/10.1016/j.cclet.2020.11.051.
- [81] R.Rafidah Raja Sulaiman, A. Hanan, J. Yu, W.Yin Wong, R. Mohamad Yunus, K. Shyuan Loh, R. Walvekar, V. Chaudhary, M. Khalid, Structurally modified mxenes-based catalysts for application in hydrogen evolution reaction: a review, Catalysts 12 (2022). https://doi.org/10.3390/catal12121576.
- [82] W. Ma, X. Zhang, W. Li, M. Jiao, L. Zhang, R. Ma, Z. Zhou, Advanced Pt-based electrocatalysts for the hydrogen evolution reaction in alkaline medium, Nanoscale 15 (2023) 11759–11776, https://doi.org/10.1039/D3NR01940C.
- [83] M.-Ibrahim Jamesh, M. Harb, Tuning the electronic structure of the earthabundant electrocatalysts for oxygen evolution reaction (OER) to achieve efficient alkaline water splitting – a review, J. Energy Chem. 56 (2021) 299–342, https://doi.org/10.1016/j.ijcchem.2020.08.001
- https://doi.org/10.1016/j.jechem.2020.08.001.
 [84] R. Qin, G. Chen, X. Feng, J. Weng, Y. Han, Ru/Ir-based electrocatalysts for oxygen evolution reaction in acidic conditions: from mechanisms, optimizations to challenges, Adv. Sci. (2024), https://doi.org/10.1002/advs.202309364.
- [85] Z. Guo, J. Zhou, L. Zhua, Z. Sun, MXene: a promising photocatalyst for water splitting, Mater. Chem. A 4 (2016) 11446–11452, https://doi.org/10.1039/ C6TA04414J.
- [86] M. Zubair, M.Muneeb Ul Hassan, M.Taqi Mehran, M.Mahmood Baig, S. Hussain, F. Shahzad, 2D MXenes and their heterostructures for HER, OER and overall water splitting: a review, Int. J. Hydrog. Energy 47 (2022) 2794–2818, https://doi.org/10.1016/j.ijhydene.2021.10.248.
- [87] J. Qiao, L. Kong, S. Xu, K. Lin, W. He, M. Ni, Q. Ruan, P. Zhang, Y. Liu, W. Zhang, L. Pan, Z. Sun, Research Progress of MXene-based catalysts for electrochemical water-splitting and metal-air batteries, Energy Storage Mater. 49 (2021) 509–530, https://doi.org/10.1016/j.ensm.2021.09.034.
- [88] J.D. Gouveia, Á. Morales-García, F. Viñes, F. Illas, J.R.B. Gomes, MXenes as promising catalysts for water dissociation, Appl. Catal. 260 (2020), https://doi. org/10.1016/j.apcatb.2019.118191.
- [89] M. Höök, X. Tang, Depletion of fossil fuels and anthropogenic climate change—a review, Energy Policy 52 (2013) 797–809, https://doi.org/10.1016/j. enpol.2012.10.046.
- [90] J.O. Abe, A.P.I. Popoola, E. Ajenifuja, O.M. Popoola, Hydrogen energy, economy and storage: review and recommendation, Int. J. Hydrog. Energy 44 (2019) 15072–15086, https://doi.org/10.1016/j.ijhydene.2019.04.068.
- [91] I. Dincer, C. Acar, Review and evaluation of hydrogen production methods for better sustainability, Int. J. Hydrog. Energy 40 (2015) 11094–11111, https://doi. org/10.1016/j.ijhydene.2014.12.035.
- [92] T.L. LeValley, A.R. Richard, M. Fan, The progress in water gas shift and steam reforming hydrogen production technologies – a review, Int. J. Hydrog. Energy 39 (2014) 16983–17000, https://doi.org/10.1016/j.ijhydene.2014.08.041.
- [93] X. Wang, Q. Meng, L. Gao, Z. Jin, J. Ge, C. Liu, W. Xing, Recent progress in hydrogen production from formic acid decomposition, Int. J. Hydrog. Energy 43 (2018) 7055–7071, https://doi.org/10.1016/j.ijhydene.2018.02.146.

- [94] E. Doustkhah, M. Hasani, Y. Ide, M.Hussein N. Assadi, Pd Nanoalloys for H₂ generation from formic acid, Int. J. ACS Appl. Nano Mater. 3 (2020) 22–43, https://doi.org/10.1021/acsanm.9b02004.
- [95] S. Sengodan, R. Lan, J. Humphreys, D. Du, W. Xu, H. Wang, S. Tao, Advances in reforming and partial oxidation of hydrocarbons for hydrogen production and fuel cell applications, Renew. Sust. Energ. Rev. 82 (2018) 761–780, https://doi. org/10.1016/j.jsser.2017.09.071
- [96] P. Mishra, S. Krishnan, S. Rana, L. Singh, M. Sakinah, Z. Ab Wahid, Outlook of fermentative hydrogen production techniques: an overview of dark, photo and integrated dark-photo fermentative approach to biomass, Energy Strategy Rev. 24 (2019) 27–37, https://doi.org/10.1016/j.esr.2019.01.001.
- [97] N. Fajrina, M. Tahir, A critical review in strategies to improve photocatalytic water splitting towards hydrogen production, Int. J. Hydrog. Energy 44 (2019) 540–577, https://doi.org/10.1016/ji.ijhydene.2018.10.200.
- [98] S.-Sha Yi, X.-Bo Zhang, B.-Ri Wulan, J.-Min Yan, Q. Jiang, Non-noble metals applied to solar water splitting, Energy Environ. Sci. 11 (2018) 3128–3156, https://doi.org/10.1039/C8EE02096E.
- [99] L. Yu, Q. Zhu, S. Song, B. McElhenny, D. Wang, C. Wu, Z. Qin, J. Bao, Y. Yu, S. Chen, Z. Ren, Non-noble metal-nitride based electrocatalysts for high-performance alkaline seawater electrolysis, Nat. Commun. 10 (2019) 3128–3156, https://doi.org/10.1038/s41467-019-13092-7.
- [100] J.D. Benck, T.R. Hellstern, J. Kibsgaard, P. Chakthranont, T.F. Jaramillo, Catalyzing the Hydrogen Evolution Reaction (HER) with molybdenum sulfide nanomaterials, ACS Catal. 4 (2014) 3957–3971, https://doi.org/10.1021/ cc500023c
- [101] Y. Jiao, Y. Zheng, M. Jaroniecb, S.Zhang Qiao, Design of electrocatalysts for oxygen- and hydrogen-involving energy conversion reactions, Chem. Soc. Rev. 44 (2015) 2060–2086, https://doi.org/10.1039/C4CS00470A.
- [102] Z. Kang, M.Arif Khan, Y. Gong, R. Javed, Y. Xu, D. Ye, H. Zhao, J. Zhang, Recent progress of mxenes and mxene-based nanomaterials for the electrocatalytic hydrogen evolution reaction, Mater. Chem. A 9 (2021) 6089–6108, https://doi. org/10.1039/D0TA11735H.
- [103] B. Ding, W.-Jun Ong, J. Jiang, X. Chen, N. Li, Uncovering the electrochemical mechanisms for hydrogen evolution reaction of heteroatom doped M₂C MXene (M = Ti, Mo), Appl. Surf. Sci. 500 (2020), https://doi.org/10.1016/j. ansusc 2019 143987
- [104] Z.-Feng Huang, J. Song, S. Dou, X. Li, J. Wang, X. Wang, Strategies to break the scaling relation toward enhanced oxygen electrocatalysis, Matter 1 (2019) 1494–1518, https://doi.org/10.1016/j.matt.2019.09.011.
- [105] N. Mahmood, Y. Yao, J.- Wen Zhang, L. Pan, X. Zhang, J.- Jun Zou, Electrocatalysts for hydrogen evolution in alkaline electrolytes: mechanisms, challenges, and prospective solutions, Adv. Sci. 5 (2018), https://doi.org/ 10.1002/advs.201700464.
- [106] C. Walter, P.W. Menezes, M. Driess, Perspective on intermetallics towards efficient electrocatalytic water-splitting, J, Chem. Sci. 12 (2021) 8603–8631, https://doi.org/10.1039/D1SC01901E.
- [107] L. Meng, F. Viñes, F. Illas, Theoretical modelling of the hydrogen evolution reaction on mxenes: a critical review, Curr. Opin. Electrochem. 40 (2023) 8603–8631, https://doi.org/10.1016/j.coelec.2023.101332.
- [108] S. Ma, X. Fan, Y. An, D. Yang, Z. Luo, Y. Hu, N. Guo, Exploring the catalytic activity of MXenes M_{n+1}C_nO₂ for Hydrogen Evolution, J. Mater. Sci. 54 (2019) 11378–11389, https://doi.org/10.1007/s10853-019-03712-4.
- [109] Y. Cheng, L. Wang, Y. Li, Y. Song, Y. Zhang, Etching and exfoliation properties of Cr₂AlC into Cr₂CO₂ and the electrocatalytic performances of 2D Cr₂CO₂ MXene, J. Phys. Chem. C. 123 (2019) 15629–15636, https://doi.org/10.1021/acs. jpcc.9b03120.
- [110] J. Liu, Y. Liu, D. Xu, Y. Zhu, W. Peng, Y. Li, F. Zhang, X. Fan, Hierarchical "Nanoroll" like MoS₂/Ti₃C₂T_x hybrid with high electrocatalytic hydrogen evolution activity, Appl. Catal. B 241 (2019) 89–94, https://doi.org/10.1016/j.apcatb.2018.08.083.
- [111] J. Liang, C. Ding, J. Liu, T. Chen, W.Chao Peng, Y. Li, F. Zhanga, X. Fan, Heterostructure Engineering of Co-Doped MoS₂ Coupled with Mo₂CT_x MXene for enhanced hydrogen evolution in alkaline media, Nanoscale 11 (2019) 10992–11000, https://doi.org/10.1039/C9NR02085C.
- [112] L. Tie, N. Li, C. Yu, Y. Liu, S. Yang, H. Chen, S. Dong, J. Sun, S. Dou, J. Sun, Self-Supported Nonprecious MXene/Ni3S2 electrocatalysts for efficient hydrogen generation in alkaline media, ACS Appl. Energy Mater. 2 (2019) 6931–6938, https://doi.org/10.1021/acsaem.9b01529.
- [113] D.A. Kuznetsov, Z. Chen, P.V. Kumar, A. Tsoukalou, A. Kierzkowska, P.M. Abdala, O.V. Safonova, A. Fedorov, C.R. Müller, Single Site Cobalt Substitution in 2D Molybdenum Carbide (MXene) enhances catalytic activity in the hydrogen evolution reaction, J. Am. Chem. Soc. 141 (2019) 17809–17816, https://doi.org/10.1021/icsc.9b09807
- [114] C.-Feng Du, X. Sun, H. Yu, Q. Liang, K. Ngoc Dinh, Y. Zheng, Y. Luo, Z. Wang, Q. Yan, Synergy of Nb doping and surface alloy enhanced on water-alkali electrocatalytic hydrogen generation performance in Ti-Based MXene, Adv. Sci. 6 (2019), https://doi.org/10.1002/advs.201900116.
- [115] Z. Chen, S. Huang, B. Huang, M. Wan, N. Zhou, Transition metal atoms implanted into MXenes (M₂CO₂) for enhanced electrocatalytic hydrogen evolution reaction, Appl. Surf. Sci. 509 (2020), https://doi.org/10.1016/j.apsusc.2020.145319.
- [116] S. Bai, M. Yang, J. Jiang, X. He, J. Zou, Z. Xiong, G. Liao, S. Liu, Recent advances of mxenes as electrocatalysts for hydrogen evolution reaction, NPJ 2D Mater. Appl. 5 (2021), https://doi.org/10.1038/s41699-021-00259-4.
- [117] B.Rani Anne, J. Kundu, M.Kanti Kabiraz, J. Kim, D. Cho, S.-Il Choi, A review on MXene as promising support materials for oxygen evolution reaction catalysts, Adv. Funct. Mater. 31 (2023), https://doi.org/10.1002/adfm.202306100.

- [118] E. Fabbri, T.J. Schmidt, Oxygen evolution reaction—the enigma in water electrolysis, ACS Catal. 8 (2018) 9765–9774, https://doi.org/10.1021/ acseatal 8b02712
- [119] D. Friebel, M.W. Louie, M. Bajdich, K.E. Sanwald, Y. Cai, A.M. Wise, M.-Jeng Cheng, D. Sokaras, T.-Chien Weng, R. Alonso-Mori, R.C. Davis, J.R. Bargar, J.K. Nørskov, A. Nilsson, A.T. Bell, Identification of Highly Active Fe Sites in (Ni, Fe)OOH for electrocatalytic water splitting, J. Am. Chem. Soc. 137 (2015) 1305–1313, https://doi.org/10.1021/ja511559d.
- [120] I.C. Man, H.-Yan Su, F. Calle-Vallejo, H.A. Hansen, J.I. Martínez, N.G. Inoglu, J. Kitchin, Ts.F. Jaramillo, J.K. Nørskov, J. Rossmeisl, Universality in oxygen evolution electrocatalysis on oxide surfaces, ChemCatChem 3 (2011) 1159–1165, https://doi.org/10.1002/cctc.201000397.
- [121] Z. -Feng Huang, J. Song, Y. Du, S. Xi, S. Dou, J. Marie Vianney Nsanzimana, C. Wang, Zhichuan J. Xu, X. Wang, Chemical and structural origin of lattice oxygen oxidation in Co–Zn oxyhydroxide oxygen evolution electrocatalysts, Nat. Energy 4 (2019) 329–338, https://doi.org/10.1038/s41560-019-0355-9.
- [122] J. Song, C. Wei, Z.-Feng Huang, C. Liu, L. Zeng, X. Wang, Z.-J. Xu, A review on fundamentals for designing oxygen evolution electrocatalysts, Chem. Soc. Rev. 49 (2020) 2196–2214, https://doi.org/10.1039/C9CS00607A.
- [123] Y. Ma, Y. An, Z. Xu, L. Cheng, W. Yuan, Activating lattice oxygen of two-dimensional M_nX_{n-1}O₂ MXenes via zero-dimensional graphene quantum dots for water oxidation, Sci. China Mater. 65 (2022) 3053–3061, https://doi.org/10.1007/s40843-022-2091-4.
- [124] N.-Tzu Suen, S.-Fu Hung, Q. Quan, N. Zhang, Y.-Jun Xu, H. Ming Chen, Electrocatalysis for the oxygen evolution reaction: recent development and future perspectives, Chem. Soc. Rev. 46 (2017) 337–365, https://doi.org/10.1039/ C6CS00328A.
- [125] Z. Yan, H. Liu, Z. Hao, M. Yu, X. Chena, J. Chen, Electrodeposition of (Hydro) oxides for an oxygen evolution electrode, J, Chem. Sci. 11 (2020) 10614–10625, https://doi.org/10.1039/D0SC01532F.
- [126] Q. Shi, C. Zhu, D. Du, Y. Lin, Robust noble metal-based electrocatalysts for oxygen evolution reaction, Chem. Soc. Rev. 48 (2019) 3181–3192, https://doi.org/ 10.1039/C8CS00671G.
- [127] F. Song, L. Bai, A. Moysiadou, S. Lee, C. Hu, L. Liardet, X. Hu, Transition metal oxides as electrocatalysts for the oxygen evolution reaction in alkaline solutions: an application-inspired renaissance, J. Am. Chem. Soc. 140 (2018) 7748–7759, https://doi.org/10.1021/jacs.8b04546.
- [128] M. Benchakar, T. Bilyk, C. Garnero, L. Loupias, C. Morais, J. Pacaud, C. Canaff, P. Chartier, S. Morisset, N. Guignard, V. Mauchamp, S. Célérier, A. Habrioux, MXene supported cobalt layered double hydroxide nanocrystals: facile synthesis route for a synergistic oxygen evolution reaction electrocatalyst, Adv. Mater. Interfaces 6 (2019), https://doi.org/10.1002/admi.201901328.
- [129] M.-Qiang Zhao, Q. Zhang, J.-Qi Huang, F. Wei, Hierarchical nanocomposites derived from nanocarbons and layered double hydroxides - properties, synthesis, and applications, Adv. Funct. Mater. 22 (2012) 675–694, https://doi.org/ 10.1002/adfm.201102222.
- [130] W. Wang, Y. Lu, M. Zhao, R. Luo, Y. Yang, T. Peng, H. Yan, X. Liu, Y. Luo, Controllable tuning of cobalt nickel-layered double hydroxide arrays as multifunctional electrodes for flexible supercapattery device and oxygen evolution reaction, ACS Nano 13 (2019) 12206–12218, https://doi.org/10.1021/ acsnano.9b06910.
- [131] N.Clament Sagaya Selvam, J. Lee, G.H. Choi, M.Jun Oh, S. Xu, B. Lim, P.J. Yoo, MXene Supported Co_xA_y (A = OH, P, Se) electrocatalysts for overall water splitting: unveiling the role of anions in intrinsic activity and stability, Mater. Chem. A 7 (2019) 27383–27393, https://doi.org/10.1039/C9TA10664B.
- [132] C. Wang, X.-Dong Zhu, Y.-Chun Mao, F. Wang, X.-Tian Gao, S.-You Qiu, S.-Ru Leb, K.-Ning Sun, MXene-supported Co₃O₄ quantum dots for superior lithium storage and oxygen evolution activities, Chem. Commun. 55 (2019) 1237–1240, https:// doi.org/10.1039/C8CC09699F.
- [133] Y. Liu, L. Bai, T. Li, H. Liu, X. Wang, L. Zhang, X. Hao, C. He, S. Guo, MXene-Supported NiMn-LDHs as efficient electrocatalysts towards enhanced oxygen evolution reactions, Mater. Adv. 3 (2022) 4359–4368, https://doi.org/10.1039/D2MA00302C.
- [134] E. Antolini, Carbon supports for low-temperature fuel cell catalysts, Appl. Catal. 88 (2009) 1–24, https://doi.org/10.1016/j.apcatb.2008.09.030.
- [135] S. Han, Y. Chen, Y. Hao, Y. Xie, D. Xie, Y. Chen, Y. Xiong, Z. He, F. Hu, L. Li, J. Zhu, S. Peng, Multi-Dimensional Hierarchical CoS₂@MXene as trifunctional electrocatalysts for zinc-air batteries and overall water splitting, Sci. China Mater. 64 (2021) 1127-1138. https://doi.org/10.1007/s40843-020-1524-5
- 64 (2021) 1127–1138, https://doi.org/10.1007/s40843-020-1524-5.
 [136] C. Hao, Y. Wu, Y. An, B. Cui, J. Lin, X. Li, D. Wang, M. Jiang, Z. Cheng, S. Hu, Interface-Coupling of CoFe-LDH on MXene as high-performance oxygen evolution catalyst, Mater. Today Energy 12 (2019) 453–462, https://doi.org/10.1016/j.
- [137] M. Yu, S. Zhou, Z. Wang, J. Zhao, J. Qiu, Boosting electrocatalytic oxygen evolution by synergistically coupling layered double hydroxide With MXene, Nano Energy 44 (2018) 181–190, https://doi.org/10.1016/j. nanoen.2017.12.003.
- [138] D. Kan, D. Wang, X. Zhang, R. Lian, J. Xu, G. Chena, Y. Wei, Rational design of bifunctional ORR/OER Catalysts Based on Pt/Pd-Doped Nb₂CT₂ MXene by firstprinciples calculations, Mater. Chem. A 8 (2020) 3097–3108, https://doi.org/ 10.1039/CPTA122554
- [139] Z. Zhu, C. Xu, Y. Wang, L. Wang, Z. Chang, Z. Fang, X. Liu, J. Cheng, The High Performance NiFe Layered Double Hydroxides@ Ti₃C₂T_x/reduced graphene oxide hybrid catalyst for oxygen evolution reaction, J. Alloy. Compd. 894 (2022), https://doi.org/10.1016/j.jallcom.2021.162393.

- [140] C. Gan, Y. Zhang, Z. Liu, W. Yan, Q. Jiang, X. Wu, J. Tang, Integrated Co₄MnFe₃/Ti₃C₂: componential and structural engineering toward boosting electrocatalytic oxygen evolution, J. Phys. Chem. C. 125 (2021) 15872–15881, https://doi.org/10.1021/acs.jpcc.1c04892.
- [141] Y. Wen, Z. Wei, J. Liu, R. Li, P. Wang, B. Zhou, X. Zhang, J. Li, Z. Li, Synergistic cerium doping and mxene coupling in layered double hydroxides as efficient electrocatalysts for oxygen evolution, J. Energy Chem. 52 (2021) 412–420, https://doi.org/10.1016/j.jechem.2020.04.009.
- [142] L. Yan, B. Zhang, Rose-like, ruthenium-modified cobalt nitride nanoflowers grown in situ on an MXene Matrix for efficient and stable water electrolysis, Mater. Chem. A 9 (2021) 20758–20765, https://doi.org/10.1039/D1TA05243H
- [143] L. Yan, Z. Du, X. Lai, J. Lan, X. Liu, J. Liao, Y. Feng, H. Li, Synergistically modulating the electronic structure of Cr-Doped FeNi LDH Nanoarrays by Ovacancy and coupling of MXene for enhanced oxygen evolution reaction, Int. J. Hydrog. Energy 48 (2023) 1892–1903, https://doi.org/10.1016/j. iihvdene.2022.10.087.
- [144] A. Navjyoti, V. Kumar Sharma, A.K. Sharma, V. Debnath, A. Saxena, Mahajan, MXene Supported nickel-cobalt layered double hydroxide as efficient bifunctional electrocatalyst for hydrogen and oxygen evolution reactions, J. Alloy. Compd. 939 (2023), https://doi.org/10.1016/j.jallcom.2023.168779.
- [145] H. Si, C. Han, Y. Cui, S. Sang, K. Liu, H. Liu, Q. Wu, Hydrophilic NiFe-LDH/ Ti₃C₂T_x/NF electrode for assisting efficiently oxygen evolution reaction, J. Solid State Chem. 295 (2021), https://doi.org/10.1016/j.jssc.2020.121943.
- [146] J.Easo George, S. Chidangil, S.Daniel George, Recent progress in fabricating superaerophobic and superaerophilic surfaces, Adv. Mater. Interfaces 4 (2017), https://doi.org/10.1002/admi.201601088.
- [147] Y. Wen, J. Yang, H. Zou, Y. Fan, J. Li, Y. Kuang, W. Liu, K. Zhanga, L. Xiong, 2D TiVCT_x Layered nanosheets grown on nickel foam as highly efficient electrocatalysts for the hydrogen evolution reaction, RSC Adv. 12 (2022) 23584–23594, https://doi.org/10.1039/D2RA03791B.
- [148] A. Kulkarni, S. Siahrostami, A. Patel, J.K. Nørskov, Understanding catalytic activity trends in the oxygen reduction reaction, Chem. Rev. 118 (2018) 2302–2312, https://doi.org/10.1021/acs.chemrev.7b00488.
- [149] A. Sarapuu, E. Kibena-Põldsepp, M. Borgheib, K. Tammeveski, Electrocatalysis of oxygen reduction on heteroatom-doped nanocarbons and transition metal-nitrogen-carbon catalysts for alkaline membrane fuel cells, Mater. Chem. A 6 (2018) 776–804, https://doi.org/10.1039/C7TA08690C.
- [150] N. Han, P. Liu, J. Jiang, L. Ai, Z. Shaob, S. Liu, Recent advances in nanostructured metal nitrides for water splitting, Mater. Chem. A 6 (2018) 19912–19933, https://doi.org/10.1039/C8TA06529B.
- [151] J. Zou, N. Han, J. Yan, Q. Feng, Y. Wang, Z. Zhao, J. Fan, L. Zeng, H. Li, H. Wang, Electrochemical compression technologies for high-pressure hydrogen: current status, challenges and perspective, Electrochem. Energ. Rev. 3 (2020) 690–729, https://doi.org/10.1007/s41918-020-00077-0.
- [152] Y. Ji, H. Dong, C. Liua, Y. Li, The progress of metal-free catalysts for the oxygen reduction reaction based on theoretical simulations, Mater. Chem. A 6 (2018) 13489–13508, https://doi.org/10.1039/C8TA02985G.
- [153] Y. Sun, W. Zhang, Q. Wang, N. Han, A. Núñez-Delgado, Y. Cao, W. Si, F. Wang, S. Liu, Biomass-Derived N,S Co-Doped 3D multichannel carbon supported Au@ Pd@Pt Catalysts for oxygen reduction, Environ. Res. 202 (2021) 13489–13508, https://doi.org/10.1016/j.envres.2021.111684.
- [154] A. Inayat, M.M. Ahmad, M.I. Abdul Mutalib, S. Yusup, Effect of process parameters on hydrogen production and efficiency in biomass gasification using modelling approach, J. Appl. Sci. 10 (2010) 3183–3190, https://doi.org/ 10.3023/ias.2010.3183.3190
- [155] Q. Wang, N. Han, A. Bokhari, X. Li, Y. Cao, S. Asif, Z. Shen, W. Si, F. Wang, J. Jaromír Klemeš, X. Zhao, Insights into MXenes-based electrocatalysts for oxygen reduction, J, Energy 255 (2022), https://doi.org/10.1016/j.energy.2022.124465.
- [156] H.A. Gasteiger, S.S. Kocha, B. Sompalli, F.T. Wagner, Activity benchmarks and requirements for Pt, Pt-Alloy, and Non-Pt oxygen reduction catalysts for PEMFCs, Appl. Catal. B: Environ. 56 (2005) 9–35, https://doi.org/10.1016/j. apcatb.2004.06.021.
- [157] F. Jaouen, E. Proietti, M. Lefèvre, R. Chenitz, J. -Pol Dodelet, G. Wu, H. Taek Chung, C. Marie Johnstonb, P. Zelenay, Recent advances in non-precious metal catalysis for oxygen-reduction reaction in polymer electrolyte fuel cells, Energy Environ. Sci. 4 (2011) 114–130, https://doi.org/10.1039/C0EE00011F.
 [158] H. Lin, L. Chen, X. Lu, H. Yao, Y. Chen, J. Shi, Two-Dimensional titanium carbide
- [158] H. Lin, L. Chen, X. Lu, H. Yao, Y. Chen, J. Shi, Two-Dimensional titanium carbidomxenes as efficient non-noble metal electrocatalysts for oxygen reduction reaction, Sci. China Mater. 62 (2019) 662–670.
- [159] Y. Pei Zhu, C. Guo, Y. Zheng, S.-Zhang Qiao, Surface, interface engineering of noble-metal-free electrocatalysts for efficient energy conversion processes, Acc. Chem. Res. 50 (2017) 915–923, https://doi.org/10.1021/acs.accounts.6b00635
- [160] Y. Guo, P. Yuan, J. Zhang, Y. Hu, I.Saana Amiinu, X. Wang, J. Zhou, H. Xia, Z. Song, Q. Xu, S. Mu, Carbon Nanosheets Containing Discrete Co-N_x-B_y-C active sites for efficient oxygen electrocatalysis and rechargeable Zn–Air Batteries, Acs. Nano. 12 (2018) 1894–1901, https://doi.org/10.1021/acsnano.7b08721.
- [161] Z. Huang, H. Pan, W. Yang, H. Zhou, N. Gao, C. Fu, S. Li, H. Li, Y. Kuang, In Situ Self-Template Synthesis of Fe–N-doped double-shelled hollow carbon microspheres for oxygen reduction reaction, Acs. Nano. 12 (2018) 208–216, https://doi.org/10.1021/acsnano.7b05832.
- [162] S. Sultan, J.N. Tiwari, J.-Hyuk Jang, A.M. Harzandi, F. Salehnia, S. Jong Yoo, K. S. Kim, Highly efficient oxygen reduction reaction activity of graphitic tube encapsulating nitrided Co_xFe_y Alloy, Adv. Energy Mater. 8 (2018), https://doi.org/10.1002/aenm.201801002.
- [163] B. Wei, Z. Fu, D. Legut, T.C. Germann, S. Du, H. Zhang, J.S. Francisco, R. Zhang, Rational design of highly stable and active mxene-based bifunctional ORR/OER

- Double-Atom Catalysts, Adv. Mater. 33 (2021), https://doi.org/10.1002/
- [164] R. Yoo, E. Pranada, D. Johnson, Z. Qiao, A. Djire, Review—the oxygen reduction reaction on mxene-based catalysts: progress and prospects, J. Electrochem. Soc. 169 (2022), https://doi.org/10.1149/1945-7111/ac766e.
- [165] L. Chen, Y. Lin, J. Fu, J. Xie, R. Chen, H. Zhang, Hybridization of binary non-precious-metal nanoparticles with d-Ti₃C₂ MXene for catalyzing the oxygen reduction reaction, ChemElectroChem 5 (2018) 3307–3314, https://doi.org/10.1002/celc.201800693.
- $[166] \ Y.\ Zhang, H.\ Jiang, Y.\ Lin, H.\ Liu, Q.\ He, C.\ Wu, T.\ Duan, L.\ Song, In situ growth of cobalt nanoparticles encapsulated nitrogen-doped carbon nanotubes among <math display="block">Ti_3C_2Tx\ (MXene)\ matrix\ for\ oxygen\ reduction\ and\ evolution,\ Adv.\ Mater.$ Interfaces 5 (2018), https://doi.org/10.1002/admi.201800392.
- [167] J. Chen, X. Yuan, F. Lyu, Q. Zhong, H. Hu, Q. Pana, Q. Zhang, Integrating MXene Nanosheets with cobalt-tipped carbon nanotubes for an efficient oxygen reduction reaction, 1281-128, Mater. Chem. A 7 (2019), https://doi.org/10.1039/ C8TA10574J.
- [168] Z. Li, Z. Zhuang, F. Lv, H. Zhu, L. Zhou, M. Luo, J. Zhu, Z. Lang, S. Feng, W. Chen, L. Mai, S. Guo, The Marriage of the FeN4 moiety and MXene boosts oxygen reduction catalysis: Fe 3d electron delocalization matters, Adv Mater. 30 (2018), https://doi.org/10.1002/adma.201803220.
- [169] D.A. Kuznetsov, Z. Chen, P.M. Abdala, O.V. Safonova, A. Fedorov, C.R. Müller, Single-Atom-Substituted Mo₂CT_x:Fe-layered carbide for selective oxygen reduction to hydrogen peroxide: tracking the evolution of the mxene phase, J. Am. Chem. Soc. 143 (2021) 5771–5778, https://doi.org/10.1021/ iacs.1c00504.
- [170] M. Ashton, N. Trometer, K. Mathew, J. Suntivich, C. Freysoldt, S.B. Sinnott, R. G. Hennig, Predicting the electrochemical synthesis of 2d materials from first principles, J. Phys. Chem. C. 123 (2019) 3180–3187, https://doi.org/10.1021/acs.jpcc.8b10802.
- [171] C. Tsounis, P.V. Kumar, H. Masood, R.P. Kulkarni, G.S. Gautam, C.R. Muller, R. Amal, D.A. Kuznetsov, Advancing MXene electrocatalysts for energy conversion reactions: surface, stoichiometry, and stability, Angew. Chem. Int. Ed. 62 (2023) e202210828, https://doi.org/10.1002/anie.202210828.
- [172] S.L. Foster, S.I. Perez Bakovic, R.D. Duda, S. Maheshwari, R.D. Milton, S. D. Minteer, M.J. Janik, J.N. Renner, L.F. Greenlee, Catalysts for nitrogen reduction to ammonia, Nat. Catal. 1 (2018) 490–500, https://doi.org/10.1038/s41929-018-0092-7.
- [173] S. Ghavam, M. Vahdati, I.A. Grant Wilson, P. Styring, Sustainable ammonia production processes, Front. Energy Res. 9 (2021), https://doi.org/10.3389/ fenrg.2021.580808.
- [174] J. Hou, M. Yang, J. Zhang, Recent advances in catalysts, electrolytes and electrode engineering for the nitrogen reduction reaction under ambient conditions, Nanoscale 12 (2020) 6900–6920, https://doi.org/10.1039/ DONR00412.J.
- [175] X. Xue, R. Chen, C. Yan, P. Zhao, Y. Hu, W. Zhang, S. Yang, Z. Jin, Review on Photocatalytic and electrocatalytic artificial nitrogen fixation for ammonia synthesis at mild conditions: advances, challenges and perspectives, Nano Res 12 (2019) 1229–1249, https://doi.org/10.1007/s12274-018-2268-5.
- [176] Z. Li, N.H. Attanayake, J.L. Blackburn, E.M. Miller, Carbon dioxide and nitrogen reduction reactions using 2d transition metal dichalcogenide (TMDC) and Carbide/Nitride (MXene) Catalysts, Energy Environ. Sci. 14 (2021) 6242–6286, https://doi.org/10.1039/D1EE03211A.
- [177] L.Miguel Azofra, N. Li, D.R. MacFarlanea, C. Sun, Promising Prospects for 2D d₂-d₄ M₃C₂ Transition Metal Carbides (MXenes) in N₂ capture and conversion into ammonia, Energy Environ. Sci. 9 (2016) 2545–2549, https://doi.org/10.1039/C6EE01800A.
- [178] J. Zhao, L. Zhang, X.-Ying Xie, X. Li, Y. Ma, Q. Liu, W. -Hai Fang, X. Shi, G. Cui, X. Sun, ${\rm Ti}_3{\rm C}_2{\rm T}_x$ (T = F, OH) MXene nanosheets: conductive 2d catalysts for ambient electrohydrogenation of N₂ to NH₃, Mater. Chem. A 6 (2018) 24031–24035, https://doi.org/10.1039/C8TA09840A.
- [179] J. Wang, C. He, J. Huo, L. Fu, C. Zhao, A theoretical evaluation of possible N₂ reduction mechanism on Mo₂B₂, Adv. Theory Simul. 4 (2021), https://doi.org/10.1002/adts.202100003.
- [180] C.Chio Leong, Y. Qu, Y. Kawazoe, S.Kam Ho, H. Pan, MXenes: novel electrocatalysts for hydrogen production and nitrogen reduction, Catal. Today 370 (2021) 2–13, https://doi.org/10.1016/j.cattod.2020.10.003.
- [181] J. Xia, H. Guo, G. Yu, Q. Chen, Y. Liu, Q. Liu, Y. Luo, T. Li, E. Traversa, 2D vanadium carbide (mxene) for electrochemical synthesis of ammonia under ambient conditions, Catal. Lett. 151 (2021) 3516–3522, https://doi.org/10.1007/s10562-021-03589-6.
- [182] H. Wei, Q. Jiang, C. Ampelli, S. Chen, S. Perathoner, Y. Liu, G. Centi, Enhancing N₂ Fixation Activity by Converting Ti₃C₂ MXenes nanosheets to nanoribbons, ChemSusChem 13 (2020) 5614–5619, https://doi.org/10.1002/cssc.202001719.
- [183] J.L. Hart, K. Hantanasirisakul, A.C. Lang, B. Anasori, D. Pinto, Y. Pivak, J.Tijn van Omme, S.J. May, Y. Gogotsi, M.L. Taheri, Control of MXenes' electronic properties through termination and intercalation, Nat. Commun. 10 (2019), https://doi.org/10.1038/s41467-018-08169-8.
- [184] A. Liu, X. Liang, Q. Yang, X. Ren, M. Gao, Y. Yang, T. Ma, Electrocatalytic synthesis of ammonia using a 2D Ti₃C₂ MXene loaded with copper nanoparticles, ChemPlusChem 86 (2021) 166–170, https://doi.org/10.1002/cplu.202000702.
- [185] C.-Feng Du, L. Yang, K. Tang, W. Fang, X. Zhao, Q. Liang, X. Liu, H. Yu, W. Qi, Q. Yan, Ni nanoparticles/V₄C3T_x MXene heterostructures for electrocatalytic nitrogen fixation, Mater. Chem. Front. 5 (2021) 2338–2346, https://doi.org/10.1039/D0QM00898B.

- [186] W. Peng, M. Luo, X. Xu, K. Jiang, M. Peng, D. Chen, T.-Shan Chan, Y. Tan, Spontaneous Atomic Ruthenium Doping in Mo₂CT_x MXene defects enhances electrocatalytic activity for the nitrogen reduction reaction, Adv. Energy Mater. 10 (2020), https://doi.org/10.1002/aenm.202001364.
- [187] Y. Guo, T. Wang, Q. Yang, X. Li, H. Li, Y. Wang, T. Jiao, Z. Huang, B. Dong, W. Zhang, J. Fan, C. Zhi, Highly efficient electrochemical reduction of nitrogen to ammonia on surface termination modified Ti₃C₂T_x MXene Nanosheets, ACS Nano 14 (2020) 9089–9097, https://doi.org/10.1021/acsnano.0c04284.
- [188] S. Zheng, S. Li, Z. Mei, Z. Hu, M. Chu, J. Liu, X. Chen, F. Pan, Electrochemical nitrogen reduction reaction performance of single-boron catalysts tuned by mxene substrates, J. Phys. Chem. Lett. 10 (2019) 6984–6989, https://doi.org/ 10.1021/acs.ipclett.9b02741.
- [189] Y. Ding, J. Zhang, A. Guan, Q. Wang, S. Li, A.M. Al-Enizi, L. Qian, L. Zhang, G. Zheng, Promoting N₂ Electroreduction to Ammonia by Fluorine-Terminating Ti₃C₂T_x MXene, Nano Converg. 8 (2021), https://doi.org/10.1186/s40580-021-00264-9
- [190] D. Liu, G. Zhang, Q. Ji, Y. Zhang, J. Li, Synergistic electrocatalytic nitrogen reduction enabled by confinement of nanosized au particles onto a twodimensional Ti₃C₂ Substrate, ACS Appl. Mater. Interfaces 11 (2019) 25758–25765, https://doi.org/10.1021/acsami.9b02511.
- [191] J. Xia, S.-Ze Yang, B. Wang, P. Wu, I. Popovs, H. Li, S. Irle, S. Dai, H. Zhu, Boosting electrosynthesis of ammonia on surface-engineered MXene Ti₃C₂, Nano Energy 72 (2020), https://doi.org/10.1016/j.nanoen.2020.104681.
- [192] A. Liu, M. Gao, X. Ren, F. Meng, Y. Yang, Q. Yang, W. Guan, L. Gao, X. Lianga, T. Ma, A Two-Dimensional Ru@MXene catalyst for highly selective ambient electrocatalytic nitrogen reduction, Nanoscale 12 (2020) 10933–10938, https://doi.org/10.1039/D0NR00788A.
- [193] Y. Zeng, X. Du, Y. Li, Y. Guo, Y. Xie, J. Huang, G. Rao, T. Lei, C. Gong, X. Wang, B. Sun, Synergistic Performance of Nitrogen and Sulfur Co-Doped Ti₃C₂T_x for electrohydrogenation of N₂ to NH₃, J. Alloy. Compd. 869 (2021), https://doi.org/10.1016/j.iall.com/2021.159335
- [194] R. Meys, A. Kätelhön, M. Bachmann, B. Winter, C. Zibunas, S. Suh, A. Bardow, Achieving Net-Zero greenhouse gas emission plastics by a circular carbon economy, J. Sci. 374 (2021) 71–76, https://doi.org/10.1126/science.abg9853.
- [195] O.S. Bushuyev, P. De Luna, C.Thang Dinh, L. Tao, G. Saur, J. van de Lagemaat, S. O. Kelley, E.H. Sargent, What Should We Make with CO₂ and how can we make it? Joule 2 (2018) 825–832, https://doi.org/10.1016/j.joule.2017.09.003.
- [196] N. Li, X. Chen, W.-Jun Ong, D.R. MacFarlane, X. Zhao, A.K. Cheetham, C. Sun, Understanding of Electrochemical Mechanisms for CO₂ capture and conversion into hydrocarbon fuels in transition-metal carbides (MXenes), ACS Nano 11 (2017) 10825–10833, https://doi.org/10.1021/acsnano.7b03738.
- [197] H. Chen, A.D. Handoko, J. Xiao, X. Feng, Y. Fan, T. Wang, D. Legut, Z.Wei Seh, Q. Zhang, Catalytic Effect on CO₂ electroreduction by hydroxyl-terminated two-dimensional MXenes, ACS Appl. Mater. Interfaces 11 (2019) 36571–36579, https://doi.org/10.1021/acsami.9b09941.
- [198] A.D. Handoko, H. Chen, Y. Lum, Q. Zhang, B. Anasori, Z.Wei Seh, Two-dimensional titanium and molybdenum carbide MXenes as electrocatalysts for CO₂ Reduction, iScience 23 (2020), https://doi.org/10.1016/j.isci.2020.101181.
- [199] N.H. Attanayake, H.R. Banjade, A.C. Thenuwara, B. Anasori, Q. Yan, D. R. Strongin, Electrocatalytic CO₂ reduction on earth abundant 2D Mo₂C and Ti₃C₂ MXenes, Chem. Commun. 27 (2021) 1675–1678, https://doi.org/10.1039/D0CC05822J.
- [200] L. Meng, E. Tayyebi, K.S. Exner, F. Viñes, F. Illas, MXenes as electrocatalysts for the CO₂ reduction reaction: recent advances and future challenges, ChemElectroChem 11 (2024), https://doi.org/10.1002/celc.202300598.
- [201] K. Eid, Q. Lu, S. Abdel-Azeim, A. Soliman, A.M. Abdullah, A.M. Abdelgwad, R. P. Forbes, K.I. Ozoemena, R.S. Varma, M.F. Shibl, Highly Exfoliated Ti₃C₂T_x MXene nanosheets atomically doped with cu for efficient electrochemical CO₂ reduction: an experimental and theoretical study, Mater. Chem. A 10 (2022) 1965–1975, https://doi.org/10.1039/D1TA09471H.
- [202] Y. Zhao, J. Zhang, X. Guo, X. Cao, S. Wang, H. Liu, G. Wang, Engineering strategies and active site identification of mxene-based catalysts for electrochemical conversion reactions, Chem. Soc. Rev. 52 (2023) 3215–3264, https://doi.org/10.1039/D2CS00698G.
- [203] C. Zhao, Y. Zhang, K. Nie, L. Yi, B. Li, Y. Yuan, X. Qu, Z. Liu, Recent advances in design and engineering of mxene-based heterostructures for sustainable energy conversion, Appl. Mater. Today 32 (2023), https://doi.org/10.1016/j. aomt.2023.101841.
- [204] Y. Cheng, X. Xu, Y. Li, Y. Zhang, Y. Song, CO₂ Reduction Mechanism on the Nb₂CO₂ MXene surface: effect of nonmetal and metal modification, Comput. Mater. Sci. 202 (2022), https://doi.org/10.1016/j.commatsci.2021.110971.
- [205] K. Kannan, M.H. Sliem, A.M. Abdullah, K. Kumar Sadasivuni, B. Kumar, Fabrication of ZnO-Fe-MXene based nanocomposites for efficient CO₂ Reduction, J. Catal. 10 (2020), https://doi.org/10.3390/catal10050549.
- [206] B.M. Daas, S. Ghosh, Fuel Cell Applications of Chemically Synthesized Zeolite Modified Electrode (ZME) as catalyst for alcohol electro-oxidation - a review, J. Electroanal. Chem. 783 (2016) 308–315, https://doi.org/10.1016/j. ielectem 2016 11 004
- [207] G. Zhao, C. Fang, J. Hu, D. Zhang, Platinum-based electrocatalysts for direct alcohol fuel cells: enhanced performances toward alcohol oxidation reactions, ChemPlusChem 86 (2021) 574–586, https://doi.org/10.1002/cplu.202000811
- [208] Y. Zuo, W. Sheng, W. Tao, Z. Li, Direct Methanol fuel cells system-a review of dual-role electrocatalysts for oxygen reduction and methanol oxidation, J. Mater. Sci. Technol. 114 (2022) 29–41, https://doi.org/10.1016/j.jmst.2021.10.031.

- [209] J. Zhao, Z. Tu, S. Hwa Chan, Carbon Corrosion mechanism and mitigation strategies in a proton exchange membrane fuel Cell (PEMFC): a review, J. Power Sources 488 (2021), https://doi.org/10.1016/j.jpowsour.2020.229434.
- [210] S. Samad, K.Shyuan Loh, W.Yin Wong, T.Khoon Lee, J. Sunarso, S.Tong Chong, W.Ramli Wan Daud, Carbon and non-carbon support materials for platinum-based catalysts in fuel cells, Int. J. Hydrog. Energy 43 (2018) 7823–7854, https://doi.org/10.1016/i.jihydene.2018.02.154.
- [211] Y.-Jie Wang, D.P. Wilkinson, J. Zhang, Noncarbon support materials for polymer electrolyte membrane fuel cell electrocatalysts, Chem. Rev. 111 (2011) 7625–7651, https://doi.org/10.1021/cr100060r.
- [212] Q. Peng, J. Zhou, J. Chen, T. Zhangab, Z. Sun, Cu Single Atoms on Ti₂CO₂ as a highly efficient oxygen reduction catalyst in a proton exchange membrane fuel cell, Mater. Chem. A 7 (2019) 26062–26070, https://doi.org/10.1039/ COTAGE 207B
- [213] Z. Fu, C. Ling, J. Wang, A Ti₃C₂O₂ supported single atom, trifunctional catalyst for electrochemical reactions, Mater. Chem. A 8 (2020) 7801–7807, https://doi.org/ 10.1039/D0TA01047B.
- [214] V. Navjyoti, V. Sharma, V. Bhullar, A. Saxena, A. Krishna Debnath, Mahajan, Modulation of Surface Ti–O Species in 2D-Ti₃C₂T_x MXene for developing a highly efficient electrocatalyst for hydrogen evolution and methanol oxidation reactions, Langmuir 39 (2023) 2995–3005, https://doi.org/10.1021/acs. langmuir.2c02845.
- [215] S.Gouse Peera, C. Liu, J. Shim, A.Kumar Sahu, T.Gwan Lee, M. Selvaraj, R. Koutavarapu, MXene (Ti₃C₂T_x) supported electrocatalysts for methanol and ethanol electrooxidation: a review, Ceram. Int. 47 (2021) 28106–28121, https://doi.org/10.1016/j.ceramint.2021.07.075.
- [216] X. Zhao, Q. Liu, Q. Li, L. Chen, L. Mao, H. Wang, S. Chen, Two-dimensional electrocatalysts for alcohol oxidation: a critical review, J. Chem. Eng. 400 (2020), https://doi.org/10.1016/j.cej.2020.125744.
- [217] J. Wang, B. Zhang, W. Guo, L. Wang, J. Chen, H. Pan, W. Sun, Toward electrocatalytic methanol oxidation reaction: longstanding debates and emerging catalysts, Adv. Mater. 35 (2023), https://doi.org/10.1002/adma.202211099.
- [218] Y. Wang, Y. Nian, A.N. Biswas, W. Li, Y. Han, J.G. Chen, Challenges and opportunities in utilizing mxenes of carbides and nitrides as electrocatalysts, Adv. Energy Mater. 11 (2021), https://doi.org/10.1002/aenm.202002967.
- [219] Y. Wang, J. Wang, G. Han, C. Du, Q. Deng, Y. Gao, G. Yin, Y. Song, Pt Decorated Ti₃C₂ MXene for enhanced methanol oxidation reaction, Ceram. Int. 45 (2019) 2411–2417, https://doi.org/10.1016/j.ceramint.2018.10.160.
- [220] M. Chandran, A. Raveendran, M. Vinoba, B.Kizhakkekilikoodayil Vijayan, M. Bhagiyalakshmi, Nickel-Decorated MoS₂/MXene nanosheets composites for electrocatalytic oxidation of methanol, Ceram. Int. 47 (2021) 26847–26855, https://doi.org/10.1016/j.ceramint.2021.06.093.
- [221] P. Zhang, C. Fan, R. Wang, C. Xu, J. Cheng, L. Wang, Y. Lu, P. Luo, Pd/MXene (Ti₃C₂T_x)/reduced graphene oxide hybrid catalyst for methanol electrooxidation, J. Nanotechnol. 31 (2020), https://doi.org/10.1088/1361-6528/ab5609.
- [222] C. Yang, Q. Jiang, W. Li, H. He, L. Yang, Z. Lu, H. Huang, Ultrafine Pt nanoparticle-decorated 3d hybrid architectures built from reduced graphene oxide and mxene nanosheets for methanol oxidation, Chem. Mater. 31 (2019) 9277–9287, https://doi.org/10.1021/acs.chemmater.9b02115.
- [223] S. Li, L. Zhao, J. Shu, H. Niu, R. Li, J. Zhao, H. Yang, J. Jin, R. Jin, Mxene Coupled Over Nitrogen-doped graphene anchoring palladium nanocrystals as an advanced electrocatalyst for the ethanol electrooxidation, J. Colloid Interface Sci. 610 (2022) 944–952, https://doi.org/10.1016/j.jcis.2021.11.142.
- [224] D.Susan Abraham, M. Chandran, M. Vinoba, R. Yamuna, M. Bhagiyalakshmi, Flower-like Layered NiCu-LDH/MXene nanocomposites as an anodic material for electrocatalytic oxidation of methanol, Langmuir 39 (2023) 4756–4765, https:// doi.org/10.1021/acs.langmuir.3c00154.
- [225] C. Yang, Q. Jiang, H. Huang, H. He, L. Yang, W. Li, Polyelectrolyte-Induced Stereoassembly of grain boundary-enriched platinum nanoworms on ti3c2tx mxene nanosheets for efficient methanol oxidation, ACS Appl. Mater. Interfaces 12 (2020) 23822–23830, https://doi.org/10.1021/acsami.0c02806.
- [226] P. Wang, H. Cui, C. Wang, In situ formation of porous trimetallic ptrhfe nanospheres decorated on ultrathin mxene nanosheets as highly efficient catalysts for ethanol oxidation, Nano Energy 66 (2019), https://doi.org/10.1016/j. nanoep. 2019 104196
- [227] C. Yang, Q. Jiang, H. Liu, L. Yang, H. He, H. Huang, W. Li, Pt-on-Pd BImetallic Nanodendrites Stereoassembled on Mxene Nanosheets for Use as High-efficiency Electrocatalysts toward the Methanol Oxidation Reaction, Mater. Chem. A 9 (2021) 15432–15440, https://doi.org/10.1039/D1TA01784E.
- [228] N. Abdullah, R. Saidur, A.Mohd Zainoodin, K.Han Tan, A.Kumar Pandey, Enhancing methanol oxidation reaction with platinum–ruthenium embedded mxene: synthesis, characterization, and electrochemical properties, J. Phys. Chem. Solids 180 (2023), https://doi.org/10.1016/j.jpcs.2023.111434.
- [229] Y.-Zhe Chen, M. Zhou, Y.-Fu Huang, Y.-Yun Ma, L.-Yi Yan, X.-Wen Zhou, X.-Zhou Ma, X.- Ling Zhao, C. Chen, J. Bai, D.- Hai Lin, Enhanced ethanol oxidation over pd nanoparticles supported porous graphene-doped mxene using polystyrene particles as sacrificial templates, Rare Met 41 (2022) 3170–3179, https://doi.org/10.1007/c12508-022-02030-5
- [230] J.B.G. Martínez, A. Ortiz, I. Ortiz, State-of-the-art and perspectives of the catalytic and electrocatalytic reduction of aqueous nitrates, Appl. Catal. B-Environ. 207 (2017) 42–59, https://doi.org/10.1016/j.apcatb.2017.02.016.
- [231] S. Wang, J. Chen, S. Zhang, X. Zhang, D. Chen, J. Zhou, Hydrochemical evolution characteristics, controlling factors, and high nitrate hazards of shallow groundwater in a typical agricultural area of Nansi Lake Basin, North China, Environ. Res. 223 (2023), https://doi.org/10.1016/j.envres.2023.115430.

- [232] X. Zhang, Y. Zhang, P. Shi, Z. Bi, Z. Shan, L. Ren, The deep challenge of nitrate pollution in River Water of China, Sci. Total Environ. 770 (2021), https://doi. org/10.1016/j.scitotenv.2020.144674.
- [233] W. Shuqing, F.Wei jiang, Z. Hongping, Origin and removal of nitrite in water, HJFNS 6 (2017) 37–42, https://doi.org/10.12677/HJFNS.2017.61006.
- [234] H. Xu, Y. Ma, J. Chen, W.-xian Zhange, J. Yang, Electrocatalytic reduction of nitrate—a step towards a sustainable nitrogen cycle, Chem. Soc. Rev. 51 (2022) 2710–2758, https://doi.org/10.1039/D1CS00857A.
- [235] A.K. Benekos, M. Tsigara, S. Zacharakis, I.-Eva Triantaphyllidou, A. G. Tekerlekopoulou, A. Katsaounis, D.V. Vayenas, Combined electrocoagulation and electrochemical oxidation treatment for groundwater denitrification, J. Environ. Manag. 285 (2021), https://doi.org/10.1016/j.jenvman.2021.112068.
- [236] S. Yuan, Y. Xue, R. Ma, Q. Ma, Y. Chen, J. Fan, Advances in iron-based electrocatalysts for nitrate reduction, Sci. Total Environ. 866 (2023), https://doi. org/10.1016/j.scitotenv.2023.161444.
- [237] Z. Huang, M. Rafiq, A. Reda Woldu, Q. -Xiao Tong, D. Astruc, L. Hu, Recent progress in electrocatalytic nitrogen reduction to ammonia (NRR), Coord. Chem. Rev. 478 (2023), https://doi.org/10.1016/j.ccr.2022.214981.
- [238] S. Garcia-Segura, M. Lanzarini-Lopes, K. Hristovski, P. Westerhoff, Electrocatalytic reduction of nitrate: fundamentals to full-scale water treatment applications, Appl. Catal. B Environ. 236 (2018) 546–568, https://doi.org/ 10.1016/i.aocatb.2018.05.041.
- [239] L. Tao, K. Pang, L. Huang, H. Jiada, G. Zhu, L. Tao, Highly efficient electrochemical reduction of nitrate to ammonia on cobalt doped Ti₃C₂ MXene nanosheets, Inorg. Chem. Commun. 161 (2024), https://doi.org/10.2139/ ssrn.4658179.
- [240] T. Hu, M. Wang, C. Guo, C.Ming Li, Functionalized MXenes for efficient electrocatalytic nitrate reduction to ammonia, Mater. Chem. A 10 (2022) 8923–8931, https://doi.org/10.1039/D2TA00470D.
- [241] D.F. Abbott, Y. Xu, D.A. Kuznetsov, P. Kumar, C.R. Müller, A. Fedorov, V. Mougel, Understanding the synergy between Fe and Mo sites in the nitrate reduction reaction on a bio-inspired bimetallic mxene electrocatalyst, Angew. Chem. Int. Ed. 62 (2023), https://doi.org/10.1002/anie.202313746.
- [242] F. Zhao, G. Li, Q. Hua, J. Cao, J. Song, L. Gao, T. Ma, X. Ren, A. Liu, A two-dimensional mxene-supported curu catalyst for efficient electrochemical nitrate reduction to ammonia, Catal., Sci. Technol. 13 (2023) 5543–5548, https://doi.org/10.1039/D3CY01009K.
- [243] Y. Wang, S. Rahimnejad, W.-J. Sun, L.-X. Li, H.-Y. Zhang, Q. Cao, J.-H. He, Bimetallic Cu-Fe Catalysts on MXene for synergistically electrocatalytic conversion of nitrate to ammonia, J. Colloid Interface Sci. 648 (2023) 595–603, https://doi.org/10.1016/j.jcis.2023.06.008.
- [244] H. Zhang, L. Li, W. Sun, J. He, Q. Xu, J. Lu, Highly dispersed in–situ grown Bi₂O₃ Nanosheets on Ti₃C₂T_x MXene for selective electroreduction of nitrate to ammonia, ChemElectroChem 10 (2023), https://doi.org/10.1002/ celc_202201001.
- [245] Z. Zhang, N. Zhang, J. Zhang, B. Deng, Z. Cao, Z. Wang, G. Wei, Q. Zhang, R. Jia, P. Xiang, S. Xia, Critical review in electrocatalytic nitrate reduction to ammonia towards a sustainable nitrogen utilization, J. Chem. Eng. 483 (2024), https://doi. org/10.1016/j.cej.2024.148952
- [246] G. Chen, M. Ding, K. Zhang, Z. Shen, Y. Wang, J. Ma, A. Wang, Y. Li, H. Xu, Cover Feature: Single–Atomic Ruthenium Active Sites on Ti₃C₂ MXene With oxygenterminated surface synchronize enhanced activity and selectivity for electrocatalytic nitrogen reduction to ammonia, ChemSusChem 15 (2022), https://doi.org/10.1002/cssc.202102352.
- [247] S. Wang, C. Song, Y. Cai, Y. Li, P. Jiang, H. Li, B. Yu, T. Ma, Interfacial polarization triggered by covalent-bonded mxene and black phosphorus for enhanced electrochemical nitrate to ammonia conversion, Adv. Energy Mater. 13 (2023), https://doi.org/10.1002/aenm.202301136.
- [248] S. Sen, S. Ganguly, Opportunities, barriers and issues with renewable energy development – a discussion, Renew. Sust. Energ. Rev. 69 (2017) 1170–1181, https://doi.org/10.1016/j.rser.2016.09.137.
- [249] J. Kwon Im, E. Jungmin Sohn, S. Kim, M. Jang, A. Son, K.-Duk Zoh, Y. Yoon, Review of MXene-based nanocomposites for photocatalysis, Chemosphere 270 (2021), https://doi.org/10.1016/j.chemosphere.2020.129478.
- [250] X. Li, Y. Bai, X. Shi, N. Su, G. Nie, R. Zhang, H. Niead, L. Ye, Applications of MXene (Ti₃C₂T_x) in photocatalysis: a review, Mater. Adv. 2 (2021) 1570–1594, https://doi.org/10.1039/D0MA00938E.
- [251] M. Tahir, A. Sherryna, R. Mansoor, A.Ali Khan, S. Tasleem, B. Tahir, Titanium carbide mxene nanostructures as catalysts and cocatalysts for photocatalytic fuel production: a review, ACS Appl. Nano Mater. 5 (2022) 18–54, https://doi.org/ 10.1021/acsanm.1c03112.
- [252] H. Chang, X. Li, L. Shi, Y.-Rong Zhu, T. Feng Yi, Towards high-performance electrocatalysts and photocatalysts: design and construction of mxenes-based nanocomposites for water splitting, J. Chem. Eng. 421 (2021), https://doi.org/ 10.1016/j.jcj.2021.129944
- [253] G. Murali, J. Kumar Reddy Modigunta, Y. Ho Park, J.- Hoon Lee, J. Rawal, S.-Yi Lee, I. In, S.-Jin Park, A Review on MXene synthesis, stability, and photocatalytic applications, ACS Nano 16 (2022) 13370–13429, https://doi.org/ 10.1021/acsnano.2c04750.
- [254] A. Migani, L. Blancafort, What controls photocatalytic water oxidation on rutile TiO₂(110) under ultra-high-vacuum conditions? J. Am. Chem. Soc. 139 (2017) https://doi.org/10.1021/jacs.7b05121.
- [255] A. Migani, L. Blancafort, Excitonic interfacial proton-coupled electron transfer mechanism inthe photocatalytic oxidation of methanol to formaldehyde on

- TiO₂(110), J. Am. Chem. Soc. 138 (2016) 16165–16173, https://doi.org/10.1021/jacs.7b05121.
- [256] D. Ontiveros, F. Viñes, C. Sousa, Bandgap Engineering of MXene compounds for water splitting, Mater. Chem. A 11 (2023) 13754–13764, https://doi.org/ 10.1039/D3TA01933K.
- [257] J. Wei, M. Zhou, A. Long, Y. Xue, H. Liao, C. Wei, Z.J. Xu, Heterostructured electrocatalysts for hydrogen evolution reaction under alkaline conditions, Nano-Micro Lett. 10 (2018), https://doi.org/10.1007/s40820-018-0229-x.
- [258] R. Tang, S. Xiong, D. Gong, Y. Deng, Y. Wang, L. Su, C. Ding, L. Yang, C. Liao, Ti₃C₂ 2D MXene: recent progress and perspectives in photocatalysis, ACS Appl. Mater. Interfaces 12 (2020) 56663–56680, https://doi.org/10.1021/ acsami_0c12905
- [259] A. Meng, L. Zhang, B. Cheng, J. Yu, Dual Cocatalysts in TiO₂ Photocatalysis, Adv. Mater. 31 (2019) 56663–56680, https://doi.org/10.1002/adma.201807660.
- [260] J. Ran, G. Gao, F.- Tang Li, T.- Yi Ma, A. Du, S.- Zhang Qiao, Ti₃C₂ MXene Cocatalyst on metal sulfide photo-absorbers for enhanced visible-light photocatalytic hydrogen production, Nat. Commun. 8 (2017), https://doi.org/ 10.1038/ncomms13907.
- [261] K. Takanabe, Photocatalytic water splitting: quantitative approaches toward photocatalyst by design, ACS Catal. 7 (2017) 8006–8022, https://doi.org/ 10.1021/acscatal.7b02662
- [262] L. Cheng, Q. Chen, J. Li, H. Liu, Boosting the photocatalytic activity of CdLa₂S₄ for Hydrogen Production Using Ti₃C₂ MXene as a Co-Catalyst, Appl. Catal. B 267 (2020), https://doi.org/10.1016/j.apcatb.2019.118379.
- [263] H. Wang, R. Peng, Z.D. Hood, M. Naguib, S.P. Adhikari, Z. Wu, Titania composites with 2 d transition metal carbides as photocatalysts for hydrogen production under visible-light irradiation, ChemSusChem 9 (2016) 1490–1497, https://doi. org/10.1002/cssc.201600165.
- [264] M. Zhang, J. Qin, S. Rajendran, X. Zhang, R. Liu, Heterostructured d-Ti₃C₂/TiO₂/g-C₃N₄ nanocomposites with enhanced visible-light photocatalytic hydrogen production activity, ChemSusChem 11 (2018) 4226–4236, https://doi.org/10.1002/cssc.201802284.
- [265] T. Su, Z.D. Hood, M. Naguib, L. Bai, S. Luo, C.M. Rouleau, I.N. Ivanov, H. Ji, Z. Qin, Z. Wu, 2D/2D Heterojunction of Ti₃C₅/g-C₃N₄ nanosheets for enhanced photocatalytic hydrogen evolution, Nanoscale 11 (2019) 8138–8149, https://doi.org/10.1039/C9NR00168A.
- [266] R. Xiao, C. Zhao, Z. Zou, Z. Chen, L. Tian, H. Xu, H. Tang, Q. Liu, Z. Lin, X. Yang, In Situ Fabrication of 1D CdS Nanorod/2D Ti₃C₂ MXene nanosheet schottky heterojunction toward enhanced photocatalytic hydrogen evolution, Appl. Catal. B 268 (2020), https://doi.org/10.1016/j.apcatb.2019.118382.
- [267] K. Huang, C. Li, X. Zhang, L. Wang, W. Wang, X. Meng, Self-assembly synthesis of phosphorus-doped tubular g-C₃N₄/Ti₃C₂ MXene schottky junction for boosting photocatalytic hydrogen evolution, Green. Energy Environ. 8 (2023) 233–245, https://doi.org/10.1016/j.gee.2021.03.011.
- [268] J. Li, J. Li, C. Wu, Z. Li, L. Cai, H. Tang, Z. Zhou, G. Wang, J. Wang, L. Zhao, S. Wang, Crystalline Carbon Nitride Anchored on MXene as an ordered schottky heterojunction photocatalyst for enhanced visible-light hydrogen evolution, Carbon 179 (2021) 387–399, https://doi.org/10.1016/j.carbon.2021.04.046.
- [269] Y. Xie, M.Mushfiqure Rahman, S. Kareem, H. Dong, F. Qiao, W. Xiong, X. Liu, N. Li, X. Zhao, Facile Synthesis of CuS/MXene nanocomposites for efficient photocatalytic hydrogen generation, CrystEngComm 22 (2020) 2060–2066, https://doi.org/10.1039/D0CE00104J.
- [270] T. Song, L. Hou, B. Long, A. Ali, G.-Jun Deng, Ultrathin MXene "Bridge" to accelerate charge transfer in ultrathin metal-free 0D/2D Black Phosphorus/g-C₃N₄ heterojunction toward photocatalytic hydrogen production, J. Colloid Interface Sci. 584 (2021) 474–483, https://doi.org/10.1016/j.jcis.2020.09.103.
- [271] J. Kang, S. Byun, S. Kim, J. Lee, M. Jung, H. Hwang, T.Woo Kim, S.Ho Song, D. Lee, Design of Three-Dimensional Hollow-Sphere Architecture of Ti₃C₂T_x MXene with graphitic carbon nitride nanoshells for efficient photocatalytic hydrogen evolution, ACS Appl. Energy Mater. 3 (2020) 9226–9233, https://doi.org/10.1021/acsaem.0c01590.
- [272] H. Wang, Y. Sun, Y. Wu, W. Tu, S. Wu, X. Yuan, G. Zeng, Z.J. Xu, S. Li, J. Wei Chew, Electrical Promotion of Spatially Photoinduced Charge Separation via Interfacial-Built-In Quasi-Alloying Effect in Hierarchical Zn₂In₂S₅/Ti₃C₂(O, OH)_x hybrids toward efficient photocatalytic hydrogen evolution and environmental remediation, Appl. Catal. B 245 (2019) 290–301, https://doi.org/10.1016/j.apcatb.2018.12.051.
- [273] H. Dong, X. Zhang, Y. Zuo, N. Song, X. Xin, B. Zheng, J. Sun, G. Chen, C. Li, 2D Ti₃C₂ as Electron Harvester Anchors on 2D g-C₃N₄ to create boundary edge active sites for boosting photocatalytic performance, Appl. Catal. A-Gen. 590 (2020), https://doi.org/10.1016/j.apcata.2019.117367.
- [274] Y. Sun, Y. Sun, X. Meng, Y. Gao, Y. Dall'Agnese, G. Chen, C. Dall'Agnese, X.-Feng Wang, Eosin Y-sensitized partially oxidized Ti₃C₂ MXene for photocatalytic hydrogen evolution, Catal. Sci. Technol. 9 (2019) 310–315, https://doi.org/10.1039/C8CY02240B.
- [275] K. Huang, C. Li, X. Meng, In-Situ Construction of Ternary Ti₃C₂ MXene@TiO₂/ ZnIn₂S₄ composites for highly efficient photocatalytic hydrogen evolution, J. Colloid Interface Sci. 580 (2020) 669–680, https://doi.org/10.1016/j. jcis.2020.07.044.
- [276] L. Tie, S. Yang, C. Yu, H. Chen, Y. Liu, S. Dong, J. Sun, J. Sun, In situ decoration of ZnS Nanoparticles with Ti₃C₂ MXene nanosheets for efficient photocatalytic hydrogen evolution, J. Colloid Interface Sci. 545 (2019) 63–70, https://doi.org/ 10.1016/j.jcis.2019.03.014.
- [277] Y. Li, Z. Yin, G. Ji, Z. Liang, Y. Xue, Y. Guo, J. Tian, X. Wang, H. Cui, 2D/2D/2D Heterojunction of Ti_3C_2 MXene/MoS $_2$ nanosheets/ TiO_2 nanosheets with exposed

- (001) facets toward enhanced photocatalytic hydrogen production activity, Appl. Catal. B 246 (2019) 12–20, https://doi.org/10.1016/j.apcatb.2019.01.051.
- [278] Z. Ai, Y. Shao, B. Chang, B. Huang, Y. Wu, X. Hao, Effective orientation control of photogenerated carrier separation via rational design of a Ti₃C₂(TiO₂)@CdS/ MoS₂ Photocatalytic System, Appl. Catal. B 242 (2019) 202–208, https://doi.org/ 10.1016/j.apcatb.2018.09.101.
- [279] Z. Yao, H. Sun, H. Sui, X. Liu, Construction of BPQDs/Ti₃C₂@TiO₂ composites with favorable charge transfer channels for enhanced photocatalytic activity under visible light irradiation, Nanomaterials 20 (2020), https://doi.org/ 10.3390/nano10030452.
- [280] Y. Sun, D. Jin, Y. Sun, X. Meng, Y. Gao, Y. Dall'Agnese, G. Chenab, X.-Feng Wang, g-C₂N₄/Ti₃C₂T_x (MXenes) composite with oxidized surface groups for efficient photocatalytic hydrogen evolution, Mater. Chem. A 6 (2018) 9124–9131, https://doi.org/10.1039/C8TA02706D.
- [281] P. Lin, J. Shen, X. Yu, Q. Liu, D. Li, H. Tang, Construction of Ti₃C₂ MXene/O-Doped g-C₃N₄ ²D-²D Schottky-Junction for enhanced photocatalytic hydrogen evolution, Ceram. Int. 45 (2019) 24656–24663, https://doi.org/10.1016/j.corg.mint.2019.8.203
- [282] Z. Li, H. Zhang, L. Wang, X. Meng, J. Shi, C. Qi, Z. Zhang, L. Feng, C. Li, 2D/2D BiOBr/Ti₃C₂ heterojunction with dual applications in both water detoxification and water splitting, J. Photochem. Photobiol. 386 (2020), https://doi.org/10.1016/j.jphotochem.2019.112099.
- [283] Y. Li, L. Ding, S. Yin, Z. Liang, Y. Xue, X. Wang, H. Cui, J. Tian, Photocatalytic H₂ Evolution on TiO₂ Assembled with Ti₃C₂ MXene and Metallic 1T-WS₂ as Co-Catalysts, Nano-Micro Lett. 12 (2019), https://doi.org/10.1007/s40820-019-0339-0
- [284] G. Zuo, Y. Wang, W.Liang Teo, A. Xie, Y. Guo, Y. Dai, W. Zhou, D. Jana, Q. Xian, W. Dong, Y. Zhao, Ultrathin ZnIn₂S₄ nanosheets anchored on Ti₃C₂T_x MXene for Photocatalytic H₂ Evolution, Angew. Chem. 132 (2020) 11383–11388, https://doi.org/10.1002/ange.202002136.
- [285] H. Wang, L. Chen, Y. Sun, J. Yu, Y. Zhao, X. Zhan, H. Shi, $\mathrm{Ti}_3\mathrm{C}_2$ MXene modified $\mathrm{SnNb}_2\mathrm{O}_6$ nanosheets schottky photocatalysts with directed internal electric field for tetracycline hydrochloride removal and hydrogen evolution, Sep. Purif. Technol. 265 (2021) 11383–11388, https://doi.org/10.1016/j. seppur.2021.118516.
- [286] X. Du, T. Zhao, Z. Xiu, Z. Xing, Z. Li, K. Pan, S. Yang, W. Zhou, BiVO4@ZnIn₂S₄/Ti₃C₂ MXene Quantum Dots Assembly All-Solid-State Direct Z-scheme photocatalysts for efficient visible-light-driven overall water splitting (h), Appl. Mater. Today 20 (2020), https://doi.org/10.1016/j.apmt.2020.100719.
- [287] Y. Li, L. Ding, Y. Guo, Z. Liang, H. Cui, J. Tian, Boosting the photocatalytic ability of g-C₃N₄ for Hydrogen Production by Ti₃C₂ MXene quantum dots, ACS Appl. Mater. Interfaces 11 (2019) 41440–41447, https://doi.org/10.1021/ accomin 0h14085
- [288] X. An, W. Wang, J. Wang, H. Duan, J. Shib, X. Yu, The Synergetic Effects of Ti₃C₂ MXene and Pt as Co-Catalysts for Highly Efficient Photocatalytic Hydrogen Evolution Over g-C₃N₄, Phys. Chem. Chem. Phys. 20 (2018) 11405–11411, https://doi.org/10.1039/C8CP01123K.
- [289] P. Tian, X. He, L. Zhao, W. Li, W. Fang, H. Chen, F. Zhang, Z. Huang, H. Wang, Ti₃C₂ Nanosheets Modified Zr-MOFs with schottky junction for boosting photocatalytic HER Performance, J, Sol. Energy 188 (2019) 750–759, https://doi. org/10.1016/j.solener.2019.06.060.
- [290] J. Zhang, M. Wu, B. He, R. Wang, Hu Wang, Y. Gong, Facile Synthesis of Rod-Like g-C₃N₄ by Decorating Mo₂C Co-Catalyst for Enhanced Visible-Light Photocatalytic Activity, Appl. Surf. Sci. 470 (2019) 565–572, https://doi.org/10.1016/j. apsgc. 2018 11.165
- [291] Y. Song, K. Xia, Y. Gong, H. Chen, L. Li, J. Yi, X. She, Z. Chen, J. Wu, H. Lib, H. Xu, Y. Gong, Controllable synthesized heterostructure photocatalyst Mo₂C@C/2D g-C₃N₄: enhanced catalytic performance for hydrogen production, Dalton Trans. 47 (2018) 14706–14712, https://doi.org/10.1039/C8bT03161D.
- [292] D. Ruan, M. Fujitsuka, T. Majima, Exfoliated Mo₂C Nanosheets Hybridized on CdS with fast electron transfer for efficient photocatalytic H₂ production under visible light irradiation, Appl. Catal. B 264 (2020) 14706–14712, https://doi.org/10.1016/j.apcatb.2019.118541.
- [293] J. Lelieveld, K. Klingmüller, A. Pozzer, V. Ramanathan, Effects of fossil fuel and total anthropogenic emission removal on public health and climate, Proc. Natl. Acad. Sci. U. S. A 116 (2019) 7192–7197, https://doi.org/10.1073/ pngs.181908011
- [294] M. Aggarwal, S. Basu, N.P. Shetti, M.N. Nadagouda, T.M. Aminabhavi, Photocatalytic Conversion of CO₂ into valuable products using emerging twodimensional graphene-based nanomaterials: a step towards sustainability, J. Chem. Eng. 425 (2021), https://doi.org/10.1016/j.cej.2021.131401.
- [295] C. Wang, Z. Sun, Y. Zheng, Y.Hang Hu, Recent progress in visible light photocatalytic conversion of carbon dioxide, Mater. Chem. A 7 (2019) 865–887, https://doi.org/10.1039/C8TA09865D.
- [296] Y. Wang, B. Ren, J. Zhen Ou, K. Xu, C. Yang, Y. Li, H. Zhang, Engineering Two-Dimensional metal oxides and chalcogenides for enhanced electro- and photocatalysis, Sci. Bull. 66 (2021) 1228–1252, https://doi.org/10.1016/j.scii.2021.02.007
- [297] T. Rao, W. Cai, H. Zhang, W. Liao, Nanostructured metal nitrides for photocatalysts, J. Mater. Chem. C. 9 (2021) 5323–5342, https://doi.org/ 10.1020/NOVENDERONAL
- [298] Y. Zhang, Y. Zhang, H. Zhang, L. Bai, L. Hao, T. Ma, H. Huang, Defect engineering in metal sulfides for energy conversion and storage, J. Coord. Chem. 448 (2021), https://doi.org/10.1016/j.ccr.2021.214147.

- [299] Y. Zhao, M. Que, J. Chen, C. Yang, MXenes as co-catalysts for the solar-driven photocatalytic reduction of CO₂, J. Mater. Chem. C. 8 (2020) 16258–16281, https://doi.org/10.1016/j.ccr.2021.214147.
- [300] F. Zhang, Y. Zhu, Q. Lin, L. Zhang, X. Zhang, H. Wang, Noble-metal single-atoms in thermocatalysis, electrocatalysis, and photocatalysis, Energy Environ. Sci. 14 (2021) 2954–3009, https://doi.org/10.1039/D1EE00247C.
- [301] Q. Zhong, Y. Li, G. Zhang, Two-dimensional MXene-Based and MXene-Derived Photocatalysts: Recent Developments and Perspectives, J. Chem. Eng. 409 (2021), https://doi.org/10.1016/j.cej.2020.128099.
- [302] J. Shen, Z. Wu, C. Li, C. Zhang, A. Genest, G. Rupprechter, L. He, Emerging Applications of MXene Materials in CO₂ Photocatalysis, FlatChem 28 (2021), https://doi.org/10.1016/j.flatc.2021.100252.
- [303] Z. Otgonbayar, W.- Chun Oh, MXene-based nanocomposite for the photocatalytic CO₂ reduction: comprehensive review, J, Mol. Catal. 541 (2023), https://doi.org/ 10.1016/i.mcat.2023.113085.
- [304] S. -Faye Ng, J. Jie Foo, W. -Jun Ong, Solar-powered chemistry: Eengineering low-dimensional carbon nitride-based nanostructures for selective CO₂ conversion to C₁-C₂ products, Info.Mat. 4 (2022), https://doi.org/10.1002/inf2.12279.
- [305] M. Khalil, J. Gunlazuardi, T.A. Ivandini, A. Umar, Photocatalytic Conversion of CO₂ Using earth-abundant catalysts: a review on mechanism and catalytic performance, Renew. Sust. Energ. Rev. 113 (2019), https://doi.org/10.1016/j. rser.2019.109246.
- [306] L. Chen, K. Huang, Q. Xie, S.Mun Lam, J.Chung Sin, T. Su, H. Ji, Z. Qin, The Enhancement of Photocatalytic CO₂ reduction by the in situ growth of TiO₂ on Ti₃C₂ MXene, Catal. Sci. Technol. 11 (2021) 1602–1614, https://doi.org/ 10.1039/D0CY02212H
- [307] K. Wang, M. Cheng, N. Wang, Q. Zhang, Y. Liu, J. Liang, J. Guan, M. Liu, J. Zhou, N. Li, Inter-Plane 2D/2D Ultrathin La₂Ti₂O₇/Ti₃C₂ MXene Schottky heterojunctions toward high-efficiency photocatalytic CO₂ reduction, Chin. J. Catal. 44 (2023) 146–159, https://doi.org/10.1016/S1872-2067(22)64155-X.
- [308] J. Zhang, J. Shi, S. Tao, L. Wu, J. Lu, Cu₂O/Ti₃C₂MXene heterojunction photocatalysts for improved CO₂ photocatalytic reduction performance, Appl. Surf. Sci. 542 (2021), https://doi.org/10.1016/j.apsusc.2020.148685.
- [309] X. Li, Y. Bai, X. Shi, J. Huang, K. Zhang, R. Wang, L. Ye, Mesoporous g-C₃N₄/ MXene (Ti₃C₂T_x) Heterojunction as a 2D electronic charge transfer for efficient photocatalytic CO₂ Reduction, Appl. Surf. Sci. 546 (2021), https://doi.org/ 10.1016/j.apsusc.2021.149111.
- [310] J. Low, L. Zhang, T. Tong, B. Shen, J. Yu, TiO₂/MXene Ti₃C₂ composite with excellent photocatalytic CO₂ reduction activity, J. Catal. 361 (2018) 255–266, https://doi.org/10.1016/j.jcat.2018.03.009.
- [311] J. Li, Y. Wang, Y. Wang, Y. Guo, S. Zhang, H. Song, X. Li, Q. Gao, W. Shang, S. Hu, H. Zheng, X. Li, MXene Ti₃C₂ Decorated g-C₃N₄/ZnO photocatalysts with improved photocatalytic performance for CO₂ reduction, Nano Mater. Sci. 5 (2023) 237–245, https://doi.org/10.1016/j.nanoms.2023.02.003.
- [312] M. Tahir, B. Tahir, İn-Situ Growth of TiO₂ Imbedded Ti₃C₂T_A Nanosheets to Construct PCN/Ti₃C₂T_A MXenes 2D/3D heterojunction for efficient solar driven photocatalytic CO2 reduction towards CO and CH₄ Production, J. Colloid Interface Sci. 591 (2021) 20–37, https://doi.org/10.1016/j.jcis.2021.01.099.
 [313] Z. Wu, C. Li, Z. Li, K. Feng, M. Cai, D. Zhang, S. Wang, M. Chu, C. Zhang, J. Shen,
- [313] Z. Wu, C. Li, Z. Li, K. Feng, M. Cai, D. Zhang, S. Wang, M. Chu, C. Zhang, J. Shen, Z. Huang, Y. Xiao, G.A. Ozin, X. Zhang, L. He, Niobium and titanium carbides (MXenes) as superior photothermal supports for CO₂ Photocatalysis, ACS Nano 15 (2021) 5696–5705, https://doi.org/10.1021/acsnano.1c00990.
- [314] H. Wang, Q. Tang, Z. Wu, Construction of Few-Layer Ti₃C₂ MXene and Boron-Doped g-C₃N₄ for enhanced photocatalytic CO₂ Reduction, ACS Sustain, Chem. Eng. 9 (2021) 8425–8434, https://doi.org/10.1021/acsnano.1c00990.
- [315] M. Ye, X. Wang, E. Liu, J. Ye, D. Wang, Boosting the Photocatalytic Activity of P25 for carbon dioxide reduction by using a surface-alkalinized titanium carbide mxene as cocatalyst, ChemSusChem 11 (2018) 1606–1611, https://doi.org/ 10.1002/cssc.201800083.
- [316] Q. Tang, Z. Sun, S. Deng, H. Wang, Z. Wu, Decorating g-C₃N₄ with Alkalinized Ti₃C₂ MXene for Promoted Photocatalytic CO₂ Reduction Performance, J. Colloid Interface Sci. 564 (2020) 406–417, https://doi.org/10.1016/j.jcis.2019.12.091.
- [317] S. Cao, B. Shen, T. Tong, J. Fu, J. Yu, 2D/2D Heterojunction of Ultrathin MXene/Bi₂WO₆ nanosheets for improved photocatalytic CO₂ Reduction, Adv. Funct. Mater. 28 (2018) 406–417, https://doi.org/10.1002/adfm.201800136.
 [318] Z. Zeng, Y. Yan, J. Chen, P. Zan, Q. Tian, P. Chen, Boosting the Photocatalytic
- [318] Z. Zeng, Y. Yan, J. Chen, P. Zan, Q. Tian, P. Chen, Boosting the Photocatalytic Ability of Cu₂O Nanowires for CO₂ conversion by mxene quantum dots, Adv. Funct. Mater. 29 (2019), https://doi.org/10.1002/adfm.201806500.
- [319] S. Zhao, D. Pan, Q. Liang, M. Zhou, C. Yao, S. Xu, Z. Li, Ultrathin NiAl-layered double hydroxides grown on 2D Ti₃C₂T_x MXene to construct core-shell heterostructures for enhanced photocatalytic CO₂ Reduction, J. Phys. Chem. C. 125 (2021) 10207–10218, https://doi.org/10.1021/acs.jpcc.1c00017.
- [320] F. He, B. Zhu, B. Cheng, J. Yu, W. Ho, W. Macyk, 2D/2D/0D TiO₂/C₃N₄/Ti₃C₂ MXene Composite S-scheme photocatalyst with enhanced CO₂ Reduction Activity, Appl. Catal. B 272 (2020), https://doi.org/10.1016/j.apcatb.2020.119006.
- [321] Q. Tang, P. Xiong, H. Wang, Z. Wu, Boosted CO₂ photoreduction performance on Ru-Ti₂CN MXene-TiO₂ Photocatalyst Synthesized by non-HF Lewis acidic etching method, J. Colloid Interface Sci. 619 (2022) 179–187, https://doi.org/10.1016/j. icis.2022.03.137.
- [322] A. Saeed, W. Chen, A.Hakim Shah, Y. Zhang, I. Mehmood, Y. Liu, Enhancement of Photocatalytic CO₂ Reduction for Novel Cd_{0.2}Zn_{0.8}S@Ti₃C₂ (MXenes) nanocomposites, J. CO₂ Util. 47 (2021), https://doi.org/10.1016/j. jcou.2021.101501.
- [323] K. Wang, Q. Wang, K. Zhang, G. Wang, H. Wang, Selective Solar-Driven CO₂ reduction mediated by 2D/2D Bi₂O₂SiO₃/MXene nanosheets heterojunction,

- J. Mater. Sci. Technol. 124 (2022) 179–187, https://doi.org/10.1016/j.imst.2021.10.059.
- [324] A. Pearson, Refrigeration with ammonia, Int. J. Refrig. 31 (2008) 545–551, https://doi.org/10.1016/j.ijrefrig.2007.11.011.
- [325] H.Ghavam Mehr, N. Torabiardekani, M.R. Rahimpour, Chapter eleven ammonia application in fabric, textile, and leather products, Prog. Ammon. Sci. Technol. Membr. (2024) 223–239, https://doi.org/10.1016/B978-0-323-88501-0.00006-0
- [326] A.G. Olabi, M.A. Abdelkareem, M. Al-Murisi, N. Shehata, A. Hai Alami, A. Radwan, T. Wilberforce, K.- Jung Chae, E. Taha Sayed, Recent progress in green ammonia: production, applications, assessment; barriers, and its role in achieving the sustainable development goals, Energy Convers. Manag. 277 (2023), https://doi.org/10.1016/j.enconman.2022.116594.
- [327] J. Zheng, L. Jiang, Y. Lyu, S.Ping Jiang, S. Wang, Green synthesis of nitrogen-to-ammonia fixation: past, present, and future, Energy Environ. Mater. 5 (2022) 452–457, https://doi.org/10.1002/eem2.12192.
- [328] D. Yan, H. Li, C. Chen, Y. Zou, S. Wang, Defect engineering strategies for nitrogen reduction reactions under ambient conditions, Small Methods 3 (2019), https:// doi.org/10.1002/smtd.201800331.
- [329] M. El-Shafie, S. Kambara, Recent advances in ammonia synthesis technologies: toward future zero carbon emissions, Int. J. Hydrog. Energy 48 (2023) 11237–11273, https://doi.org/10.1016/j.ijhydene.2022.09.061.
- [330] B. Sun, S. Lu, Y. Qian, X. Zhang, J. Tian, Recent progress in research and design concepts for the characterization, testing, and photocatalysts for nitrogen reduction reaction, Carbon Energy 5 (2023), https://doi.org/10.1002/cey2.305.
- [331] Y. Wei, W. Jiang, Y. Liu, X. Bai, D. Hao, B.-Jie Ni, Recent advances in photocatalytic nitrogen fixation and beyond, Nanoscale 14 (2022) 2990–2997, https://doi.org/10.1039/D2NR00198E.
- [332] R. Li, Photocatalytic Nitrogen Fixation: An attractive approach for artificial photocatalysis, Chinese J. Catal. 39 (2018) 1180–1188, https://doi.org/10.1016/ 51872-2067(18)63104-3.
- [333] M. Hiep Vu, M. Sakar, S. Ali Hassanzadeh-Tabrizi, T.-On Do, Photo(electro) catalytic nitrogen fixation: problems and possibilities, Adv. Mater. Interfaces 6 (2019), https://doi.org/10.1002/admi.201900091.
- [334] Y. Pang, C. Su, L. Xu, Z. Shao, When nitrogen reduction meets single-atom catalysts, Prog. Mater. Sci. 132 (2023), https://doi.org/10.1016/j. pmatsci.2022.101044.
- [335] G. Zhuang, J. Yan, Y. Wen, Z. Zhuang, Y. Yu, Two-dimensional transition metal oxides and chalcogenides for advanced photocatalysis: progress, challenges, and opportunities, Sol. RRL 5 (2021), https://doi.org/10.1002/solr.202000403.
- [336] T. Heliso Dolla, T. Matthews, N. Wendy Maxakato, P. Ndungu, T. Montini, Recent Advances in transition metal sulfide-based electrocatalysts and photocatalysts for nitrogen fixation, J. Electroanal. Chem. 928 (2023), https://doi.org/10.1016/j. ielechem.2022.117049.
- [337] Y. Sun, Y. Ahmadi, K.-Hyun Kim, J. Lee, The use of bismuth-based photocatalysts for the production of ammonia through photocatalytic nitrogen fixation, Renew. Sust. Energ. Rev. 170 (2022), https://doi.org/10.1016/j.rser.2022.112967.
- [338] L. Zhang, S. Hou, T. Wang, S. Liu, X. Gao, C. Wang, G. Wang, Recent advances in application of graphitic carbon nitride-based catalysts for photocatalytic nitrogen fixation, Small 18 (2022), https://doi.org/10.1002/smll.202202252.
- [339] S. Lu, L. Shen, X. Li, B. Yu, J. Ding, P. Gao, H. Zhang, Advances in the photocatalytic reduction functions of graphitic carbon nitride-based photocatalysts in environmental applications: a review, J. Clean. Prod. 378 (2022), https://doi.org/10.1016/j.jclepro.2022.134589.
- [340] J. Liu, M.S. Kelley, W. Wu, M.G. Kanatzidis, Nitrogenase-mimic iron-containing chalcogels for photochemical reduction of dinitrogen to ammonia, Proc. Natl. Acad. Sci. U. S. A 113 (2016) 5530–5535, https://doi.org/10.1073/ pnas.1605512113
- [341] L.- fei Hong, R.-tang Guo, Y. Yuan, X.- yin Ji, Z.- sheng Li, Z.- dong Lin, W.-guo Pan, Recent Progress of Two-Dimensional MXenes in photocatalytic applications: a review, Mater. Today Energy 18 (2020), https://doi.org/10.1016/j.mtener.2020.100521.
- [342] N. Shah, X. Wang, J. Tian, Recent advances in MXenes: A Promising 2D Material for Photocatalysis, Mater. Chem. Front. 7 (2023) 4184–4201, https://doi.org/ 10.1039/D3OM00216K.
- [343] H. Yu, H. Jiang, S. Zhang, X. Feng, S. Yin, W. Zhao, Review of two-dimensional MXenes (Ti₃C₂T_x) materials in photocatalytic applications, Processes 11 (2023), https://doi.org/10.3390/pr11051413.
- [344] T. Amrillah, A. Hermawan, V.Novita Alviani, Z.Wei Seh, S. Yin, MXenes and Their derivatives as nitrogen reduction reaction catalysts: recent progress and perspectives, Mater. Today Energy 22 (2021), https://doi.org/10.1016/j. mtener.2021.100864.
- [345] Q. Li, J.-liang Xu, S.-mei Wang, K.-fu Yu, W.-kun Zhu, T.-ting Hou, L.-tian Zhang, W.-hua Zhang, S.-quan Liang, L.-bing Wang, Ti₃C₂T_x MXene doped by w atoms for full-spectrumphotofixation of nitrogen, Trans. Nonferrous Met. Soc. China 32 (2022) 233–250, https://doi.org/10.1016/S1003-6326(21)65790-4.
- [346] H. Jiang, C. Zang, Y. Zhang, W. Wang, C. Yang, B. Sun, Y. Shenad, F. Bian, 2D MXene-Derived Nb₂O₅/C/Nb₂C/g-C₃N₄ heterojunctions for efficient nitrogen photofixation, Catal. Sci. Technol. 10 (2020) 5964–5972, https://doi.org/ 10.1006/NOCESCEN.
- [347] B. Chang, Y. Guo, D. Wu, L. Li, B. Yang, J. Wang, Plasmon-enabled N₂ photofixation on partially reduced Ti₃C₂ MXene, J, Chem. Sci. 12 (2021) 11213–11224, https://doi.org/10.1039/D1SC02772G.
- [348] T. Hou, Q. Li, Y. Zhang, W. Zhu, K. Yu, S. Wang, Q. Xu, S. Liang, L. Wang, Near-Infrared Light-Driven Photofixation of Nitrogen Over Ti₃C₂T_x/TiO₂ hybrid

- structures with superior activity and stability, Appl. Catal. B 273 (2020), https://doi.org/10.1016/j.apcatb.2020.119072.
- [349] B. Sun, P. Qiu, Z. Liang, Y. Xue, X. Zhang, L. Yang, H. Cui, J. Tian, The Fabrication of 1D/2D CdS Nanorod@Ti₃C₂ MXene composites for good photocatalytic activity of hydrogen generation and ammonia synthesis, J. Chem. Eng. 406 (2021), https://doi.org/10.1016/j.cej.2020.127177.
- [350] J. Qin, X. Hu, X. Li, Z. Yin, B. Liu, K.-ho Lam, 0D/2D AgInS₂/MXene Z-scheme heterojunction nanosheets for improved ammonia photosynthesis of N₂, Nano Energy 61 (2019) 27–35, https://doi.org/10.1016/j.nanoen.2019.04.028.
- [351] X. Chen, Y. Li, Z. Wu, X. Xu, W. Zhu, X. Gao, Bi₄O₅Br₂ Anchored on Ti₃C₂ MXene with Ohmic Heterojunction in Photocatalytic NH₃ production: insights from combined experimental and theoretical calculations, J. Colloid Interface Sci. 602 (2021) 553–562, https://doi.org/10.1016/j.jcis.2021.06.049.
- [352] L. Wang, J. Zhang, Y. Liu, J. Wang, X. Xu, R. Guan, Y. Zhang, W. Shi, Y. Liu, Z. Zhao, Bisphenol A Assisted Ti₃C₂T_x/CuZnInS Schottky heterojunction for highly efficient photocatalytic nitrogen fixation, Colloids Surf. A Physicochem. Eng. Asp. 648 (2022), https://doi.org/10.1016/j.colsurfa.2022.129430.
- [353] Y. Fang, Y. Cao, B. Tan, Q. Chen, Oxygen and titanium vacancies in a BiOBr/ MXene-Ti₃C₂ composite for boosting photocatalytic N₂ fixation, ACS Appl. Mater. Interfaces 13 (2021) 42624–42634, https://doi.org/10.1021/acsami.1c08888.
- [354] W. Gao, X. Li, S. Luo, Z. Luo, X. Zhang, R. Huang, M. Luo, In situ modification of cobalt on MXene/TiO₂ as composite photocatalyst for efficient nitrogen Fixation, J. Colloid Interface Sci. 585 (2021) 20–29, https://doi.org/10.1016/j. icis 2020 11 064
- [355] B. Chang, Y. Guo, H. Liu, L. Li, B. Yang, Engineering a Surface Defect-Rich Ti₃C₂ Quantum Dots/Mesoporous C₃N₄ hollow nanosphere schottky junction for efficient N₂ photofixation, Mater. Chem. A 10 (2022) 3134–3145, https://doi. org/10.1039/D1TA09941 H.
- [356] F. Kordbacheh, G. Heidari, Water pollutants and approaches for their removal, Mater. Chem. Horiz. 2 (2023) 139–153, https://doi.org/10.22128/ MCH 2023 684 1039
- [357] W. Siong Chai, J. Ying Cheun, P. Senthil Kumar, M. Mubashir, Z. Majeed, F. Banat, S.-Hsin Ho, P. Loke Show, A review on conventional and novel materials towards heavy metal adsorption in wastewater treatment application, J. Clean. Prod. 296 (2021), https://doi.org/10.1016/j.jclepro.2021.126589.
- [358] A. Yusuf, A. Sodiq, A. Giwa, J. Eke, O. Pikuda, G. De Luca, J.Luque Di Salvo, S. Chakraborty, A review of emerging trends in membrane science and technology for sustainable water treatment, J. Clean. Prod. 266 (2020), https://doi.org/ 10.1016/j.iclepro.2020.121867.
- [359] A.S. Adeleye, J.R. Conway, K. Garner, Y. Huang, Y. Su, A.A. Keller, Engineered nanomaterials for water treatment and remediation: costs, benefits, and applicability, J. Chem. Eng. 286 (2016) 640–662, https://doi.org/10.1016/j. cei.2015.10.105.
- [360] M.A. Oturan, J.-Jacques Aaron, Advanced oxidation processes in water/ wastewater treatment: principles and applications. a review, Crit. Rev. Environ. Sci. Technol. 44 (2014) 2577–2641, https://doi.org/10.1080/ 10643389.2013.829765.
- [361] A.Shafi Ganie, S. Bano, N. Khan, S. Sultana, Z. Rehman, M.M. Rahman, S. Sabir, F. Coulon, M.Zain Khan, Nanoremediation technologies for sustainable remediation of contaminated environments: recent advances and challenges, Chemosphere 275 (2021), https://doi.org/10.1016/j.chemosphere.2021.130065.
- [362] X. Li, Y. Chen, Y. Tao, L. Shen, Z. Xu, Z. Bian, H. Li, Challenges of photocatalysis and their coping strategies, Chem. Catal. 2 (2022) 1315–1345, https://doi.org/ 10.1016/j.checat.2022.04.007.
- [363] K. Rasool, R.P. Pandey, P.Abdul Rasheed, S. Buczek, Y. Gogotsi, K.A. Mahmoud, Water Treatment and environmental remediation applications of twodimensional metal carbides (MXenes), Mater. Today 30 (2019) 18–102, https:// doi.org/10.1016/j.mattod.2019.05.017.
- [364] R. Mantovani Ronchi, J. Teodoro Arantes, S. Ferreira Santos, K.A. Mahmoud, Synthesis, structure, properties and applications of MXenes: current status and perspectives, Ceram. Int. 45 (2019) 18167–18188, https://doi.org/10.1016/j. ceramint.2019.06.114.
- [365] S. Lim, J.Hyung Kim, H. Park, C. Kwak, J. Yang, J. Kim, S.Young Ryua, J. Lee, Role of Electrostatic interactions in the adsorption of dye molecules by Ti₃C₂-MXenes, RSC Adv. 11 (2021) 6201–6211, https://doi.org/10.1039/D0RA10876F.
- [366] A. Shahzad, K. Rasool, M. Nawaz, W. Miran, J. Jang, M. Moztahida, K. A. Mahmoud, D.Sung Lee, Heterostructural ${\rm TiO_2/Ti_3C_2T_x}$ (MXene) for photocatalytic degradation of antiepileptic drug carbamazepine, J. Chem. Eng. 349 (2018) 748–755, https://doi.org/10.1016/j.cej.2018.05.148.
- [367] Z. Chen, Y. Ma, W. Chen, Y. Tang, L. Li, J. Wang, Enhanced Photocatalytic degradation of ciprofloxacin by heterostructured BiOCl/Ti₃C₂T_x MXene nanocomposites, J. Alloy. Compd. 950 (2023), https://doi.org/10.1016/j. isllnow.2020.160707.
- [368] A. Grzegórska, I. Wysocka, P. Głuchowski, J. Ryl, J. Karczewski, A. Zielińska-Jurek, Novel Composite of Zn/Ti-layered double hydroxide coupled with mxene for the efficient photocatalytic degradation of pharmaceuticals, Chemosphere 308 (2022), https://doi.org/10.1016/j.chemosphere.2022.136191.
- [369] K. Gao, L.-an Hou, X. An, D. Huang, Y. Yang, BiOBr/MXene/g-C₃N₄ Z-scheme heterostructure photocatalysts mediated by oxygen vacancies and MXene quantum dots for tetracycline degradation: process, mechanism and toxicity analysis, Appl. Catal. B 323 (2023), https://doi.org/10.1016/j. apcatb.2022.122150.
- [370] Z. Othman, A. Sinopoli, H.R. Mackey, K.A. Mahmoud, Efficient photocatalytic degradation of organic dyes by AgNPs/TiO₂/Ti₃C₂T₅ MXene composites under UV and Solar Light, ACS Omega 6 (2021) 33325–33338, https://doi.org/10.1021/ acsomega.1c03189.

- [371] Z. Yang, J. Wang, Enhanced photocatalytic degradation of emerging contaminants using Ti₃C₂T_x MXene-Supported CdS Quantum Dots, Langmuir 39 (2023) 4179–4189, https://doi.org/10.1021/acs.langmuir.3c00223.
- [372] M.Abdullah Iqbal, A. Tariq, A. Zaheer, S. Gul, S.Irfan Ali, M.Z. Iqbal, D. Akinwande, S. Rizwan, Ti₃C₂-MXene/bismuth ferrite nanohybrids for efficient degradation of organic dyes and colorless pollutants, ACS Omega 4 (2019) 20530–20539, https://doi.org/10.1021/acsomega.9b02359.
- [373] Q. Liu, X. Tan, S. Wang, F. Ma, H. Znad, Z. Shen, L. Liu, S. Liu, MXene as a Non-Metal Charge Mediator in 2D Layered CdS@Ti₃C₂@TiO₂ COmposites with Superior Z-scheme Visible Light-driven Photocatalytic Activity, Environ. Sci.: Nano 6 (2019) 3158–3169, https://doi.org/10.1039/C9EN00567F.
- [374] Y. Cao, Y. Fang, X. Lei, B. Tan, X. Hu, B. Liu, Q. Chen, Fabrication of Novel CuFe₂O₄/MXene hierarchical heterostructures for enhanced photocatalytic degradation of sulfonamides under visible light, J. Hazard. Mater. 387 (2020), https://doi.org/10.1016/j.jhazmat.2020.122021.
- [375] V. Sharma, A. Kumar, A. Kumar, V. Krishnan, Enhanced photocatalytic activity of two dimensional ternary nanocomposites of ZnO-Bi₂WO₆-Ti₃C₂ MXene under natural stulight irradiation, Chemosphere 287 (2022), https://doi.org/10.1016/ ichemosphere 2021 132119
- [376] X. Fu, Y. Kong, M. Wang, T. Cai, Q. Zeng, MXene Derived Ti₃C₂/TiO₂/Ag Persistent Photocatalyst with enhanced electronstorage capacity for round-theclock degradation of organic pollutant, J. Colloid Interface Sci. 656 (2024) 233–240, https://doi.org/10.1016/j.jcis.2023.11.079.
- [377] C. Cui, R. Guo, H. Xiao, E. Ren, Q. Song, C. Xiang, X. Lai, J. Lan, S. Jiang, Bi₂WO₆/Nb₂CT_x MXene Hybrid Nanosheets with Enhanced Visible-Light-Driven Photocatalytic Activity for Organic Pollutants Degradation, Appl. Surf. Sci. 505 https://doi.org/10.1016/j.apsusc.2019.144595.
- [378] S.-Mun Lam, M.-Kit Choong, J.-Chung Sin, H. Zeng, L. Huang, L. Hua, H. Li, Z. Haider Jaffari, K. Hwa Cho, Construction of Delaminated Ti₃C₂ MXene/ NiFe₂O₄/V₂O₅ Ternary Composites for expeditious pollutant degradation and bactericidal property, J. Environ. Chem. Eng. 10 (2022), https://doi.org/ 10.1016/j.jece.2022.108284.
- [379] H. Song, Y. Wang, Z. Ling, D. Zu, Z. Li, Y. Shen, C. Li, Enhanced Photocatalytic Degradation of Perfluorocotanoic Acid by Ti₃C₂ MXene-derived heterojunction photocatalyst: application of intercalation strategy in DESs, Sci. Total Environ. 746 (2020). https://doi.org/10.1016/j.scitoteny.2020.141009.
- [380] S. Zhang, M. Cai, J. Wu, Z. Wang, X. Lu, K. Li, J.-Min Lee, Y. Min, Photocatalytic Degradation of TiO₂ via Incorporating Ti₃C₂ MXene for methylene blue removal from water, Catal. Commun. 174 (2023), https://doi.org/10.1016/j. catcom.2022.106594.
- [381] B. Liu, X. Zhang, J. Chu, F. Li, C. Jin, J. Fan, 2D/2D BiOIO₃/Ti₃C₂ MXene nanocomposite with efficient charge separation for degradation of multiple pollutants, Appl. Surf. Sci. 618 (2023), https://doi.org/10.1016/j.ansusc.2023.156565.
- [382] Y. Zhou, M. Yu, H. Liang, J. Chen, L. Xu, J. Niu, Novel dual-effective z-scheme heterojunction with g-C₃N₄, Ti₃C₂ MXene anD Black Phosphorus for Improving Visible Light-induced Degradation of Ciprofloxacin, Appl. Catal. B 291 (2021), https://doi.org/10.1016/j.apcatb.2021.120105.
- [383] H. Wang, R. Zhao, H. Hu, X. Fan, D. Zhang, D. Wang, 0D/2D Heterojunctions of Ti₃C₂ MXene QDs/SiC as an efficient and robust photocatalyst for boosting the visible photocatalytic no pollutant removal ability, ACS Appl. Mater. Interfaces 12 (2020) 40176–40185, https://doi.org/10.1021/acsami.0c01013.
- [384] K. Huang, C. Li, L. Wang, W. Wang, X. Meng, Layered Ti₃C₂ MXene and Silver Co-Modified g-C₃N₄ with enhanced visible light-driven photocatalytic activity,
 J. Chem. Eng. 425 (2021), https://doi.org/10.1016/j.cej.2021.131493.
 [385] H. Zhang, M. Li, J. Cao, Q. Tang, P. Kang, C. Zhu, M. Ma, 2D a-Fe₂O₃ Doped Ti₃C₂
- [385] H. Zhang, M. Li, J. Cao, Q. Tang, P. Kang, C. Zhu, M. Ma, 2D a-Fe₂O₃ Doped Ti₃C₂ MXene composite with enhanced visible light photocatalytic activity for degradation of rhodamine B, Ceram. Int. 44 (2018) 19958–19962, https://doi.org/10.1016/j.ceramint.2018.07.262.
- [386] G. Sharma, A. Kumar, S. Sharma, M. Naushad, D. -Viet, N. Vo, M. Ubaidullah, S. M. Shaheen, F.J. Stadler, Visible-light driven dual heterojunction formed between g-C₃N₄/BiOCl@MXene-Ti₃C₂ for the effective degradation of tetracycline, Environ. Pollut. 308 (2022), https://doi.org/10.1016/j.envpol.2022.119597.
- [387] Y. Wang, J. Chen, M. Que, Q. Wu, X. Wang, Y. Zhou, Y. Ma, Y. Li, X. Yang, MXene-Derived Ti₃C₂T_x/Bi₄Ti₃O₁₂ heterojunction photocatalyst for enhanced degradation of tetracycline hydrochloride, rhodamine b, and methyl orange under visible-light irradiation, Appl. Surf. Sci. 639 (2023), https://doi.org/10.1016/j.assusc.2023.158270.
- [388] H. Liu, C. Yang, X. Jin, J. Zhong, J. Li, One-pot hydrothermal synthesis of MXene Ti₃C₂/TiO₂/BiOCl ternary heterojunctions with improved separation of photoactivated carries and photocatalytic behavior toward elimination of contaminants, Colloids Surf. A Physicochem. Eng. Asp. 603 (2020), https://doi. org/10.1016/j.colsurfa.2020.125239.
- [389] M. Abdullah Iqbal, S. Irfan Ali, F. Amin, A. Tariq, M.Z. Iqbal, S. Rizwan, La- and Mn-Codoped Bismuth Ferrite/Ti₃C₂ MXene composites for efficient photocatalytic degradation of congo red dye, ACS Omega 4 (2019) 8661–8668, https://doi.org/ 10.1016/j.ceramint.2018.07.262.
- [390] T. Lunkenbein, J. Schumann, M. Behrens, R. Schlögl, M.G. Willinger, Formation of a ZnO Overlayer in Industrial Cu/ZnO/Al₂O₃ catalysts induced by strong metalsupport interactions, Angew. Chem. Int. Ed. 54 (2015) 4544–4548, https://doi. org/10.1002/anie.201411581.
- [391] E. Lam, K. Larmier, P. Wolf, S. Tada, O.V. Safonova, C. Copéret, Isolated Zr Surface Sites on Silica Promote Hydrogenation of CO₂ to CH₃OH in Supported Cu Catalysts, J. Am. Chem. Soc. 140 (2018) 10530–10535, https://doi.org/10.1021/ jacs.8b05595.

- [392] H. Zhou, Z. Chen, A.Vidal López, E.D.íaz López, E. Lam, A. Tsoukalou, E. Willinger, D.A. Kuznetsov, D. Mance, A. Kierzkowska, F. Donat, P.M. Abdala, A. Comas-Vives, C. Copéret, A. Fedorov, C.R. Müller, Engineering the Cu/Mo₂CT_x (MXene) interface to drive CO₂ hydrogenation to methanol, Nat. Catal. 4 (2021) 860–871, https://doi.org/10.1038/s41929-021-00684-0.
- [393] R. Morales-Salvador, J.D. Gouveia, Á. Morales-García, F. Viñes, J.R.B. Gomes, F. Illas, Carbon capture and usage by MXenes, ACS Catal. 11 (2021) 11248–11255, https://doi.org/10.1021/acscatal.1c02663.
- [394] H. Zhou, Z. Chen, E. Kountoupi, A. Tsoukalou, P.M. Abdala, P. Florian, A. Fedorov, C.R. Müller, Two-Dimensional Molybdenum Carbide 2D-Mo₂C as a superior catalyst for CO₂ Hydrogenation, Nat. Commun. 12 (2021), https://doi. org/10.1038/s41467-021-25784-0.
- [395] H.-Ulrich Blaser, C. Malan, B. Pugin, F. Spindler, H. Steiner, M. Studer, Selective Hydrogenation for fine chemicals: recent trends and new developments, Adv. Synth. Catal. 345 (2003) 103–151, https://doi.org/10.1002/adsc.200390000.
- [396] G. Vilé, D. Albani, N. Almora-Barrios, N. López, J. Pérez-Ramírez, Advances in the design of nanostructured catalysts for selective hydrogenation, ChemCatChem 8 (2016) 21–33, https://doi.org/10.1002/cctc.201501269.
- [397] K. Li, T. Jiao, R. Xing, G. Zou, Q. Zhao, J. Zhou, L. Zhang, Q. Peng, Fabrication of Hierarchical MXene-Based AuNPs-containing core-shell nanocomposites for high efficient catalysts, Green. Energy Environ. 3 (2018) 147–155, https://doi.org/ 10.1016/j.gee.2017.11.004.
- [398] G. Fan, X. Li, C. Xu, W. Jiang, Y. Zhang, D. Gao, J. Bi, Y. Wang, Palladium supported on titanium carbide: a highly efficient, durable, and recyclable bifunctional catalyst for the transformation of 4-chlorophenol and 4-nitrophenol, Nanomater 8 (2018), https://doi.org/10.3390/nano8030141.
- [399] X. Xie, Z. Wu, N. Zhang, Robust and Easily Retrievable Pd/Ti₃C₂T_xCgraphene hydrogels for efficient catalytic hydrogenation of nitroaromatic compounds, Chin. Chem. Lett. 31 (2020) 1014–1017, https://doi.org/10.1016/j.cclet.2019.10.012.
- [400] M.M. Trandafir, F. Neaţu, I.M. Chirica, Ş. Neaţu, A.C. Kuncser, E.I. Cucolea, V. Natu, M.W. Barsoum, M. Florea, Highly efficient ultralow Pd loading supported on MAX phases for chemoselective hydrogenation, ACS Catal. 10 (2020) 5899–5908, https://doi.org/10.1021/acscatal.0c00082.
- [401] Q. Chen, W. Jiang, G. Fan, Pt Nanoparticles on Ti₃C₂T_x-Based MXenes as efficient catalysts for the selective hydrogenation of nitroaromatic compounds to amines, Dalton Trans. 49 (2020) 14914–14920, https://doi.org/10.1039/D0DT02594A.
- [402] Y. Wang, D. Zhao, D. Rodríguez-Padrón, C. Len, Recent ADvances in Catalytic Hydrogenation of Furfural, J. Catal. 9 (2019), https://doi.org/10.3390/ catal9100796.
- [403] M. Naguib, W. Tang, K.L. Browning, G.M. Veith, V. Maliekkal, M. Neurock, A. Villa, Catalytic Activity of Ti-based MXenes for the hydrogenation of furfural, ChemCatChem 12 (2020) 5733–5742, https://doi.org/10.1002/cctc.202000977.
- [404] M. Crespo-Quesada, F. Cárdenas-Lizana, A.-Laure Dessimoz, L. Kiwi-Minsker, Modern Trends in catalyst and process design for alkyne hydrogenations, ACS Catal. 2 (2012) 1773–1786, https://doi.org/10.1021/cs300284r.
- [405] Y. Yan, D. Sall, L. Loupias, S. Célérier, M. Aouine, P. Bargiela, M. Prévot, F. Morfin, L. Piccolo, MXene-supported single-atom and nano catalysts for effective gas-phase hydrogenation reactions, Mater. Today Catal. 2 (2023), https://doi.org/10.1016/j.mtcata.2023.100010.
- [406] K.Tom Rommens, M. Saeys, Molecular views on Fischer Tropsch synthesis, Chem. Rev. 123 (2023) 5798–5858, https://doi.org/10.1021/acs. chemrey 2c00508
- [407] L. Fratalocchi, C.Giorgio Visconti, G. Groppi, L. Lietti, E. Tronconi, Intensifying Heat Transfer in Fischer—Tropsch TUbular Reactors through the Adoption of Conductive Packed Foams, J. Chem. Eng. 349 (2018) 829–837, https://doi.org/ 10.1016/j.cei.2018.05.108.
- [408] E. Kountoupi, A.J. Barrios, Z. Chen, C.R. Müller, V.V. Ordomsky, A. Comas-Vives, A. Fedorov, The impact of oxygen surface coverage and carbidic carbon on the activity and selectivity of two-dimensional molybdenum carbide (2D-Mo₂C) in Fischer–Tropsch Synthesis, ACS Catal. 14 (2024) 1834–1845, https://doi.org/ 10.1021/acscatal.3c03956.
- $[409] \label{eq:continuous} J. \ Diao, M. \ Hu, Z. \ Lian, Z. \ Li, H. \ Zhang, F. \ Huang, B. \ Li, X. \ Wang, D. Sheng Su, H. \ Liu, Ti_3C_2T_x \ MXene \ catalyzed ethylbenzene dehydrogenation: active sites and mechanism exploration from both experimental and theoretical aspects, ACS Catal. 8 (2018), https://doi.org/10.1021/acscatal.8b02002.$
- [410] P. Tomkins, M. Ranocchiari, J.A. van Bokhoven, Direct conversion of methane to methanol under mild conditions over Cu-Zeolites and beyond, Acc. Chem. Res. 50 (2017) 418–425, https://doi.org/10.1021/acs.accounts.6b00534.
- [411] X. Sun, Y. Gao, C. Zhao, S. Deng, X. Zhong, G. Zhuang, Z. Wei, J.-guo Wang, Palladium Dimer Supported on Mo₂CO₂ (MXene) for direct methane to methanol conversion, Adv. Theory Simul. 2 (2019), https://doi.org/10.1002/ adts.201800158
- [412] S. Dey, G. Chandra Dhal, Controlling carbon monoxide emissions from automobile vehicle exhaust using copper oxide catalysts in a catalytic converter, Mater. Today Chem. 17 (2020) 5124–5134, https://doi.org/10.1016/j. mtchem.2020.100282.
- [413] A.F. Zedan, S. Gaber, A.S. AlJaber, K. Polychronopoulou, CO oxidation at near-ambient temperatures over TiO₂-Supported Pd-Cu catalysts: promoting effect of Pd-Cu Nanointerface and TiO₂ Morphology, Nanomater 25 (2021), https://doi.org/10.3390/nano11071675.
- [414] H. Zhang, S. Fang, Y.Hang Hu, Recent advances in single-atom catalysts for CO Oxidation, Catal. Rev. Sci. Eng. 64 (2020) 491–532, https://doi.org/10.1080/ 01614940.2020.1821443.
- [415] C.T. Campbell, G. Ertl, H. Kuipers, J. Segner, A molecularbeam study of the catalytic-oxidation of CO on a Pt(111) Surface, J. Chem. Phys. 73 (1980) 5862–5873, https://doi.org/10.1063/1.440029.

- [416] I. Tezsevin, M.C.M. van de Sanden, S. Er, Surface charging activated mechanism change: a computational study of O, CO, and CO₂ interactions on Ag electrodes, J. Energy Chem. 50 (2020) 307–313, https://doi.org/10.1016/j. iechem. 2020.03.080
- [417] S. Hussain Talib, Z. Lu, B. Bashir, S. Hussain, K. Ahmad, S. Khan, S. Haider, Z. Yang, K. Hermansson, J. Li, CO Oxidation on MXene (Mo₂CS₂) supported single-atom catalyst: a termolecular eley-rideal mechanism, Chin. Chem. Lett. 34 (2023), https://doi.org/10.1016/j.cclet.2022.04.010.
- [418] Q. Peng, X. Zhang, Z. Geng, Z. Yang, J. Yang, Single Zn atom catalyst on Ti₂CN₂ MXenes for Efficient CO Oxidation, Phys. E Low. Dimens. Syst. Nanostruct. 147 (2023), https://doi.org/10.1016/j.physe.2022.115595.
- [419] B. Cai, J. Zhou, D. Li, Z. Ao, New Insights into the Single-Atom-Decorated Zr₂CO₂ (MXene) as an Efficient Catalyst for CO oxidation in incomplete combustion gas, Appl. Surf. Sci. 575 (2022), https://doi.org/10.1016/j.apsusc.2021.151777.
- [420] C. Zhu, J.-Xia Liang, Y.-Gang Wang, J. Li, Non-noble metal single-atom catalyst with mxene support: Fe1/Ti₂CO₂ for CO Oxidation, J. Catal. 43 (2022) 1830–1841, https://doi.org/10.1016/S1872-2067(21)64027-5.

- [421] M. Usman, W.M.A. Wan Daud, H.F. Abbas, Dry reforming of methane: influence of process parameters-a review, Renew. Sust. Energ. Rev. 45 (2015) 710–744, https://doi.org/10.1016/j.rser.2015.02.026.
- [422] R. Thakur, A. VahidMohammadi, J. Smith, M. Hoffman, J. Moncada, M. Beidaghi, C.A. Carrero, Insights into the genesis of a selective and coke-resistant mxenebased catalyst for the dry reforming of methane, ACS Catal. 10 (2020) 5124–5134, https://doi.org/10.1021/acscatal.0c00797.
- [423] R. Thakur, A. VahidMohammadi, J. Moncada, W.R. Adams, M. Chi, B. Tatarchuk, M. Beidaghi, C.A. Carrero, Insights into the thermal and chemical stability of multilayered V₂CT_x MXene, Nanoscale 11 (2019) 10716–10726, https://doi.org/10.1039/C9NR03020D.
- [424] A. Kurlov, E.B. Deeva, P.M. Abdala, D. Lebedev, A. Tsoukalou, A. Comas-Vives, A. Fedorov, C.R. Müller, Exploiting two-dimensional morphology of molybdenum oxycarbide to enable efficient catalytic dry reforming of methane, Nat. Commun. 11 (2020), https://doi.org/10.1038/s41467-020-18721-0.
- [425] N. Huang, T. Su, Z. Qin, H. Ji, Nickel supported on multilayer vanadium carbide for dry reforming of methane, ChemistrySelect 7 (2022), https://doi.org/ 10.1002/slct.202203873.